CZECH TECHNICAL UNIVERSITY IN PRAGUE
Faculty of Nuclear Sciences and Physical Engineering
Department of Nuclear Chemistry

Study and development of track etch detectors for dosimetric purposes

Kateřina Pachnerová Brabcová

supervisors: Prof. Ing. František Spurný, DrSc.
Ing. Iva Ambrožová, PhD.

Prague, 2010

Acknowledgement

My greatest thanks go to my supervisor František Spurný, who unfortunately could not stand by me till the end. I will never forget long inspiriting discussions; all I can say is - it was of great help. Thank you.

Without Iva Ambrožová nothing would be completed, her brief encouragements kept me afloat even in times of my biggest doubts.

I am grateful to Marie Davídková and Jana Fejfarová, who patiently corrected the worst English mistakes; however I still had plenty of time to commit several others. I would also like to express my gratitude to have felt the supportive spirit of the whole Department of Radiation Dosimetry, namely of Natalie Megisová, Ivo Světlík, or Zlata Mrazová.

Several people kindly provided me professional help. Alexandr Malušek, far from Sweden, advised me about statistical hurdles, and Miroslava Novotná from the Institute of Chemical Technology provided me expert opinion about FT-IR analysis.

The studies were partially supported by grants GACR No. 205/09/0171, GAAV KJB100480901, IAA No. 100480902 AS CR and research project AVOZ10480505. Experiments were also partially realized in the frame of ESA DOBIES project and ICCHIBAN project. I am also obliged to kind HIMAC staff.

Nothing would have been possible without my incredibly supportive and patient family, my parents and my old sea rats Šimon and Daniel. They all together worked hard to make background for me, I am proud of them.

Thanks to all of you.

A new monk at the monastery asked Joshu: "What is the secret of Zen?"

Joshu answered: "Have you eaten breakfast?"

"Yes", the new monk said.

"Well, wash your bowl."

Sayings of Zen master Joshu

Content

1. INTRODUCTION

Step by step, radiation dosimetry reaches fundamental position among scientific branches during last century and since the human activities deal with ionizing radiation more and more, its importance will probably even rise. The future will have to challenge such issues as interplanetary flights, or, whether we like it or not, the essential energetic dependence on nuclear resources and nuclear waste disposal.

The aim of radiation dosimetry is to recognize, estimate and minimize radiation risks for environment and the mankind in general, as well as for human individuals themselves. The basic optimization approach, with respect to the complexity of radiation protection, is minimization of risk "as low as reasonably achievable" known under the abbreviation ALARA. Of course, there will probably always be special fields of random or planned activities, where this protecting approach cannot be and is not kept; in such cases radiation dosimetry should quantify the risk and educate itself for the future.

Radiation dosimetry has to be up-to-date with current knowledge of ionization radiation biological impacts and it is developing very fast indeed. Yet roughly one hundred years ago, people had no idea about any radiation danger and since then huge progress has been made; it ranges from general observation of deterministic and stochastic effects to very full-scale understanding of cellular processes. Still, many questions remain, like an impact of very low doses, and some new have appeared, like mesmeric bystander effect few years ago.

There are many measuring instruments trying to estimate quantity and/or quality of ionization radiation, but since it covers heterogeneous principles there does not exist a single instrument capable of characterizing whatever radiation. Track etched detectors TED are one of the instruments able to classify and quantify particles with linear energy transfer from about 5 $keV.\mu m^{-1}$ in water, which impacts on humans is dominant according to research (Zhou et al, 2009). LET describes an ionizing density of charged particles, whereas the density relates to biological efficiency of radiation. From the LET, further dosimetric quantities can be calculated.

One might be wondering whether track etched detectors are able to compete with other modern detector systems; we are not alone in confidence that they still are. There still are some applications for which there is no better detector choice regarding power independence, spatial modesty and simple evaluation together with magnificent wide-spectral detector abilities of TED. On the other hand, there still remains a space for improvement and upgrade either of TED materials or the method in some way. Some of them are presented in this work.

The aim of this work is to study the possibilities of TED applied as LET spectrometers in two applications: dosimetry and microdosimetry in beams of heavy ions and neutrons. These radiation fields accompany various human activities, especially radiotherapy and space research. Two full-range studies have been performed and proved TED as very efficient instrument. Further, five different materials used as TED were included in the experiments, as well as in several methodological analysis, which were performed. Thus, it was an opportunity for complex comparison, which has not been available so far. We assumed, there were certain benefits, which offer utilization of various combinations of various TED materials in applications, where TED are usually employed. Following the findings resulting from all tests, we intended to find the most effective combination and apply it in complex dosimetry on board of spacecraft.

The work is divided into four main parts. The INTRODUCTION briefly outlines linear energy transfer spectrometry as the possibility of radiation classification, history and basic principles of TED follows, and it is completed with eventual application resume. The MATERIALS AND METHODS chapter introduces different TED materials, which are applied in our department. The chapter deals with different methodological problems; especially the uncertainties of calculation and calibration are analyzed. The result of this analysis is the assessment of dosimetric quantities with appropriate uncertainties including the whole measuring and analyzing process. Further, this chapter examines material environmental changes, as well as chemical differences among materials. The APPLICATIONS chapter describes TED detection abilities in realized experiments with heavy ions as the primary and neutrons as the secondary particles and considers the differences among the studied materials. The observed material differences result in proposition of PADC combination, which is approved in an experiment performed on board of spacecraft. The results are discussed in final chapter CONCLUSIONS, where all acquired results are summed up.

1.1 Introduction to microdosimetry

Soon after the studies of biological effects of ionizing radiation began, it became apparent that an estimation of absorbed dose does not need to be the most appropriate approach in some cases. Since the absorbed dose D is just statistical average quantity defined as the mean energy $d\varepsilon$ deposited in volume of mass dm, it neglects any random fluctuation of imparted energy. These fluctuations can be very important, especially in case of small

volumes, small doses, or densely ionizing radiations. During the fiftieth of the past century, increasing demand for different approach, especially within the cell studies led to the foundation of the whole new scientific branch called microdosimetry. Microdosimetry deals with energy transfer of ionizing radiation on microscopic level; it respects randomness and discontinuity of the transfer. Compared to quantities in classic dosimetry, microdosimetry operates with stochastic quantities; it means unpredictable, directly measurable ones, represented usually by distribution functions (Sedlák, 1989).

The main microdosimetric quantities are specific energy z and lineal energy y. These are defined as energies deposited in elemental volume of a material within passage of ionizing particle, whereas the volume is characterized with mass m, or mean chord length $\bar{l}$ respectively (ICRU 36, 1983):

$$z = \frac{\varepsilon}{m} \text{ and } y = \frac{\varepsilon}{\bar{l}} \tag{1}$$

Experimental microdosimetric methods have to evade the problem of impossibility of direct detector placement in elemental volume of micro size; the measuring has to be indirect. Since it is not simple to measure and interpret obtained microdosimetric quantities, there is certain intermediate conception between microdosimetry and dosimetry - conception of linear energy transfer (LET). LET is defined only for charged particles; the indirectly ionizing particles can be classified only via secondary particles, according to (ICRU 16, 1970):

$$LET_{\Delta} = \left(\frac{dE}{dl} \right)_{\Delta}, \tag{2}$$

where dE is deposited energy, which is lost along particle path l in inelastic collisions, where only deposition events lesser then Δ are included. With the restriction of an imparted energy we exclude secondary electrons, thus the restricted LET could be considered as the energy imparted in a vicinity of particle track (Kovář, 1984). Without any restriction, LET_{∞} is equal to stopping power. Of course, LET represents just a mean value, without considering any fluctuation of imparted energy. LET does not allow identifying the particles; different particles with different charge and different biological impacts can have the same value of LET (ICRU 36, 1983)

Moreover, even mono-energetic particle beam can not be characterized with single LET value, but with the whole LET spectra. Distribution can be followed either with particle path, or absorbed dose. Corresponding average values can be expressed according to track or dose densities of probabilities (Kovář, 1984):

$$\overline{LET}_T = \int t(LET) LET dLET \tag{3}$$

$$\overline{LET}_D = \int d(LET) LET dLET \tag{4}$$

The basic microdosimetric experimental equipment is **tissue equivalent proportional counter**. Tissue equivalent gas, usually based on methane, is closed in chamber with electrode. Walls are engaged as the cathode and can be made from tissue equivalent polymer, which could be covered with thin conducting layer. Anode is usually made from stainless steel (Kovář, 1984).

Excited and ionized gas atoms create ion pairs, which express themselves as the electric current regarding electrode voltages. The energy necessary for such an expression stays constant under constant working conditions. Because of the tissue equivalency, the counter measures energy deposition in tissue volume; the size of micrometers could be achieved with lowering of pressure. In this case, the counter is directly able to measure microdosimetric quantities lineal and specific energy. Dose equivalent could be extracted from multiplying of lineal energy by corresponding quality factor Q (Waker et al., 2002).

Further experimental equipment is available, for example **recombination ionization chamber**. Detecting efficiency is dependent on LET with respect to low pressure in the first chamber and is compared to total efficiency measured under normal conditions with saturated gas in second chamber. Similarly, total dose obtained with ionization chamber can be compared to response of **Geiger-Müller counter** with low pressure or to scintillation yield of **organic scintillator**; in both cases, the response of detector decreases with decreasing LET.

There is a special group of detectors, where the track of particles could be visualized in some way. For example, sharp cooling of gas in **cloud chamber** leads to its condensation among the path of ionization particle, **nuclear emulsion** use the photochemical reaction for this purpose, and, finally, there are **track etched detectors (TED)** also called **solid state nuclear track detectors (SSNTD)** with sensitivity for etching (Kovář, 1984; Ullmann, 2002). This thesis deals with the last types of detectors.

In last decade, there is an ambition to develop silicon-based spectrometers of LET, since they usually advantage in small proportion and low demand on power supply. One device of this type is Liulin by team of Tsvetan Dachev from Bulgarian Academy of Science (Dachev, 2009), but there are few more variants there. These spectrometers measure energy spectrum deposited in silicon, which can be converted into LET spectrum in tissue. The

conversion of deposited energy uses the ratio of energy loss in tissue and silicon; for example the ratio for 100 MeV protons is 1.31 (Badhwar and O'Neill, 2001).

1.2 Track etch detectors

At the beginning, there was a discovery of (Young, 1958), that LiF crystals could form stable damages after irradiation with thermal neutrons in contact with uranium foil. Damages were treated with a chemical agent to obtain etch pits, number of which corresponded with the number of recoiled fission fragments. In sequence, other materials with the same ability were recognized, as for example mica (Silk and Barnes, 1959), glasses, other mineral crystals and also plastics (Fleischer et al., 1965a), more recently track effect was found in some metals, intermetallic compounds and superconducting oxides (Nikezic and Yu, 2007). All these materials can create more or less stable microscopic damages called latent tracks after passage of charged particles.

The most common way of the enlarging latent tracks is chemical etching; it was discovered by Paul B. Price and Robert M. Walker and it is dated back to the year 1962 (Price and Walker, 1962). The principle consists in faster removal of damaged material in the regions of tracks, while the undamaged areas are dissolved more slowly. Thus, originally latent tracks are deepened and enlarged, and become visible on the surface with optic microscope; the process is outlined on the Figure 1.

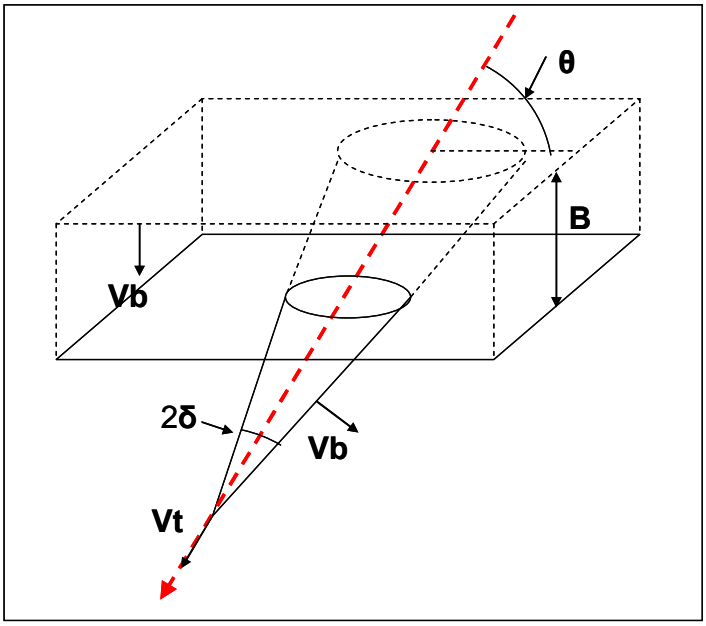

Figure 1 *Particle (red) hits the detector surface under angle θ. Track is formed by etching because of different etching velocities (Vb: etching velocity of undamaged material, Vt: etching velocity of damaged areas, B: thickness of removed layer).*

1.2.1 Tracks formation

One of the first attempts to explain latent track formation in inorganic materials was thermal spike model (Billington and Crawford, 1961). This model described very high localized temperatures in small cylindrical region around particle trajectory, which would lead to recrystallization and melting processes. After a while, it turned out that the model does not reflect observed track parameters. After this failure, a new model was suggested - called ion explosion spike model (Fleischer et al., 1965b). This model explained production of a positively charged region around particle trajectory, which leads to rejection of some ions to interstitial positions by coulomb interactions leaving vacancies behind. It is interesting, that models predicted track formation in metals and semiconductors, although the formation had been observed only in insulators in that time.

Likewise, mechanism of track formation in organic materials is quite well described, but up to now, there is still no unique theory of track creation. .The process is subdivided into the three following stages: physical, physical-chemical, and chemical. During the first, shortest, phase, particle looses its energy along its path in material. It can happen via the interactions with electrons of target nuclei, thus ionizations and excitations occur, or via the interactions directly with target nuclei, which leads to rejection of nuclei out of polymer chain. Another way of losing energy is bremsstrahlung, emission of electromagnetic radiation, but it is related to marginal group of particles with rarely high velocities. Physical stage usually does not last over 10^{-17} s (Durrani and Bull, 1987; Nikezic and Yu, 2007; L'Annunziata et al., 2003).

Second, physical-chemical phase is characterized by interactions of products formed during the previous processes; they are ions, excited atoms, and free electrons, along with molecules of material, free radicals and so on, until thermodynamic equilibrium is reached. Exact chemical composition and its particular reactions are not known. There is a general conception of polymer structure damage in plastics; molecular chains are broken and average molecular weight decreases. Lifetime of created chemical species is reaching even minutes. An ejection of CO and CO_2 from plastics was observed during irradiation, which may suggest scission of ester bonds in chains. Also, some studies confirm the accumulation of -OH groups along the particle path. In the end, latent tracks are created (please, see Figure 2). They are made up from **track cores** of about 10 nm in diameter with dramatically reduced molecular weight, that are surrounded by **track halos** of diameters corresponding to range of delta

electrons, where chemical properties are modified in some way also (L'Annunziata et al., 2003; Yamauchi, 2003).

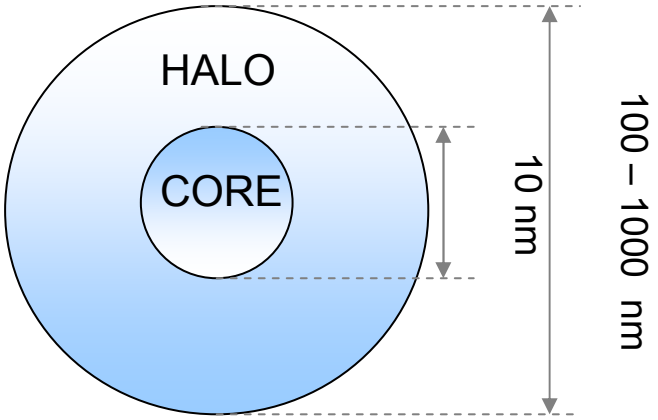

Figure 2 *Concept of latent track in plastic materials*

It was proved that oxygen plays an important role in track formation process in plastics, whereas it has no effect for track formation in glasses. Study of plastic response under vacuum showed clear evidence of track size decrement. It is supposed that free polymer radicals have to react with dissolved oxygen to form a latent track. If the amount of oxygen is decreased, radicals incline to recombine and latent track formation fails (Yamauchi, 2003; Drach et al., 1987).

The last, chemical, stage is etching, where tracks are somehow fixed and enlarged. In the case of plastic materials there is usually employed sodium, potassium hydroxide eventually with concentration ranging from 1 to 12 M and temperature ranging from 40 to 70 ºC. As mentioned above, areas of damages are etched with greater velocity, thus cone tracks rise and they manifest as the ellipses on the surface. Geometry is discussed in following chapter.

Again, there is no general conception of chemistry during etching. It is assumed that increased amount of OH- groups provide for easier penetration of etching agent along the latent tracks (Yamauchi, 2003).

1.2.2 Little geometric outline

Track formation geometry was already described many times, for example in (Durrani and Bull, 1987). Tracks can be initially figured as the cones, as the etching continues, they became more open (effect of over etching is discussed thereinafter); on the surface they appear as the ellipses, as it is figured on 3.

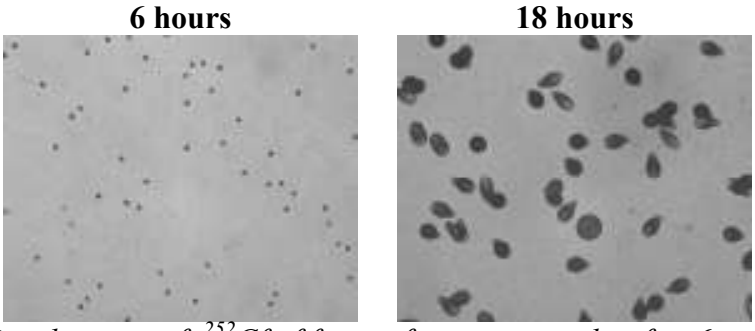

Figure 3 *Development of ^{252}Cf of fission fragments tracks after 6 and 18 hours of etching in material TD1*

I would like to emphasize just few final equations. If the constant etch rate is expected, which is valid presumption for uniform material composition and constant etching conditions, construction results in formulas for major *a* and minor *b* axis of elliptical track visible on the surface, as follows:

$$a = \frac{2V_B t\sqrt{V^2-1}}{V\sin\theta+1} \text{ and } b = 2V_B t\sqrt{\frac{V\sin\theta-1}{V\sin\theta+1}}; \tag{5}$$

where V_B, V_T are bulk rate, etch rate respectively, correspond to notation in Figure 1, V is their ratio V_B/V_T, t is etching time, and θ is angle, under which is particle strikes on the surface. Angle θ_C, defined as $sin\ \theta_C=1/V$ is called critical angle; it is minimal angle of incidence, where track can be observed and are not etched out. Since the critical angle is function of particle type and energy, as well as etching conditions, counted number of tracks per area should be correct with k_θ to estimate all particles able to create tracks in case of isotopic irradiation (Durrani and Bull, 1987):

$$k_\theta = \frac{V^2}{V^2-1} \tag{6}$$

It is possible, that antioxidant doped materials are dip angle dependent (Doke et al., 1997). It means that their track formation sensitivity is dependent on dip angle of incident particle and some particles are not registered, although they strike detector upon the angle lesser than the critical one. The effect can be corrected by different methods (Tawara, H. et al., 2008; Yasuda et al., 2008).

Minor and major axis are usually parameters, which can be easily measured. Further consideration results in following formula of etch ratio V calculation:

$$tg\theta = \frac{B}{2a}\left(1-\frac{b^2}{B^2}\right) \text{ and } V = \frac{1}{\sin\theta}, \tag{7}$$

where $B=V_Bt$ is thickness of removed layer according to Figure 1.

There are few methods to establish thickness of removed layer (Nikezic and Yu, 2004; Kodaira et al., 2007). Rather rough method is **direct measuring of thickness** before and after etching, the result is usually average from several determinations. Since the thickness of material can not be completely uniform, uncertainty of the method is more than ± 1 μm. Dr. Fujii and Dr. Yasuda developed more advanced method of measuring in their **step method** (Fujii et al., 1984; Yasuda et al., 1998); part of detector is masked by resin to avoid etching and step difference representing removed layer is measured. Dr. Yasuda upgraded this method by employment of atomic force microscope. Farther, **gravimetric method** recognizes weight shortage after etching. **Method of fission fragments** is also being applied in our department. This method comes from great etch rate of spontaneous fission fragments of ^{252}Cf incident under normal angle, thus it is valid that $tan\theta = 0$, and following $min = B$. The method is limited by short range of fission fragments (~ 15 μm in PADC), therefore can be employed just for shorter etching times (Kodaira et al, 2007).

1.2.3 Track etched detectors in applications

Track etched detectors have been commonly used for more then thirty years, especially because of their low price, small size, power independence, and rather easy method of evaluation. Track etched detectors are able to register charged particles; usually a number of registered particles is counted and thus an exposition level is quantified. Furthermore, they may be used as spectrometers of linear energy transfer to even estimate a quality of a radiation.

One of the most common applications is radon monitoring (Nikezic and Yu, 2004), the advantage of which is the possibility of automatic evaluation. Among other applications there should also be mentioned dosimetry onboard of aircrafts or spacecrafts (Spurný, 2001; Benton et al., 1986a), personal neutron dosimetry (Tanner et al., 2005), and occasionally dosimetry in various radiation fields including radiotherapy and fragmentation studies (Golovchenko et al., 2001). Track etched detectors are also effective as materials for production of micro membranes, which may be helpful in filtration process (Fleischer et al., 1963) or different biological applications; or in dating of geological samples (Fleischer et al., 1975).

2. MATERIALS AND METHODS

Our department deals with track etched detectors employed as linear transfer spectrometers since the 90's. Detailed methodology focused especially on etching conditions and an evaluation process of data was developed in (Charvát, J., 1985) for cellulose nitrate initially, later the procedure was extended in (Jadrníčková, 2010) for PADC (polyallyldiglycol carbonate). Following section outlines the way, how detectors are treated nowadays.

Materials are stored under -20 ºC in hermetic packing to reduce environmental influences. Our traditional etching conditions include 5 M NaOH during 18 hours at 70 ºC, hydroxide solution is always made fresh. Just before etching, one corner of detector is exposed to ^{252}Cf source, while the rest is shielded; it serves as an instrument for estimation of etched layer thickness as it is described in chapter 1.2.2.

Dimensions of tracks and fission fragments are analyzed with a one of the two software used in our department. Until recently we used automatic optic analyzer LUCIA G/NIS with Leitz microscope and software NIS-Elements 2.30, which is product of Laboratory Imaging, s.r.o. (www.lim.cz). During 2010, our department acquired new microscope device HSP-1000 system by SEIKO Precision INC., which includes microscope and evaluation software HspFit (Yasuda et al., 2005). The first system processes image outputs in real time, one by one, whereas the second one enables evaluating of a scanned image, which makes available easy access to evaluated images to revise it. Also, the software differ in possibilities of zoom and resolution, as well as in editing tools and solution of over-lapping tracks. Anyway, in both cases, analysis requires a human operator to make proper analysis. In spite of different approach and different benefits and disadvantages, no differences in outputs have been found.

Following chapters introduce materials usually employed as track etch detectors and several analysis of various PADC performed from various point of view; procedural matters of uncertainty analysis, calibration, analysis of material and fading task are discussed.

2.1 Materials used as track etch detectors

Today, several different materials are applied as track etch detectors. Above all, it is polyallyldiglycol carbonate (PADC), which successively substitutes previous materials such cellulose nitrate, Makrofol based on polycarbonate and others.

PADC was developed by American Acrylics Inc. in 1939 and it was distributed under the name of CR-39. This symbol became so familiar that it is commonly used up to this day in

spite of fact that this registered trademark is no more available. The material was recognized as a possible solid state detector in the late 1970s (Cartwright et al., 1978). PADC is produced by a free radical polymerisation of diethylene glycol bis-allyl carbonate monomer, which is represented by the summary formula $C_{12}H_{18}O_7$. Configuration of the monomer is introduced on the Figure 4.

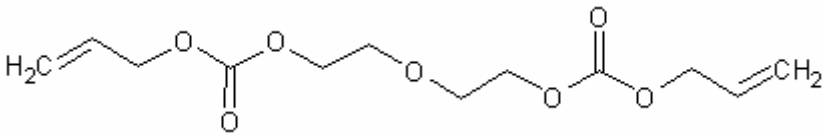

Figure 4 *Monomer used for PADC polymer manufacture*

Qualities of a PADC applied as a nuclear track detector are strongly dependent on curing conditions, such as temperature, or concentration of additives. Several works were published to deal with this problem (Portwood and Stejny, 1984; Somogyi et al., 1986; Ahmad and Stejny, 1991). They imply the more complete polymerization process, the better sensitivity of PADC occurs. The polymerization extent is usually controlled with an infrared technique; density of cross-links increases, whereas amount of diethylene monomer residua decreases.

In a closer view, the polymerization starts with addition of an initiator, isopropyl or cyclohexyl peroxycarbonates (IPP, CHPC respectively) are usually used, or, regarding to their low decomposition temperature, benzoyl peroxide can be applied (Nadkarni and Samant, 1996). A sensitivity of a material as a function of the initiator concentration shows a maximum, higher concentration would lead to shortening of length of polyallyl chains, thus decreasing of polymer density as well.

After the previous fact was cleared up, further effort was aimed at temperature polymerisation conditions. The base was outlined in (Ahmad and Stejny, 1991), where the better sensitivity and the corresponding cross-linking density were achieved with curing cycle at higher temperatures. Actual concepts of polymerization regime usually result from their work.

Besides, a lot of scientific attention is paid to effects of various additives, which would upgrade PADC as a nuclear track detector. First of all, some plasticizers are used to improve the post etched surface; phthalate esters, mainly dioctyl phthalate, are usually employed. Plasticizers would eliminate the opaqueness of detector surface, which exhibits after etching. Unfortunately, benzene ring of phthalate behaves as an electron sink; thereby sensitivity of the polymer is suppressed. The effect would be greater for lower LET values. In most of

applications, reduced sensitivity is unwanted side-effect, except of some application, where, for example, low LET background should be suppressed to underline a response of high LET component (Kodaira, S. et al., 2009).

On the other hand, increased sensitivity for lower LET particles would enable to extend range of applications. After intensive searching for another, more sensitive polymer (Ogura et al., 1995), scientists got back to PADC. Antioxidants turned out to be an answer (Benton et al., 1986b). PADC with small amount of antioxidant have better sensitivity to low LET particles, while response is not affected in higher LET regions. There is usually used 4,4'-bis(alpha, alpha-dimethylbenzyl) diphenylene, which is distributed under the name Naugard 445 (Ogura et al., 1997).

Besides, they are used some other additives in specialized application, such as carbon dope in dosimetry of thermal neutrons.

Today, several worlds' producers fabricate several PADC; let me together with (Tanner et al., 2005) to sum up the differences in industrial process:

- methods of dimmers or trimmers rising, thus different composition of initial polymerisation mixture or its purity;
- temperature and duration of polymerisation regime;
- polymerisation orientation (horizontal or vertical);
- type and concentration of initiator;
- additives.

At the time, our department tests five different materials produced by four different manufacturers; **Page** from Mouldings (Pershore) Ltd, **Tastrak** from Track Analysis Systems Ltd, both from Great Britain, **USF4** from American Technical Plastics from USA and two products of Japan Fukuvi Chemical Industry Co., Ltd – **TD1** and **Baryotrak**. They differ in composition and detection abilities as it is discussed in following chapters.

2.2 FT-IR material analysis

In few last years, several techniques including transformed Fourier infra red (FT-IR) and ultra-violet analysis (FT-UV), and electron spin resonance spectroscopy (ESR) were employed to inspect changes of TED materials chemical composition during latent tracks creating (Böhlke and Hermsdorf, 2008). It was especially described several materials, as Page (Lounis-Mokrani et al., 2003), Baryotrak (Mori et al., 2009; Yamauchi et al., 2008), Tastrak

(Böhlke and Hermsdorf, 2008) and others (Tripathy et al., 2001), in virgin forms and irradiated by protons, heavy ions, or gamma rays.

For deeper understanding of PADC material characteristic, the material analysis was performed in cooperation with the Institute of Chemical Technology in Prague. Materials were investigated using the Fourier transform infrared absorption spectroscopy in total attenuation reflection mode (FT-IR/ATR). There were obtained infrared spectra with instrument Nicolet 6700 FT-IR spectrometer operated by software OMNIC, which is provided with 4 cm^{-1} resolution from 4000 to 600 cm^{-1}.

Materials were studied in virgin form, for each, three different positions were measured and average spectra were calculated. The whole absorbance spectra are figured in 5. One can distinguish several important wave number regions of major infrared absorption frequencies (marked on Figure 5) and recognize some functional group according to (Novotná, 2010; Kania, 2007; Hummel and Scholl, 1971), which are similar for all analysed PADC.

Region around 3471 cm^{-1} indicates presence of OH groups. The formation of OH group is usually observed in irradiated forms of PADC (Mori et al., 2009), but it is clear, they are presented even in virgin forms of all investigated PADC. It might indicate intra-molecular hydrogen bonding.

Further region corresponds to asymmetric vibration of C-H in CH_3 (2940 cm^{-1}) and CH_2 (2922 cm^{-1}), followed by untagged frequencies related to the corresponding symmetric vibrations in opposite order. The ratio of CH_2 and CH_3 is one of the indicators of polymerization degree and range of polymer cross-linking.

Typical, the most intensive absorption frequencies are related to carbonate stretching; >C=O (1735 cm^{-1}) and ether C-O-C (1239 cm^{-1}). Their relative absorbance linearly decreases with a dose induced by gamma rays (Mori et al., 2009), as well as heavy ions (Yamauchi et al., 2008).

In agreement with literature (Lounis-Mokrani et al., 2003), there are also obvious peaks in 1453 and 1399 cm^{-1} (bending vibrations of CH_2 and CH_3), 1136, 1092 and 1026 cm^{-1} (additional stretching of ether C-O-C) and some others typical stretching in the area bellow 1000 cm^{-1}.

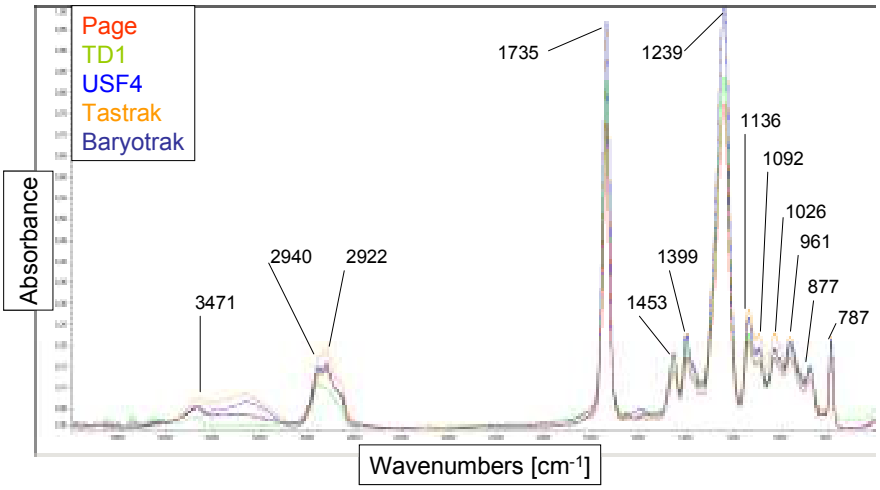

Figure 5 *Average absorbance spectra of five different PADC with major absorption frequencies tagged with corresponding wave number in* cm^{-1}

Besides, if the spectra are inspected more closely, one can see interesting absorption frequencies in region from 1700 to 1500 cm^{-1}, see Figure 6. The frequency 1648 cm^{-1} is probably related to amid groups C-N-H (they are accompanied with other stretching in region around 3200 cm^{-1}). Broader band in 1580 cm^{-1} is characteristic for an aromatic group. It should be followed by additional broads with wave number up to 780 cm^{-1} approximately; however it is not possible to distinguish them. The evidence of amid and aromatic groups indicates the presence of some additives. It is very interesting, that one can found a similarity of TD1 and USF4 materials, although these materials are manufactured by different producers. Alike, materials Tastrak and Baryotrak have similar spectra shape, different to the previous two. Page appears to be somewhere in the middle.

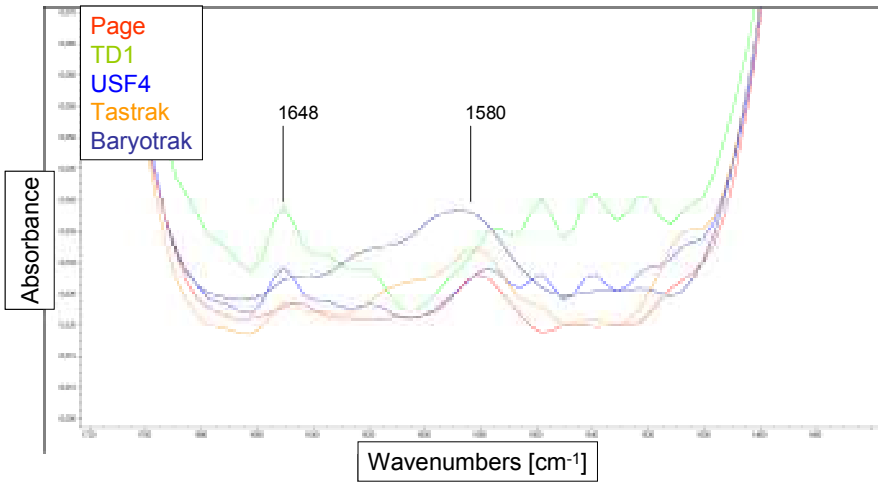

Figure 6 *Differences in average absorbance spectra of inspected PADC in region from 1700 to 1500* cm^{-1}*, close view.*

These findings are in agreement with our information about material chemical composition (summarized in Table 5). Main differences in FT-IR spectra are probably related to (non)presence of antioxidant additives.

2.3 Calibration and uncertainty analysis

During enthusiastic data analysis an error task stays often apart, although any data could not represent anything until the proper uncertainty analysis follows. If PADC is employed as linear energy transfer spectrometer, first it is necessary to find relation between detector response and linear energy transfer, this relation is called calibration. Afterwards, it is possible to calculate dosimetric characteristics, dose and dose equivalent. The method is described in following chapter.

2.3.1 Estimation of dose and dose equivalent

For track etched detectors, a multistage measurement model can be constructed according to (JCGM:104, 2009), as it is figured on 7.

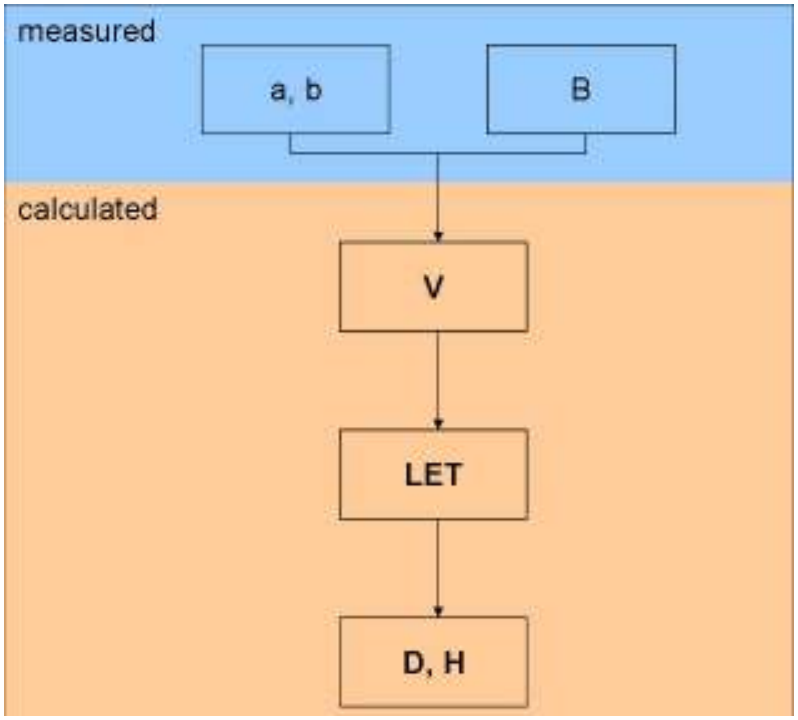

***Figure** 7 In multistage measurement model, the etch rate V is evaluated from the measured track dimensions a and b, and thickness of removed layer B. The etch rate is used to evaluate the linear energy transfer LET, which can further be used to evaluate absorbed dose D and dose equivalent H.*

There are three measured quantities: dependent *a* and *b* representing maximal and minimal dimension of track; and independent *B* representing thickness of removed layer by etching. All three quantities are measured with analytical software with negligible error, but they are stochastic quantities considered having normal distribution. As such they can be described with corresponding normal distribution parameters.

Etched rate *V* for every damaged area is counted via geometric consideration described in chapter 1.2.2 according to (7) from the measured track parameters. It is also considered having normal distribution, which characteristics are obtained from characteristics of measured quantities.

There is a relation between *V* and linear energy transfer *LET*, this dependence is found with calibration and corresponding uncertainties are discussed.

Finally, dose *D* in mGy and dose equivalent *H* in mSv are evaluated according to (8) and (9).

$$D_{LET} = \int const * LET \frac{dN}{dLET} dLET \tag{8}$$

$$H_{LET} = \int const * LET \frac{dN}{dLET} Q(LET) dLET , \tag{9}$$

where *(dN/dLET)* is number of particles per area within LET interval (corrected if necessary according to (X)) in cm^{-2}, LET is linear energy transfer in $keV.\mu m^{-1}$ and Q is quality factor dependent on LET according to (ICRP 60, 1991); its values are included in Table 1. *Const* = 1.602* 10^{-6} results from unit transformation, where eV = $1.602.10^{-19}$ J.

Table 1 *LET dependent quality factor Q (ICRP 60, 1991)*

LET [keV.µm^{-1}]	**Q(LET)60**
< 10	1
10 -100	0.32LET-2.2
> 100	$300/LET^{0.5}$

One should consider, what the dose and dose equivalent obtained with track etch detectors represent. TED are detectors based on the first moment of energy distribution (Kovář et al., 1984), for which a measured dose and a required dose in tissue are somehow proportional. It is necessary to inspect detector response to different irradiations to describe

this relation. Situation is rather simply for detection of heavy charged particles directly registered in detector and it becomes very complicated for detection of secondary particles as it is in case of neutrons or protons.

2.3.2 Normal distribution of measured quantities

A random variable X is normally distributed with mean μ and variance σ^2, if its distribution can be hit off with probability density function (pdf) according to

$$f(x) = \frac{1}{\sqrt{2\pi\sigma^2}} \exp\left(-\frac{(x-\mu)^2}{2\sigma^2}\right) \tag{10}$$

Random vector (X,Y) has two-dimensional normal distribution with vector of mean μ and covariance matrix Σ, if its distribution can be hit off with pdf according to (Novovičová, 1999)

$$f(x,y) = \frac{1}{2\pi\sqrt{|\Sigma|}} \exp\left(-\frac{(x-\mu)^T \Sigma^{-1} (x-\mu)}{2}\right) \tag{11}$$

$$\mu = (\mu_{x,}\mu_y)^T \text{ and } \Sigma = \begin{pmatrix} \sigma_x^2 & \sigma_{xy} \\ \sigma_{yx} & \sigma_y^2 \end{pmatrix} \tag{12}$$

Searching of parameters of normal distribution is described on following experiment. Carbon ions with energy 135 MeV/u were aimed upright to the surface of detector without any shielding, hence, in theory, there should be observed tracks of circular shape and one size.

Unfortunately various conjunctures affect the track development; such as non-homogeneity of detector material composition and thickness, concentration and temperature differences during etching, eventual residua after washing out of hydroxide, and also competence of human factor, since the personal view and ability to recognize and focus tracks can differ. All these factors eventuate in development of tracks of different sizes and different elliptical shapes; as it is figured on 8a.

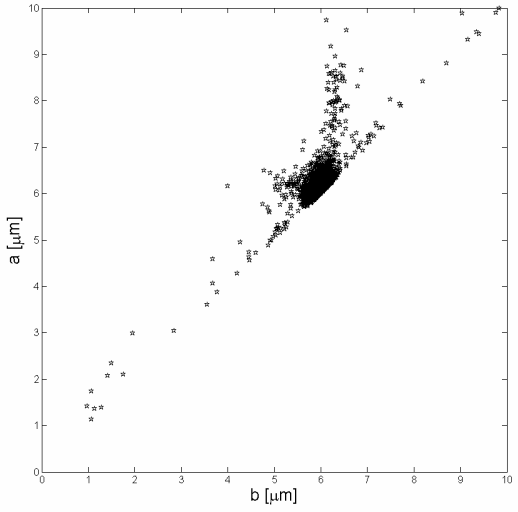

Figure 8a *Scatter plot for track parameters a and b (maximal and minimal track dimension)*

The reconstruction of normal distribution of track size was calculated as follows. Since *a* is always greater or equal to *b*, domain of *[a, b]* is upper half of quadrant, beyond the quadrant axis. Hence, corresponding mirror data were added to avoid distortion of distribution. The mirroring of data is valid under the assumption of most probable data incidence right on the quadrant axis. Also, data domain was specified by exclusion of very small or very great tracks originating from other then primary source; final data selected for analysis and corresponding mirror ones are figured on 8b.

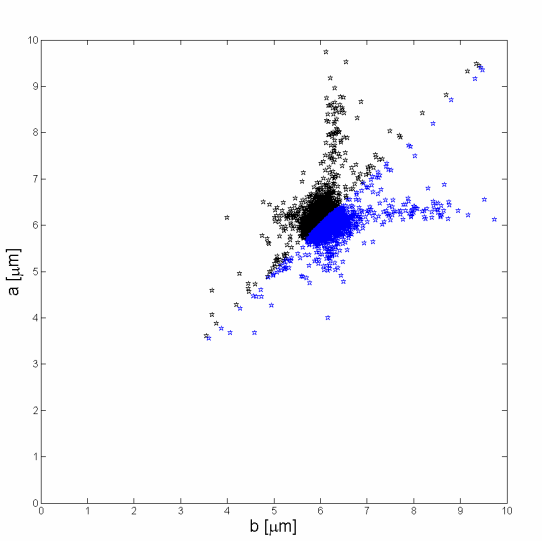

Figure 8b *Data selection (removing of outliers) and mirror data addition*

The distribution of track sizes was described with two-dimensional normal distribution $N(\mu, \sigma^2)$ with corresponding parameters according to (11) and (12). There is a clear relationship of vector (X,Y) with normal distribution $N(\mu, \sigma^2)$ and vector (U,V) with normalized normal distribution $N(0,1)$ in according to

$$\begin{bmatrix} X \\ Y \end{bmatrix} = T \begin{bmatrix} U \\ V \end{bmatrix} + \mu \,, \qquad (13)$$

where T is lower triangular matrix of Cholesky decomposition of covariance matrix Σ (Genz, 1992) and μ is vector of mean values, the data transposition is figured on 8c.

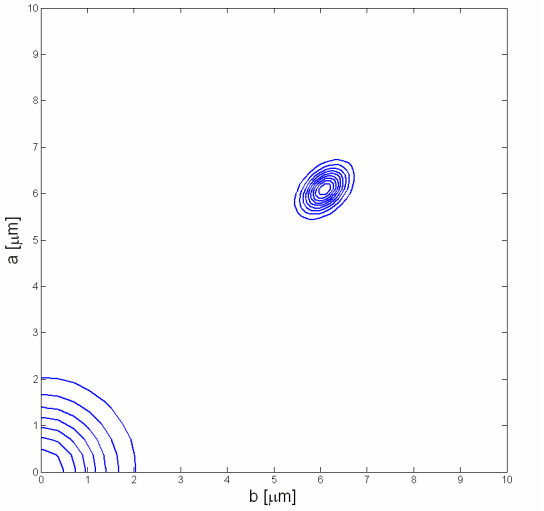

Figure 8c *2-D normal and normalized distribution of a and b*

A sum of k independent random variables with normalized normal distribution has chi-square distribution with k degrees of freedom $\chi^2(k)$. In our case, quantity $ch = U^2+V^2$ has $\chi^2(2)$.

There can be found values of 95 % and 99 % quantiles for chi-square distribution, since the quantiles are tabulated. Radius of corresponding circle of normalized normal distribution is square root quantile value. Radius of corresponding ellipse of previous normal distribution can be derived by formula mentioned above. Resulting curves are figured on 8d; note that the total number of points is 4872 (without mirror data) in this case.

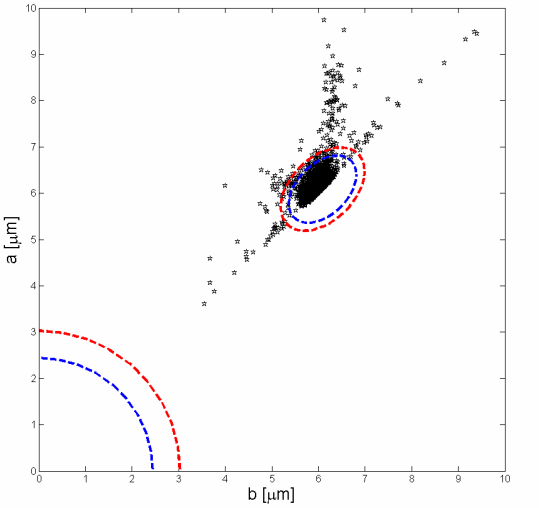

Figure 8d *95 % quantile (blue) and 99 % quantile (red) of normal and normalized distribution*

Third measured quantity *B* is expected to be also normally distributed, corresponding mean value and standard deviation are obtained alike for previous quantities, except it is one-dimensional distribution (10).

Etch rate *V* can be calculated from measured quantities according to formula resulting from (7).

$$V = f(a,b,B) \tag{14}$$

Etch rate is also expected being normally distributed; this presumption is verified on Figure 9, where probabilities of number of tracks per area distribution are compared for data measurement and corresponding theoretical prediction based on estimation of normal distribution parameters.. The mean value of V was estimated as

$$\mu_V \approx f(\mu_a, \mu_b, \mu_B), \tag{15}$$

where μ_i are corresponding mean values; and standard deviation of *V* can be expressed as:

$$\sigma_V = \sqrt{(\frac{\partial f}{\partial B}\sigma_B)^2 + (\frac{\partial f}{\partial a}\sigma_a)^2 + (\frac{\partial f}{\partial b}\sigma_b)^2 + 2\frac{\partial f}{\partial a}\frac{\partial f}{\partial b}\sigma_{ab}}, \tag{16}$$

according to propagation of uncertainties low; σ_i are corresponding standard deviations and σ_{ab} is covariance of *a* and *b* quantities.

The next step is calibration of etch rate response to values of linear energy transfer; the procedure is described in following chapter.

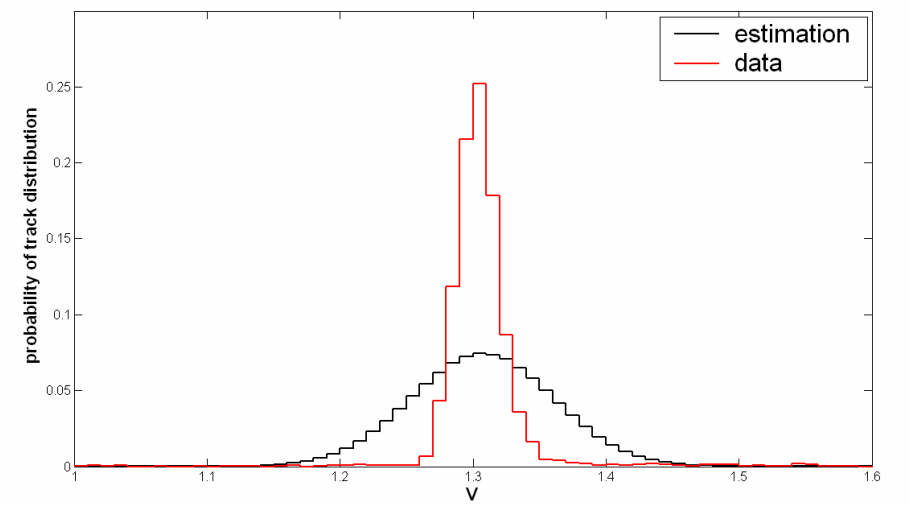

Figure 9 *Comparison of track distribution along etch rate V probabilities: measured data (red) and corresponding theoretical prediction (black) of the law of uncertainty propagation*

2.3.3 Calibration curves

Calibration consists in finding of a relation between etch rate *V* and linear energy transfer *LET*. First and fundamental challenge for me was creating of calibration curves for materials, which have not been applied in our department yet. For those already used before, there was opportunity to inspect and upgrade the old curves.

During 2008 and 2009 we performed series of experimental expositions on HIMAC facility (Heavy Ion Medical Accelerator in Chiba) in Biology room in cooperation with the Japanese National Institute of Radiological Sciences. The expositions were performed in frame of ICCHIBAN projects (Yasuda et al., 2006a) and within several approved beam time proposals, which HIMAC kindly offers (HIMAC P241 and P242: "Measurements and analysis of LET distributions at HIMAC BIO: Development of the LET distributions database"). Detectors were exposed in bare and shielded beams of various ions, whose energies and linear transfer energies are outlined in Table 2, then they were treated as described in chapter 2. We obtained about fifty calibration points for each material, which covered the whole operational spectrum of LET (from 10 to 500 keV.um^{-1} approximately).

Each calibration point characterized with mean value and standard deviation was obtained by consecution of steps described in previous chapter. Figure 10 is an example of all calibration points for material TD1; despite of including results from several different experiments they can be described as very consistent. Etched rate is traditionally figured as the value minus one.

Table 2 *Ions and their energies and linear transfer energies[1] used in calibration relation searching*

	nominal energy MeV/n	LET in water keV.um^{-1}
$^{12}C^{6+}$	290	13-41
$^{20}Ne^{10+}$	400	31-83
$^{28}Si^{14+}$	490	57, 75
$^{40}Ar^{18+}$	500	95-166
$^{56}Fe^{26+}$	420	197-335
$^{84}Kr^{36+}$	320	443

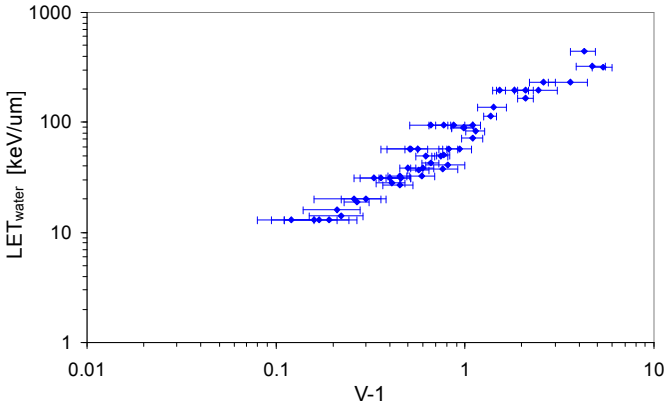

Figure 10 *A scatter plot of LET in water against shifted etch rate V-1 for several TD1 detectors irradiated and processed separately; error bars indicate 95% confidence intervals. Note the logarithmic scale on both axes.*

The uncertainties of reference LET values, which are provided by staff of HIMAC facility, are supposed to be minor. The operator staff measure absorbed dose with ionization chamber and calculate LET of primary particles. Uncertainty of nominal energy of accelerating process is less than 0.1 %, after the passing through the air it is about 2-3 % (Yasuda, 2010). This uncertainty is bellow TED discrimination. It was verified during repetitive exposition to carbon beam of 135 MeV/u, which nominal energy is considered to be constant from the view of TED. Figure 11 shows 99 % intervals of track diameters for all three expositions; there are no significant differences.

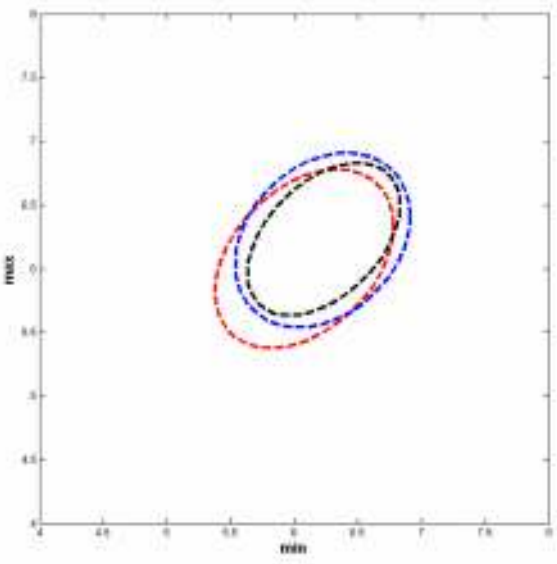

Figure 11 *99 % quantiles of distribution of track diameters for three repetitive exposures to the same beam, evaluated with material Page*

In previous formation of calibration curves, the data were fitted with simple polynomial function, but this approach does not reflect any physical characteristics of detection abilities. These characteristics can be described as follows. Each material has its own operational range. On the side of low LET it is limited by detection threshold; material cannot detect any particles with LET bellow this point. On the side of great LET values saturation effect exists; the area, where real size of track can not be distinguished anymore. In this area material cannot work as spectrometer of LET, we can just count the number of tracks. This effect occurs due to similarity of etch velocity of analysed tracks and tracks by fission fragments, which are used for estimation of bulk etched rate (chapter 1.2.2). Overall, such detection behaviour can be well described with Weibull's distribution with four parameters, as follows:

$$LET = a - (a - b)\exp^{-(k*(V-1))^d} \tag{17}$$

First iteration step of parameter searching was performed without considering of uncertainties, which enabled to estimate uncertainty *σ(LET)* of dependent value LET from the errors of independent value V-1 according to formula similar to (16):

$$\sigma(LET) = \left(\frac{dLET}{d(V-1)}\right)\sigma(V-1) \tag{18}$$

Consequently, the data were fitted by Weibull's distribution with weighting $1/\sigma(LET)^2$. The reason for weighting are differences in standard deviations of individual calibration points; it should be said, that uncertainty of etch rate estimation is roughly increasing for increased liner energy transfer, the example for TD1 material is figured on 12.

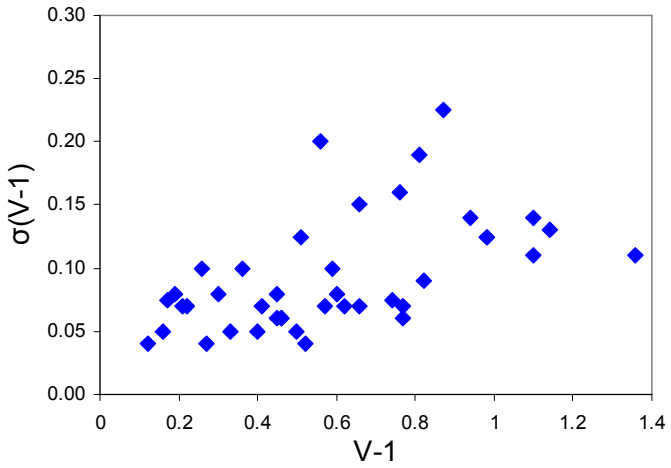

Figure 12 *Standard deviations of calibration points versus shifted track etch rate V-1 for material TD1*

First of all, let me compare old and new calibration curves for two materials, Page and Tastrak, which have been used in our department for some time (Spurný et al, 2005). Figure 13 illustrates a good similarity of the curves, except the slight deviation in the part of the greatest LET values. It is caused by the fact, that previous calibration did not take into the account the saturation effect and polynomial fit was prolonged without considering this effect. Also, Tastrak shows greater detection threshold, which corresponds to published data (for example Pálfalvi et al., 2008) and our experience. This satisfactory comparison validates calibration even for other materials.

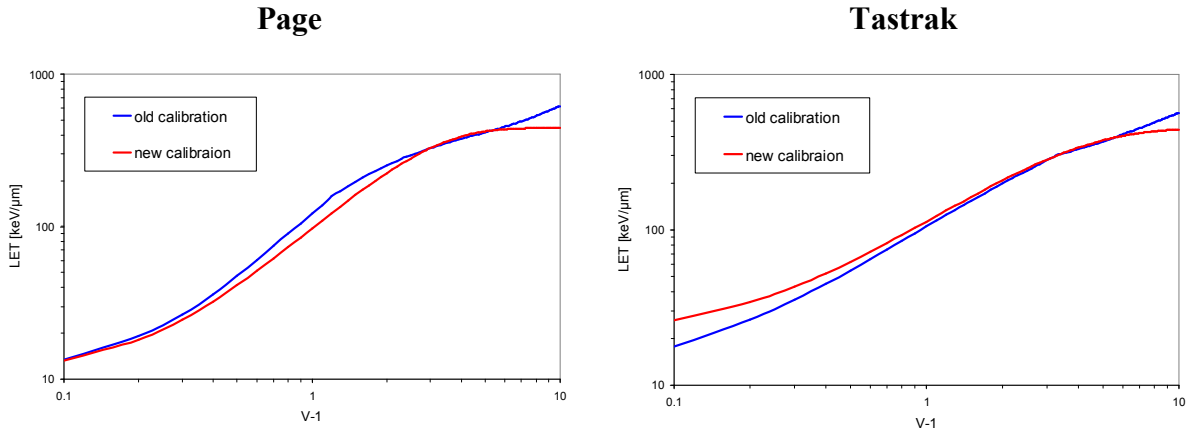

Figure 13 *Comparison of new and previous calibration dependences of LET in water and V-1 for material Page and Tastrak*

Figure 14 includes calibration curves for all five materials; corresponding parameters are summarized in Table 3. There are significant differences among them; according to expectation the curves have different detection thresholds, but also they behave differently in higher LET ranges. Very sensitive material TD1 shows early saturation in high LET range, which means there can not be distinguished particles with LET value higher than a 340 keV.um^{-1}. Behaviour of Page is very similar, in spite of different producer and therefore probably different production conditions. Tastrak and Baryotrak have higher detection thresholds, but Tastrak is saturated earlier. USF4 is the most interesting, multipurpose material; it has very low detection threshold (about 8 keV.um^{-1}), but it also has the greatest tolerance to the saturation in higher LET range among three more sensitive PADC. It should be emphasized that behaviour of tested materials is specific for our etching conditions, which were mentioned previously.

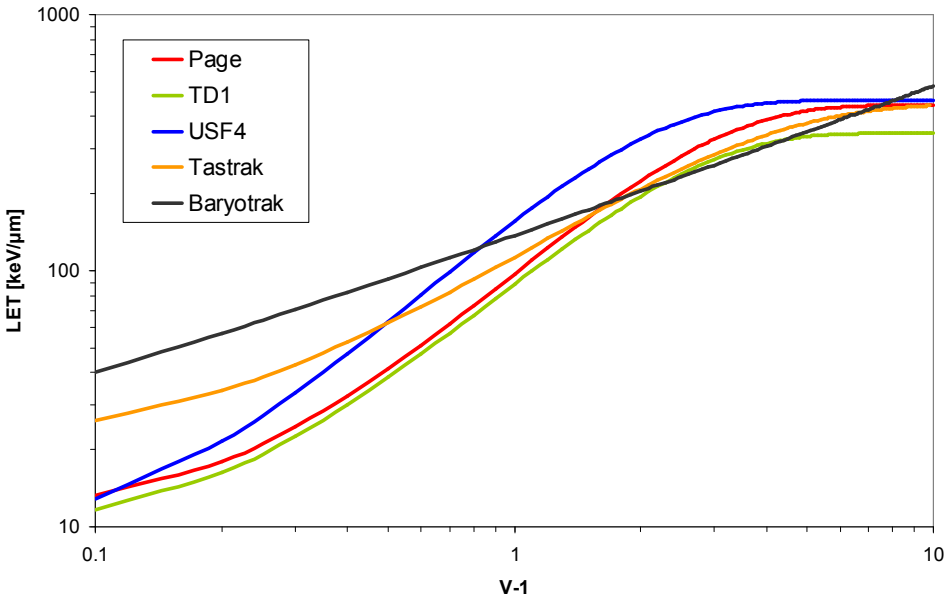

Figure 14 *Calibration curves for tested TED materials. The linear energy in water LET is plotted as a function of the shifted etch rate V-1; note the logarithmic scale on both axes*

Table 3 *Parameters a, b, k and d of calibration equations LET = f(V-1) for tested PADC, etching conditions: 5 M NaOH, 70 ˚C, 18 hours*

$$LET = a - (a - b)\exp^{-(k*(V-1))^{d}}$$

	a	b	k	d
Page	443.34	10.92	1.61	0.39
TD1	334.75	9.27	1.58	0.44
USF4	462.79	8.53	1.61	0.56
Tastrak	447.71	20.07	1.24	0.32
Baryotrak	$1.14.10^{6}$	7.98	0.60	$2.92.10^{-7}$

Detection threshold characteristics outlined in Figure 14 respect corresponding results obtained in calibration experiments. Anyway, in special cases, detection threshold can be reduced beyond 5 keV.um^{-1} as it resulted from expositions in helium beam and it is in agreement with literature (Yasuda et al, 2000). There were observed clear presence of detected primary particles for all three sensitive materials for helium beam, which energy corresponds to 5 keV.um^{-1}; the LET was calculated with code SRIM (Ziegler et al., 2008). The demonstration behind 127.69 mm binary filter is figured on 15 for material Page, where

plenty small tracks of primary helium particles is registered (together with greater tracks from secondary particles).

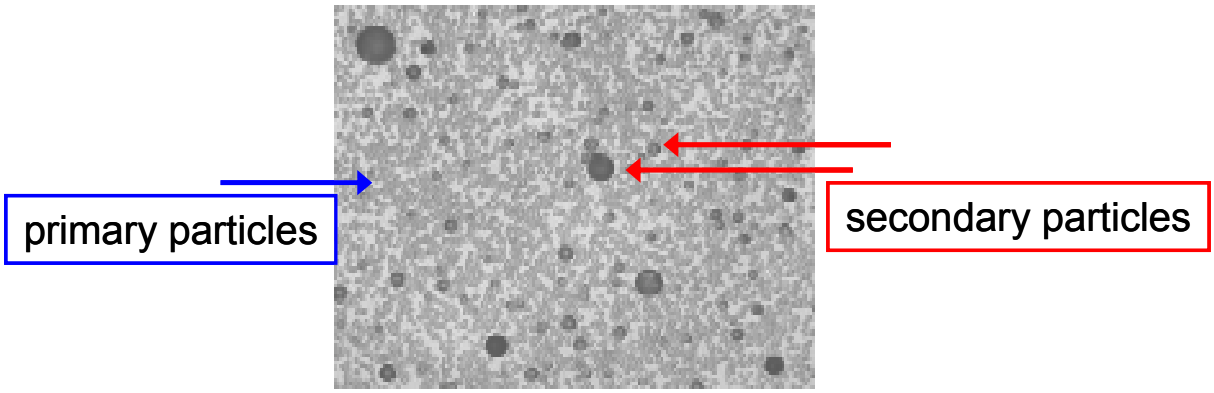

Figure 15 *A photograph of the etched surface of the Page detector irradiated to150 MeV/u helium beam behind PMMA binary filter of 127.69 mm thick. This corresponds to LET of 5 keV.um^{-1}. Small-diameter tracks were created by primary helium ions; large-diameter tracks are produced by from secondary fragments.*

Uncertainties of LET calibration curves were estimated as 95 % confidence regions with using linearization of calibration equation, and are figured in attachment as figure 47.

Dose can be expressed as simple linear dependence on LET_i and N_i number of particles per area and LET_i interval, the total dose is summed dose increments for all LET intervals according to (16). As such, dose uncertainties result also from error propagation formula:

$$\sigma(D_i) = \sqrt{(\frac{\partial D}{\partial LET}\sigma(LET_i))^2 + (\frac{\partial D}{\partial N}\sigma(N_i))^2}\ , \text{where} \qquad (19)$$

$\sigma(LET_i)$ results from width of confidence region in corresponding interval and $\sigma(N_i) = \sqrt{N_i}$, since the N_i is considered to have Poisson distribution.

Dose equivalent increments are function of corresponding dose increments and quality factor, which uncertainties are not included into our calculations. The uncertainty calculation is similar to dose uncertainties.

2.4 Environmental effects on PADC

Even though the PADC is exceptionally stable material, it is also influenced with different environmental impacts. The changes have impact for applications with long-term duration, which occur for example during space exposition or radon monitoring. Changes operating prior to irradiation are called "ageing", while the changes occurring after irradiation

are called "fading". It is clear the both processes are essentially connected and should be considered together.

All polymer materials undergo the ageing processes as the molecular reorganisation takes place regarding non-equilibrium state (Hutchinson, 1995). Ageing of PADC means changing of sensitivity and response of detector; it is strongly dependent on material composition and its manufacture, as well as on storage conditions (Hardcastle and Miles, 1996). It is known ageing should be partially suppressed by storing under a low temperature and without the air access (Bartlett, 1987).

On the other hand, fading means there is no guarantee of stability of latent tracks in plastics before they are fixed by etching. Part of damages can be recombined as the broken molecular bonds can be repaired with time going on. It is supposed that the velocity of reparation process is greater in few hours or days after the irradiation, and then it is established on more or less constant value. Fading mechanism is critically dependent on an oxygen amount dissolved in the material; at exposures in vacuum or in conditions with lower oxygen concentration (for example in trial balloons) there was observed huge oxygen leaking from the material, which leads to increasing recombination of latent tracks and increasing fading (L'Annunziata et al., 2003). It was verified that oxygen stimulates oxidation process resulting in stable low-molecular chain fragments, and further, oxygen leakage can be partially compensated by diffusion of oxygen from deeper layers of sample in dependence on material composition (Böhlke and Hermsdorf, 2008). The PADC detection abilities are also affected by humidity and temperature, UV and γ irradiation (Durrani and Bull, 1987; L'Annunziata et al., 2003; Dorschel et al, 2005).

Significant part of our experiments is aimed at monitoring of radiation risk during space missions; where long exposition times within more then few month are expected, and, furthermore, there is other time delay caused by delivery from and to coordinators; thus the elapsed time between exposition and etching is not negligible and demands some fading investigation.

2.4.1 Tests of environmental effects on PADC

During 2008 and 2009 we performed some fading tests with four PADC materials (Page, TD1, USF4 and Tastrak) to investigate stability to environmental effects. The goal of the experiment was to recommendation of one material or two, which would be useful for long-term monitoring in the future.

Ten packs of tested materials were prepared, and then they were individually exposed to ^{252}Cf at month intervals roughly. Products of spontaneous californium fission are neutrons, alpha particles and fission fragments with upper nucleon number, which are used in estimation of bulk etch rate as it is described earlier. The source of radiation was always in close touch with surface of a PADC detector, thus the particles should strike upon the detectors upright.

All time, detectors were stored in laboratory under the room conditions, it means before and also after irradiation to the time of etching. Temperature and humidity in the laboratory were changing according to season. Etching was performed for all samples together after another six months following last irradiation. Thus, the experiment conditions include ageing and fading processes together as it is during long-term expositions in real. The total time of experiment was 546 days, which is also the longest available fading time from our tested samples.

First of all, we observed material surfaces under our microscope. In a first view, it is obvious, that etched surface of materials looks different, an example is figured on 16.

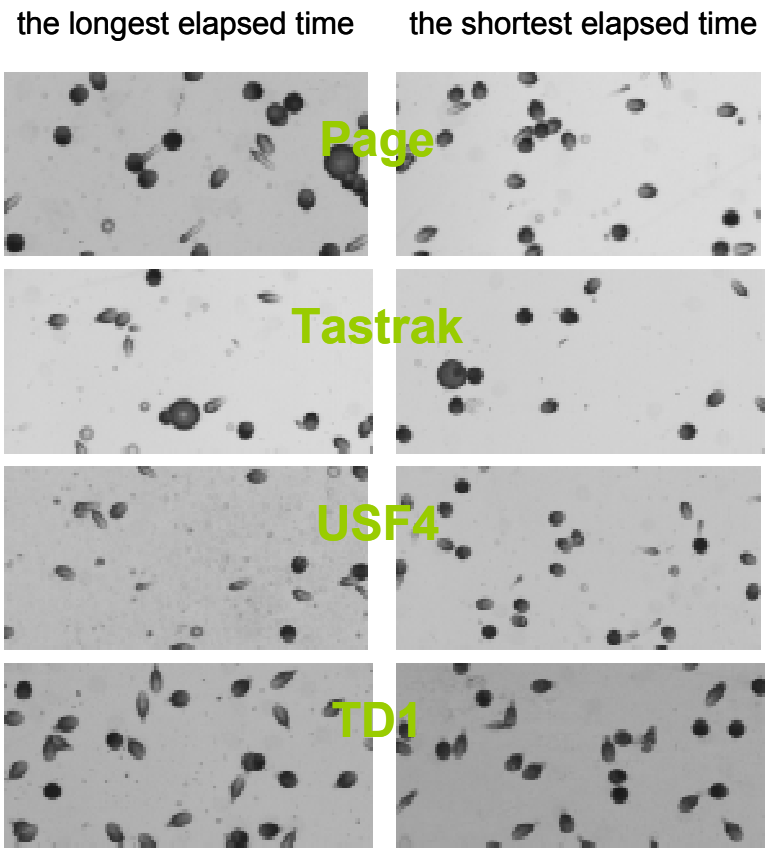

Figure 16 *Surface photographs of tested etched detectors; comparison for the longest and shortest time (546 and 257 days) elapsed between exposition and etching*

There can be observed increasing numbers of small dark objects, when elapsed time between exposure and etching was the longest (546 days). Objects have clearly different character dependent on material; those on TD1 surface are sharply bordered and they disappear with decreasing elapsed time, those on USF4, Page and Tastrak surfaces are fuzzy and greater and their number is also decreased with elapsed time, but they do not completely vanish even for the shortest elapsed time (257 days). It means, the number of "false track" increases with elapsed time for all materials. If we keep at least one background sample for every experiment, this increase should be compensate.

The problem occurs for extreme situation of higher exposure together with long elapsed time; the evaluation of the detector surface may not be possible under such circumstances, since the etched surface can look also as it is figured on 17.

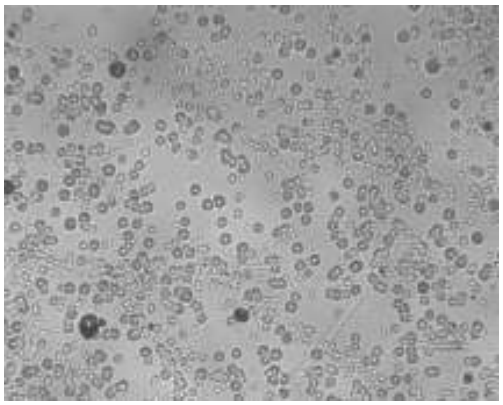

Figure 17 *Surface of an etched material after neutron irradiation with Am-Be source and 400 days of storage under room conditions; an evaluation becomes impossible*

Analysis of upright alpha particles and fission fragments parameters were performed, etch rates were calculated and corresponding LET values were assigned; results are summarized in Figure 18. Alpha particles derived from californium source should have energy 6.12 MeV (Rytz, 1991); corresponding LET was calculated as 80 keV.μm^{-1} by simulation code SRIM (Ziegler et al., 2008).

In general, one can see complex ambiguous dependence on time, which occurs for all materials. There are usually one or more maximum overall for individual materials, but their position is different. Most of previous investigators found decreasing etch rate leading to decreasing linear energy transfer and thus underestimating of dose and dose equivalent (Zhou et al, 2010). The magnitude of decreasing was found dependent on radiation type. It was usually investigated for alpha particles (Portwood et al, 1986) or neutrons (for example Gilvin et al, 1988). In spite of that, our results indicate more complicated sensitivity dependence related to the extent of ageing and fading and their ratio. Some other investigators came to similar results. For example (Tanner et al, 1995) described changing of fading in time expressed as possible detector response decrease or increase as the function of material cure cycle. Since the ageing can be very probably also material dependent, these two functions together could affect etch ratio in more complicated way.

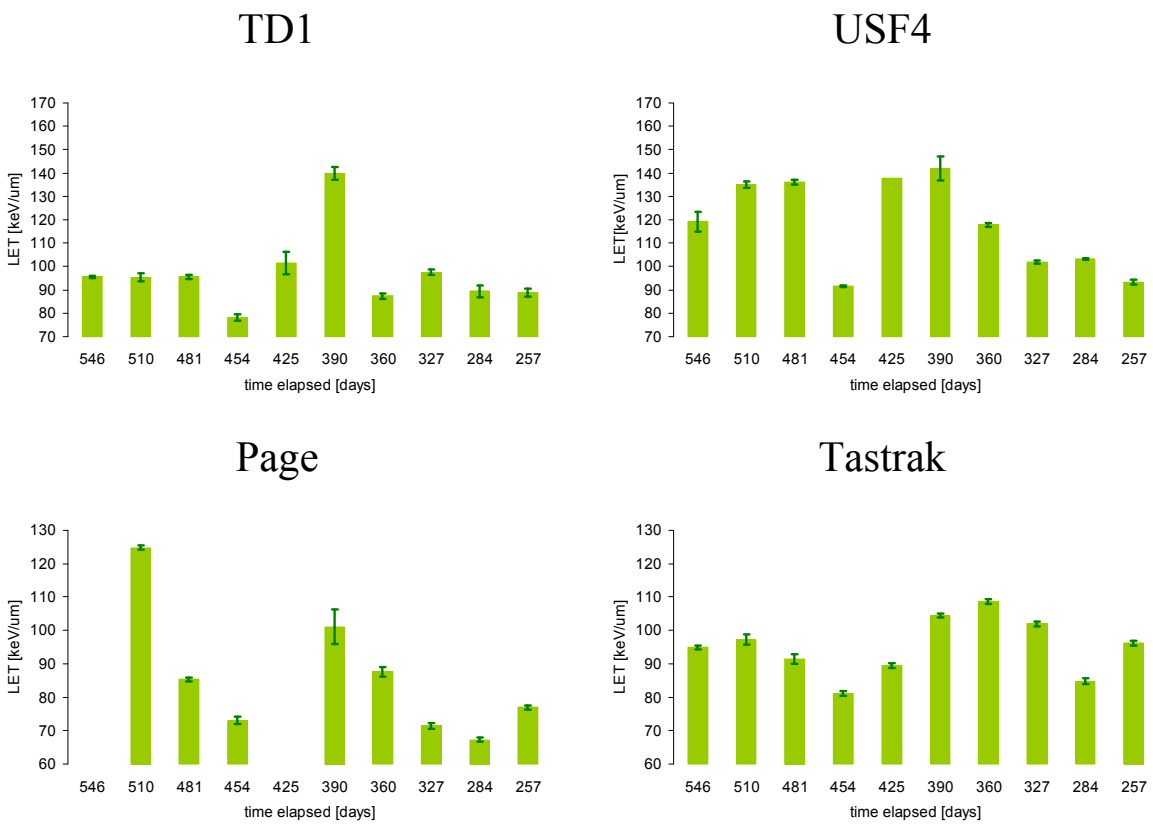

Figure 18 *Linear energy transfer LET calculated for upright alpha particles of ^{252}Cf spontaneous fission after elapsed time ranging from 257 to 546 days*

Further, a room temperature was regularly measured in the frame of another experiment. Detectors had been placed in the room from July 2008 to November 2009, the corresponding temperature history is figured on 19. The maxima recorded by PADC materials can be connected to this history.

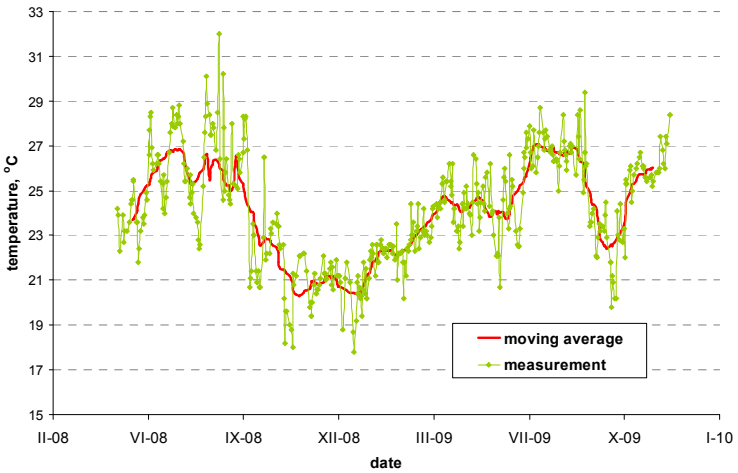

Figure 19 *Temperature history recorded in the room, where detectors were placed from July 2008 to November 2009*

One possible way to assess materials from the point of environmental stability is the extent of possible changing LET during time. Following Table 4 includes such ranges for our materials. Three more sensitive materials obviously undergo more dramatic material changes manifesting as LET variations within 50 keV.μm^{-1} approximately. Tastrak, material with higher detection threshold, does not change during the time as much. Apparently, we need more tests focused on the environmental changes, but for our next long-term experiments it would be probably useful to apply a material with higher detection threshold together with a sensitive material and their results compare together.

Table 4 *Linear energy transfer mean value and individual ranges for upright alpha particles estimated for elapsed time from 267 to 546 days, all values are expressed in keV.μm^{-1}*

	mean value			ranging from	to	width of LET range
TD1	96.90	±	21.47	78.19	139.95	61.76
USF4	117.76	±	35.89	91.48	136.11	44.63
Page	85.95	±	27.52	67.31	124.77	57.46
Tastrak	95.03	±	26.38	81.07	108.67	27.60

During long-term experiments as e.g. monitoring in space there is never available the knowledge about exact time of individual tracks creation; thus we know just a range of elapsed time, but not the ratio of ageing and fading time. Recently, a method of fading correction was developed by (Zhou et al., 2009). The method is based on internal LET calibration to 137 keV.μm^{-1} iron peak, which results in formula correcting etch ratio in dependence on time and several other parameters. This method appears as very promising.

2.5 Summary of PADC procedural tests

One of the most obvious detector characteristics is its detection range. PADC as LET spectrometer registers charged particles with linear energy transfer above a detection threshold and bellow a saturation area. This restriction is described in chapter 2.3.3. Under our etching conditions, USF4 has the lowest detection threshold (8 keV.um^{-1}), on the other side Baryotrak can register particle even with LET above 700 keV.um^{-1}.

Further, it is desired to achieve a consistent response with any detector. In our case, the calibration experiments could be used to assess the consistency of response, namely the width of confidence region (Figure 47 in attachment). The better consistency, the narrower confidence region is obtained. From this point of view, USF4 achieved the best results.

The results of chapter 2.3.1, where the environmental changes on PADC were investigated, indicates that more sensitive materials undergo more dramatic changes during time (Table 4). In average, material Page was able to make the best evaluation of registered particles LET. On the other hand, except less sensitive material Tastrak, USF4 is material with the highest stability and the smallest fluctuation of LET.

FT-IR analysis showed similarity of material USF4 with TD1 and material Tastrak with Baryotrak; Page stays behind. Since Baryotrak was not involved to experiment focused on environmental changes, it is opportunity to treat this material similar to Tastrak and expect similar relative stability.

Besides, one should consider additional material characteristics, which are not obvious, but they can be important from a practical point of view. In our case, it is especially a possibility to evaluate etch detectors with both types of analysis systems available in our laboratory. For Lucia system, material should be not coloured, which is the case of TD1 material; for Hsp system material should be thicker, since for 0.5 mm materials we have difficulties to scan their surface.

There are other aspects of choosing appropriate material, as price and availability.

Several available material information and our findings are summarized in following Table 5. It is obvious, that producers have great reasons against supplying any details about exact composition, or production conditions, therefore the table could not be completed.

Table 5 *Characteristics of different PADC materials*

material	thickness (mm)	plasticizer	antioxidant	LET detection threshold ($keV.um^{-1}$)	LET saturation ($keV.um^{-1}$)
Page	0.5	?	no	10	440
Tastrak	0.5	yes	no	20	450
USF4	0.6	?	yes	8	460
TD1	0.8	yes	yes	9	340
Baryotrak	0.9	no	no	30	>700

3. APPLICATIONS

This thesis introduces the results of track etch detectors applied as linear energy transfer spectrometers in several applications, where various dosimetric characteristics were estimated.

The first application was a study of fields of heavy ions. Light ions have been recently used in cancer therapy. Soon after the expansion of heavy ion radiation therapy, a possible risk of secondary cancers and other non-malign complications have been recognized (Matsufuji et al., 2003; Schardt et al., 2007). These complications occur due to nuclear reaction and fragmentation of primary particles, at which a plenty of various secondary particles can be produced. The knowledge of primary beam modification after the passing through the matter is crucial for understanding of radiation biological effect.

There are several possibilities how to study the beam quality (Endo et al., 2007); one of them is the description with spectra of linear energy transfer, or with depth-dose distribution.

It was already proved, that TED are effective instruments in description of therapeutic ion beam (Kohno et al., 2005, Brabcová et al., 2010). TED are able to register primary particles (with LET over the detection thresholds), as well as secondary particles created in a TED material itself or in surroundings. TED are one of few instruments available for high LET component studies. For several heavy ion beams, we studied depth-dose distribution, spectra of linear energy transfer and contribution of fragments. The results were compared to literature.

Secondly, TED were exposed to neutron beams with various energies and their response was examined. TED are commonly used in personal neutron dosimetry, but they are usually not applied as LET spectrometers. Results were compared to literature, or reference values.

The experiments utilized the same five PADC materials, which were investigated in the previous procedural analyses. Thus, further inspection of the material detection abilities could follow and some useful combination was searched.

Finally, some results obtained onboard spacecraft are introduced. In a spacecraft dosimetry TED advantage especially because of their spatial modesty and power independence. Since the radiation field is also composing of heavy ions, as well as neutrons we can apply our experiences from the previous analysis and experiments. The recommended PADC combination was applied and the results were compared to literature.

3.1 Hadron therapy

Despite its signification, hadron therapy includes techniques of oncological radiation therapy, which uses protons, light ions, and neutrons respectively (Braccini, 2007). Unique advantages of hadron therapy have been known since 1946, when Robert Wilson published the first promising conclusion about heavy ion treatment. It took many years of negotiation and technical obstructions to realize this great idea. Nowadays, hadron therapy is applied to patients in thirty world's medical centers – for example HIMAC (Japan), GSI (Germany), Loma Linda University Medical Center (USA) and others (for actual overall survey please see on web site of PTCOG: Particle Therapy Co-Operative Group, http://ptcog.web.psi.ch). In some special tumor cases hadron therapy turned out as peerless technique.

The main concern of radiotherapy is searching the greatest biological effect of applied dose together with maximum precision. Let me compare convenient therapeutic techniques, such as X rays, gamma, or electron applications with beams of protons, neutrons, so called hadrons, or heavy ions. There are two main indicators for therapeutic effects: relative biological effectiveness (RBE) and oxygen enhancement ratio (OER). RBE is defined as the ratio of reference radiation dose and dose delivered by radiation under the study, where both produce the same biological effect; reference radiation is usually gamma rays of ^{60}Co. The greater the RBE, the better is the destroying effect on cancer tumour. OER, on the other side, is required to be as low as possible; its value represents sensitivity of hypoxic cancer cells to radiation. It is defined as ratio of doses in tissue without and with oxygen, where, again, they produce the same biological effect. Figure 20 (left) suggests that heavy ions have benefits in both RBE and OER. Beside that, there is a question of radiation stress of health tissue surrounding tumour target. Comparing depth dose distribution on Figure 20 (right), we can clearly observe the disadvantages of great doses in front of target volume in case of X and gamma rays, as well as neutron beam. Doses are exponentially reduced passing through the body; distribution of sufficient dose to the tumour volume is necessarily accompanied with great unwanted exposition of health tissue. Very modern technique of Intensity Modulated Radio-Therapy (IMRT) targets a tumour from several different directions to distribute undesirable dose in larger volume of health issue, but it is affected anyway. In contrast, proton and ion beams can be targeted directly to tumour volume and thus almost spare surrounding issues (Kraft, 2007; Amaldi and Kraft, 2005).

Existence of secondary cancers risk has been known and discussed for convenient therapeutic techniques for long time. Soon, there was also recognized a risk of fast neutron

therapy considering its poor dose depth distribution and consequently high stress of healthy tissues. In case of hadron therapy, any attention had not been paid to potential risk until recently. In few last years, several studies have occurred in the fields of secondary neutrons and nuclear fragments, which can change the radiation characteristic of used beams and perhaps can increase secondary cancer risk. Their presence has to be taken into consideration (Chaudhri, 2007; Schardt et al., 2007). It was proved, that a contribution of fragments with the dangerous biological impacts increases with increasing proton number of primary ion. Hence, radiotherapy prefers light ions, especially carbon (Matsufuji et al., 2003).

Radiation characteristics of heavy ions are often described with depth in tissue-dose distribution, so-called Bragg's curve (note the Figure 20). The most of the dose is delivered close to the particle end; it leads to sharp peak on the curve, which can be target to a tumor. To fit exactly a tumor shape, maximal delivered dose area of clinic beam is usually spread out in a broad area. It can be achieved in a number of ways (Babkin et al., 2010); in case of HIMAC it is a passive shaping with so called ridge filters (Kanai et al., 1999; Inaniwa et al., 2005). However, the beam spreading increases delivered dose in the plateau (Jayaraman and Lanzl, 2004). Generally, part of absorbed dose before (plateau) and all absorbed dose behind (tail) the Bragg's maximum is due to fragmentation and will be discussed further.

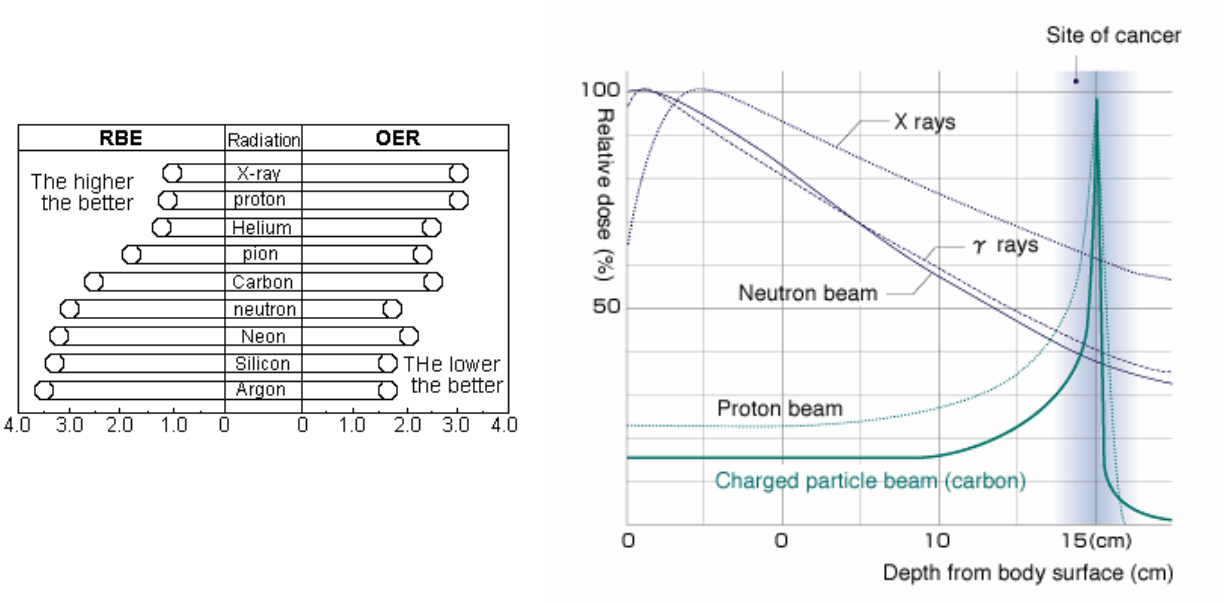

Figure 20 *Radiation characteristics of several therapeutic beams (www.nirs.go.jp) - relative biological effectiveness (RBE) and oxygen enhancement ratio (OER) (both on the left), and depth-dose distribution (right)*

3.2 Experiments in heavy ion beams

Our department started collaboration with the Japanese National Institute of Radiological Sciences during 2007. Since that there have been performed many experiments trying to assist in characterization of radiation situation in ion beams similar to those used for patient's exposition in HIMAC facility (Kanai et al., 1999). The experiments were performed in the frame of ICCHIBAN project (Yasuda et al., 2006a) and approved HIMAC proposals for beam time. In following chapter I present a compilation of all relevant results and discussion of possibilities of track etched detectors in this scope.

Various types of passive and active detectors were employed in our measurements. Beside track etch detectors, passive detectors included two types of thermoluminescent detectors ($CaSO_4$:Dy and Al_2O_3:C). As the active detector there was employed Liulin, the spectrometer of energy deposition in silicon, and Hawk, tissue-equivalent proportional counter. This work is focused on the TED results only; results of the other employed detectors and comparison with TED results are available in (Brabcová et al., 2010; Jadrníčková et al., 2010a; Spurný et al., 2010; Ploc et al., 2010; Spurný et al., 2009).

Arrangement of experiments was following: five various PADC materials employed as the TED were put in holders, which were specially designed for this occasion (see Figure 21). One quarter of inner space was reserved for thermoluminescent detectors, in remaining positions TED were placed in several layers.

Figure 21 *Special holders designed for experiments*

Holders were upright exposed in a beam of several ions; they were carbon ions with primary energy 290 MeV/u, neon ions with 400 MeV/u and helium ions with 150 MeV/u. For every ion type, sets of holders were exposed behind increasing thickness of binary filters to simulate individual increasing depths in tissue. Binary filters are plates of PMMA (polymethyl methacrylate), which is considered having similar characteristics to water regarding nuclear interactions. As the tissues are composed mainly from water, it can be also consider having similar characteristics to tissue target. The thickness of PMMA is usually expressed as water-equivalent thickness in mm (Matsufuji et al., 2003).

Some of the ion beams had two possible configurations; it was either mono energetic (MONO), or spread-out-Bragg-peak (SOBP).

The detailed exposition conditions are included in Table 6 - the thickness of binary filters and nominal fluencies.

All PADC were treated under our usual conditions and evaluated with a one of the two evaluation systems available in our department; it was described in chapter 2.

Table 6 *Exposition conditions in HIMAC BIO. Desired fluencies Φ for corresponding thickness of binary filters (B.F.) for MONO or SOBP setup of three ions*

C 290 MeV/u				Ne 400 MeV/u				He 150 MeV/u	
MONO		SOBP		MONO		SOBP		MONO	
B.F. mm	**Φ** cm^{-2}	B.F. mm	**Φ** cm^{-2}	B.F. mm	**Φ** cm^{-2}	B.F. mm	**Φ** cm^{-2}	B.F. mm	**Φ** cm^{-2}
0.00	10^5	0	97500	0.00	$5*10^4$	0	21450	0	$5*10^6$
30.05	10^5	48.13	97500	1.14	$5*10^4$	30.05	22100	57.87	$4.96*10^6$
63.26	10^5	71.36	97500	20.78	$5*10^4$	59.64	22100	88.91	$5*10^6$
95.03	10^5	85.83	97500	59.64	$5*10^4$	84.15	21450	127.68	$4.93*10^6$
104.93	10^5	86.97	97500	69.59	$5*10^4$	113.65	22100	135.2	10^5
117.24	10^5	117.24	97500	89.42	$5*10^4$	140.85	21450	143.16	10^5
129.81	10^5	136.34	97500	109.69	$5*10^4$	143.16	22100	145.61	10^5
138.02	10^5	146.78	97500	120.18	$5*10^4$	143.84	22100	146.78	10^5
142.53	10^5	147.92	97500	128.31	$5*10^4$	145.61	22100	147.92	10^5
144.47	10^5	152.46	97500	132.75	$5*10^4$	154.91	22100		
146.15	10^5			136.88	$2*10^4$				
147.29	10^5			141.39	$2*10^4$				
147.92	$2*10^4$			142.53	$2*10^4$				
149.01	$2*10^4$			143.84	10^4				
149.64	$2*10^4$			144.47	10^4				
150.15	$2*10^4$			144.98	10^4				
150.78	10^5			145.61	$2*10^4$				
151.32	10^5			147.29	$2*10^4$				
154.91	10^5								

3.2.1 Spectra of linear energy transfer

There is a possibility to classify particles according to their linear energy transfer, since the LET is related to biological impacts. As mentioned previously, track etched detectors are ranked among LET spectrometers, thus they can provide us information with distribution of particles along LET range.

Spectra of linear energy transfer were created as a distribution of particles within LET intervals related to length of the interval. Following examples were obtained by measurement with material Page in MONO (Figure 22a) and SOBP configuration (Figure 22b) of carbon beam; similar spectra can be also calculated for the other inspected ions. The figures illustrate increasing average LET of particles in main peak behind increasing thickness of select binary filters, as well as spreading peaks due to scattering of beam. It means, the beam acquires

completely different biological effects in dependence on material thickness. It is also obvious that a number of particles in main peak decrease due to fragmentation processes, while a number of secondary particles increase.

In spectra, one can see somewhat increasing response in the area of the lowest LET, which is related to a dust.

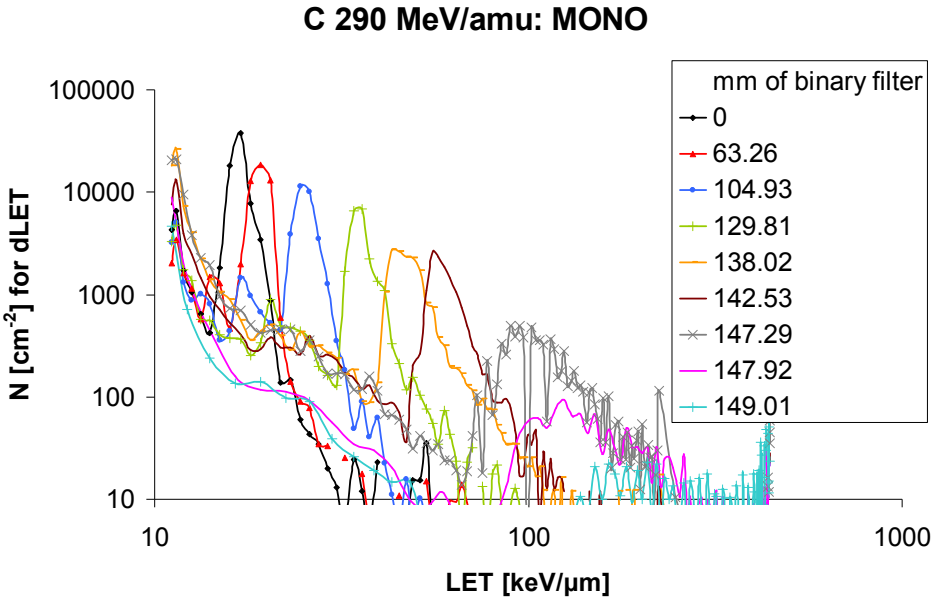

a)

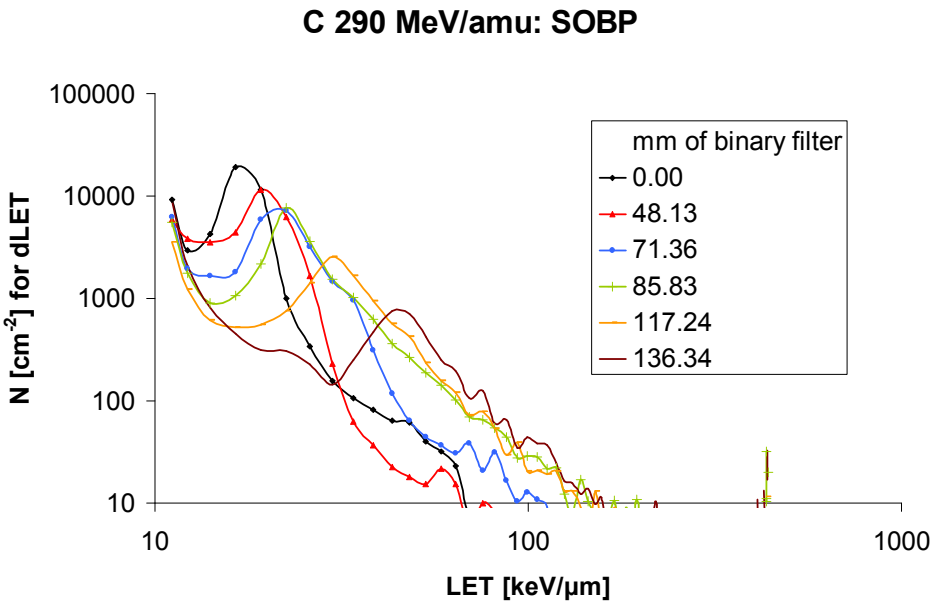

b)

Figure 22 *Spectra of linear energy transfer behind increasing thickness of selected binary filters in MONO (a) and SOBP (b) carbon beam measured with Page detector; a number of particles within a LET interval was normalized for length of the LET interval*

As it was expected, SOBP spectra have different profiles compared to the same beam of MONO configuration; example for 290 MeV/u carbon beam is on Figure 23. Primary particles of MONO setup have restricted uniform energy, whereas SOBP beam includes primary particles with energy within certain interval. SOBP average LET is the same or higher than for the corresponding MONO configuration, which is in agreement with literature (Courdi et al., 1994).

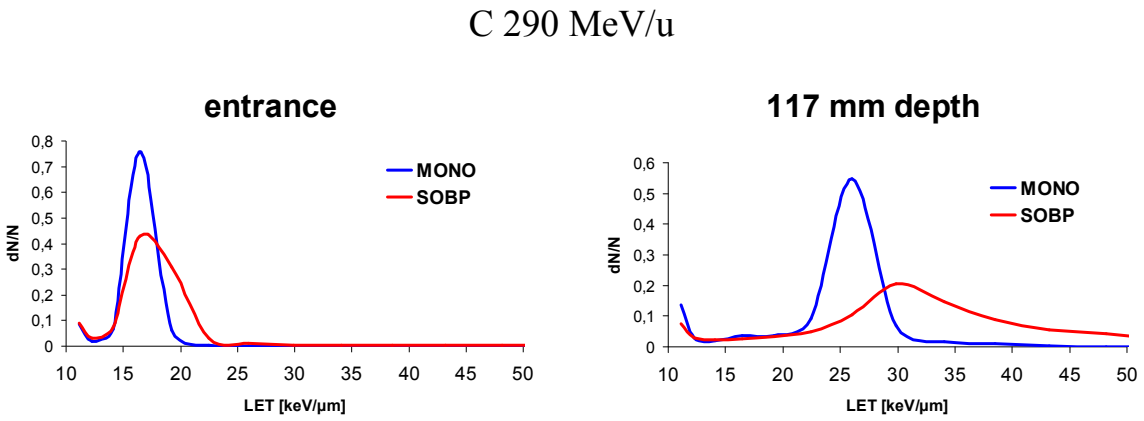

Figure 23 *Comparison of LET spectra for MONO and SOBP setup of irradiation with 290 MeV/u carbon beams in the entrance and behind 177 mm PMMA filter; recorded with material Page*

As was mentioned, all five tested PADC were applied in these experiments, thus it was an opportunity to inspect possible differences among them. Spectra of linear energy transfer for several selected binary filters were compared for irradiation with carbon in both setups on Figure 25. Similar spectra comparisons for neon and helium beam follow on Figure 26 and 27.

Since the materials were arranged in several layers, there are obvious spectra shifts with depth according to individual position in holders. For plateau area of small binary filter thickness, there are no other differences in detection, except the detection range. Materials Baryotrak and Tastrak with approximately 20 and 30 keV.µm^{-1} detection thresholds did not record particles bellow these points, thus in case of carbon SOBP and helium configuration they did not record almost anything and were not included.

On the other hand, these materials can be utilized for study of high LET particles. If we are inspected very high LET secondary particles, it is sometimes difficult to distinguish them in a background of low LET primary particles. An example of the effect is on Figure 24, where is a comparison of detector surfaces after helium beam irradiation for two PADC

materials. Since the fluency of primary particles was high, there would not be possible to study high LET components on material with low detection threshold.

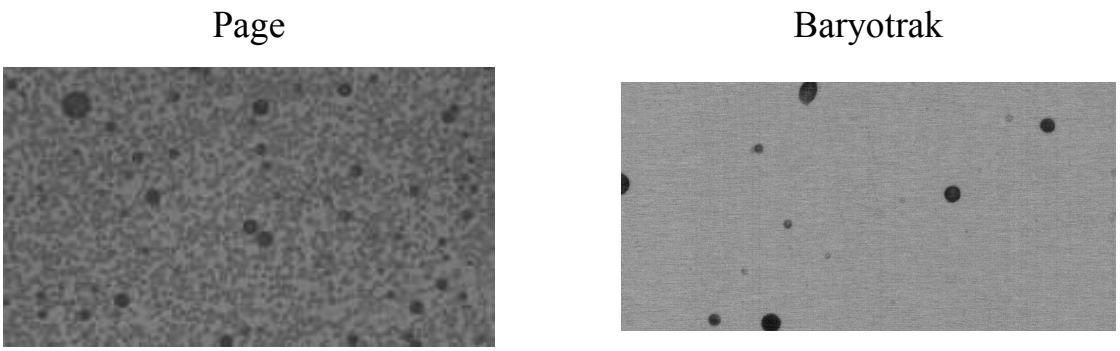

Figure 24 *Etch detector surfaces of Page (detection threshold ~ 10 keV.μm^{-1}) and Baryotrak (detection threshold ~ 30 keV.μm^{-1}) after irradiation to helium beam with energy 150 MeV/u behind binary filter of 127.68 mm. Page registered low LET primary particles, Baryotrak registered only higher LET secondaries.*

Further spectral differences can be observed for irradiations in area close to the Bragg's maximum. In this area, primary particles are at the end of their path and lot of secondary particles are created. Spectra recorded by individual materials are quit different; one can see considerable variations in LET of detected particles (note the differences of spectra for Ne beam behind 69 mm and thicker binary filters on Figure 26a). This effect originates from a failure of the relation (7), which is not valid anymore and neither etch rate, nor LET can be assess. Consequently the detectors did not work as LET spectrometers properly. Why it is so, it is described for example in (Pálfalvi, 2009, Nikezic and Yu, 2003). Calculation of track parameters given by (7) is restricted to tracks, for which etching does not reach their end point. It means the tracks keep conical shape. After the etching passes the end of particle path, track becomes spherical and (7) cannot be considered as valid. These tracks are called over-etched. There are two basic approaches how to deal with this problem. Together with some others, we consider these tracks as the normal ones, since we are usually not able to distinguish them anyhow. This leads to overestimation of V as well as LET and dose consequently. The second possible approach is focused on recognizing and excluding of such tracks, which, on the contrary, leads to underestimation of dose. It is possible to avoid over etching with using of short and long etch times combination, after which the tracks are analyzed with atomic force microscope, this technique is described in (Yasuda et al., 2006b). Such a technique is unfortunately not available in our department. However, one should keep this restriction in mind and consider any data from this point of view.

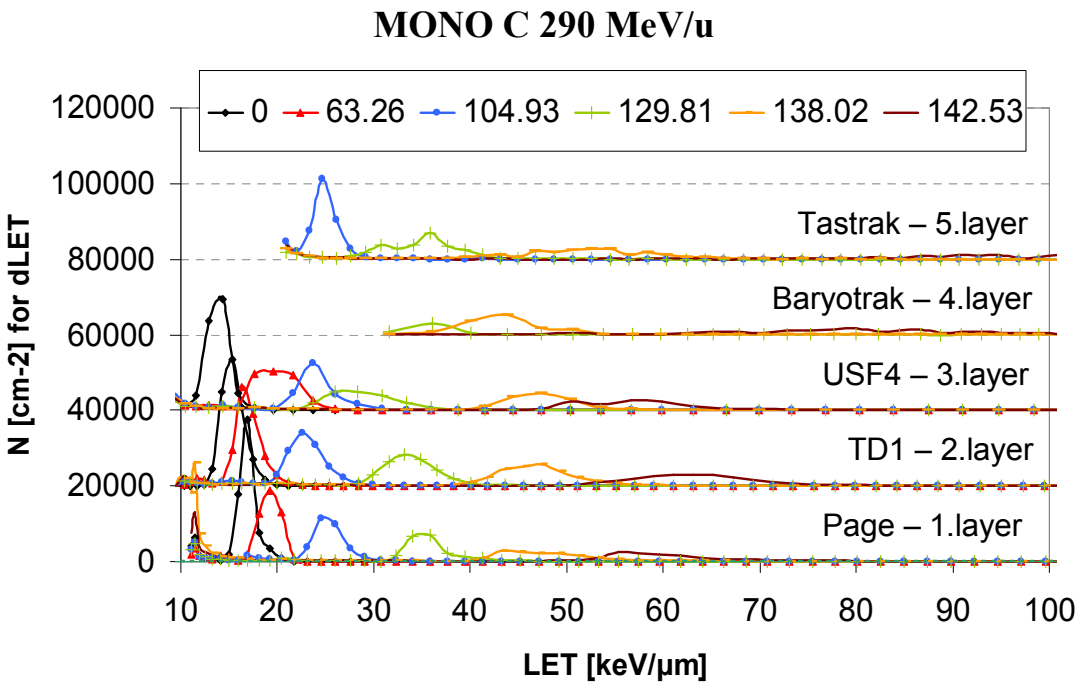

a)

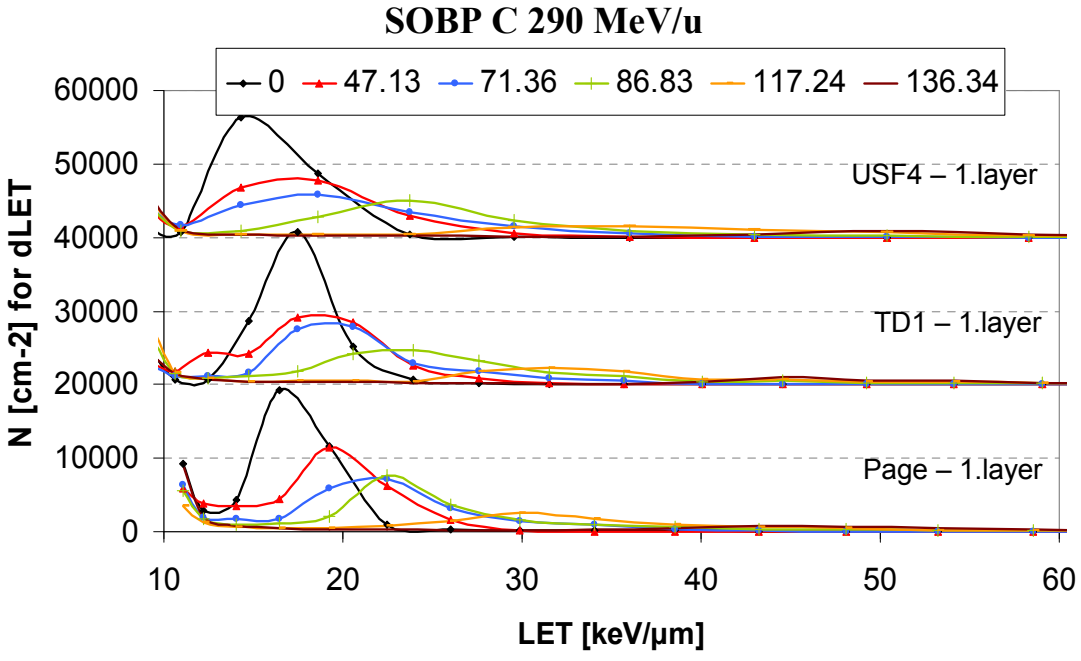

b)

Figure 25 *LET spectra for several different thickness of binary filter (expressed in water-equivalent mm) for MONO (a) and SOBP (b) carbon beam measured with different PADC; a number of particles per area were corrected for the width of corresponding LET interval. For better lucidity, the absolute values are incremented by k*20000, where k is 0 for Page, 1 for TD1, and 2 for USF4, 3 for Baryotrak, and 4 for Tastrak (Baryotrak and Tastrak are not included for SOBP configuration regarding to their high detection threshold).*

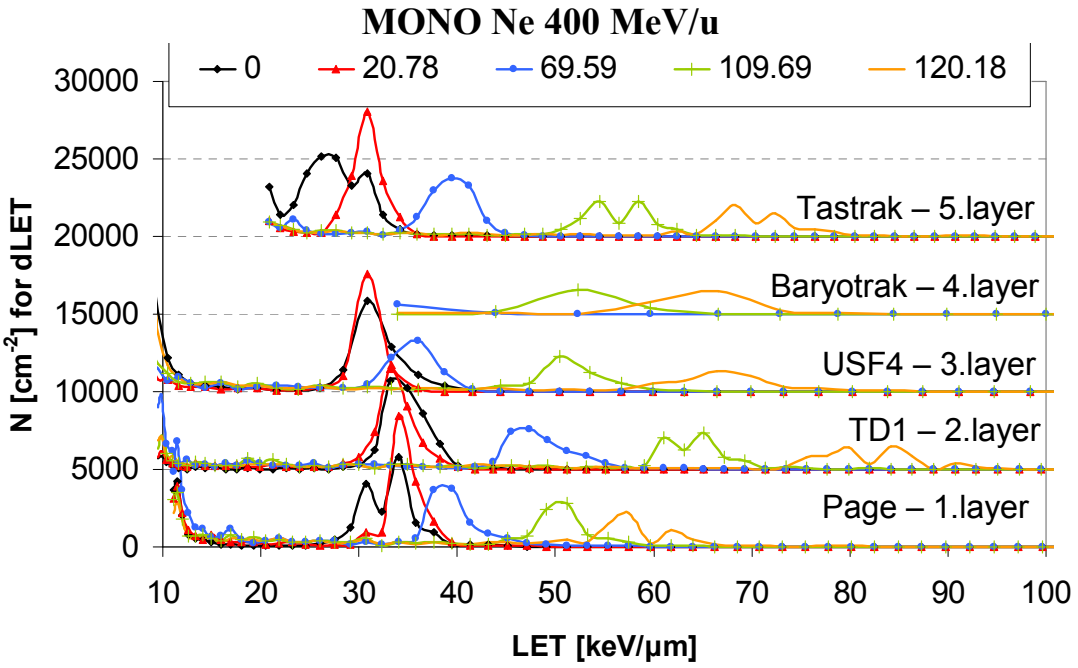

a)

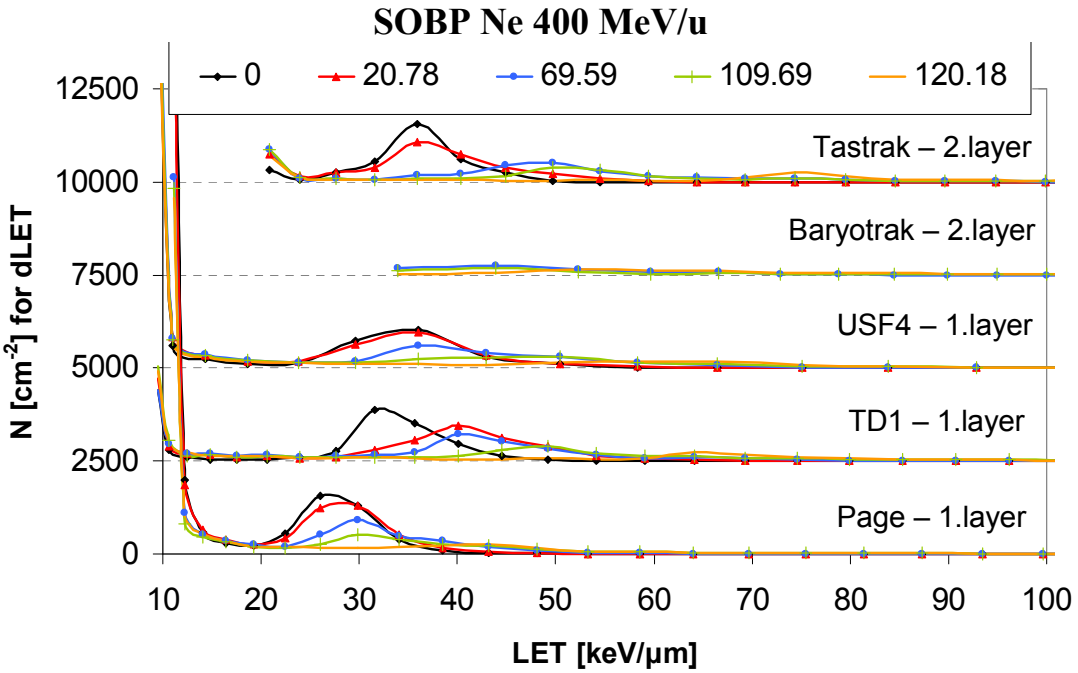

b)

Figure 26 *LET spectra for several different thickness of binary filter (expressed in water-equivalent mm) for MONO (a) and SOBP (b) neon beam measured with five PADC; a number of particles per area were corrected for a width of corresponding LET interval. For better lucidity, the absolute values are incremented by factor k*5000 (a), or k*2500 (b), where k is 0 for Page, 1 for TD1, 2 for USF4, 3 for Baryotrak, and 4 for Tastrak.*

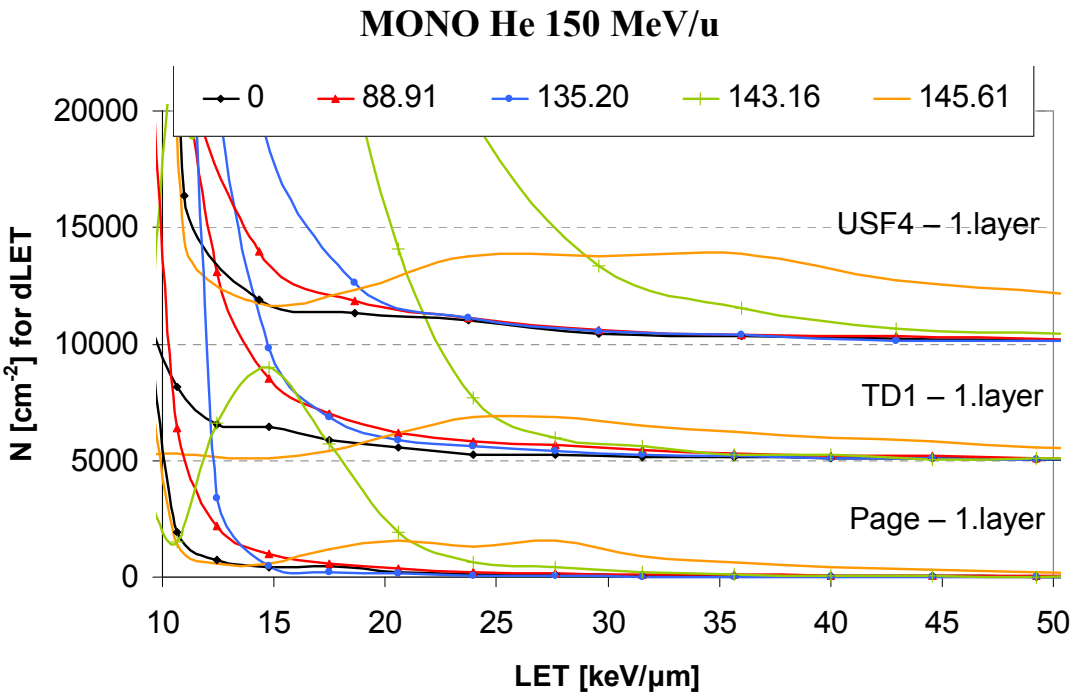

Figure 27 *LET spectra for several different thickness of binary filter (expressed in water-equivalent mm) for MONO helium beam measured with three PADC; a number of particles per area were corrected for a width of corresponding LET interval. For better lucidity, the absolute values are incremented by factor k*5000, where k is 0 for Page, 1 for TD1, and 2 for USF4.*

3.2.2 Depth-dose distribution

From a LET value in keV.um^{-1}, an absorbed dose in mGy can be obtained according to (8), thus we can construct absorbed dose response in dependence on depth in binary filter. HIMAC operating staff supplied us with reference curves of dose dependence on depth, which were estimated with ionization chamber.

If we want to compare our results with the reference values, it is necessary to normalize the relative reference values to fluencies applied in our experiments. Therefore, we calculated absorbed doses for irradiation without any shielding and normalized the reference curves for this entrance values.

The absorbed doses were obtained using measured "real" fluency for individual case and corresponding LET value. Linear energy transfer was calculated with calculation code SRIM (Ziegler et al., 2008) from known beam nominal energies for MONO setups. For SOBP setup, it is more complicated to obtain energies for LET calculation, since the beam is coming through a ridge filter. Hence, the LET values were derived from measured LET spectrum for SOBP setup as an average LET measured with materials from the most upper layer.

The number of primary particles per area, particle fluency, is estimated as an average of several measurements with scintillator before experiment, but it is not guaranteed it is constant during the whole time of irradiations. Thus, the real fluency may vary from the demanded one. The possible beam changes were partially corrected with estimation of "real" fluency as the number of primary particles recorded with upper material (or an average in case of several materials in upper layer) for irradiation without any binary filter. Unfortunately, this correction cannot be done separately for all positions in depth, since the primary particles for deeper positions could not be recognized anymore. Furthermore, this recognition was also impossible for He beam, where primary particles for unshielded irradiation had linear energy transfer 2.23 keV.μm^{-1}, which is bellow detection threshold of all tested materials. Beside, since the fluencies within a one beam were different for different thickness of a binary filter (as it is noted in Table 6), the doses in depth were normalized for a uniform fluency.

Further, it should be noticed that materials were arranged in several layers inside of holders. Thus, the exact depth for individual material had to be corrected for thickness of materials in previous layers according to dimensions tabulated in 5.

The comparison of planned and measured fluencies together with LET estimation is summarized in Table 7.

Table 7 *Parameters used for absorbed dose calculation (measured fluency and LET); comparison of measured and demanded fluencies for irradiations without shielding*

MeV/u	setup	fluency [cm^{-2}]		LET [keV.μm^{-1}]
		demanded	measured	
C 290	MONO	100000	96457*	13.06***
	SOBP	97500	95400 ± 1331**	17.05 ± 0.58**
Ne 400	MONO	50000	36630*	31.30***
	SOBP	21450	14358 ± 609**	32.75 ± 3.16**
He 150	MONO	500 000	undetectable	2.33***

** value for single upper material (Page)*
*** average for three upper materials (Page, USF4, TD1) with statistic uncertainty only*
**** calculated with SRIM*

Results are compiled on Figures 28 for helium and 29 and 30 for carbon and neon of both setups. Figures illustrate well known and described rapid increase of dose close to the end of particle path, which is called Bragg's maximum; its extent is in order of mm for

MONO setup and in order of tens of cm for SOBP. Uncertainties were not included for better readability, but they are about 20 %.

For all three investigated beams of both setups, the dose situation is quit well described with track etched detectors, except the materials with the higher detection thresholds - Tastrak and Baryotrak, which stay completely or partially blind in the area of low LET. Also, note the blindness of all materials for plateau area in case of He, where LET of particles is out of the detection range for all of them.

Anyway, one can see few surprising values, particularly in the area of Bragg's maximum, where higher doses were occasionally recorded. It was recorded with TD1 and USF4 for MONO helium beam (Figure 28), with Page and TD1 for MONO carbon beam, (Figure 29a), and with TD1 and Baryotrak for MONO neon beam (Figure 30a); all these exceptionalities will be discussed in following chapter.

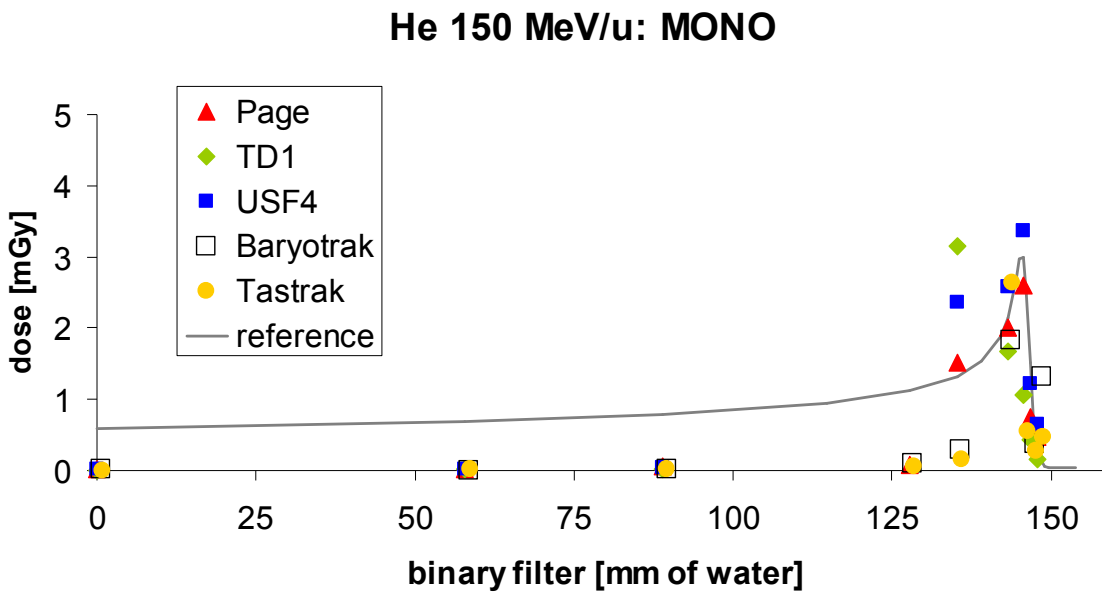

Figure 28 *Depth-dose distribution for MONO setup of He 150 MeV/u; comparison of measurement with different track etch detectors (dots) and reference distribution (line)*

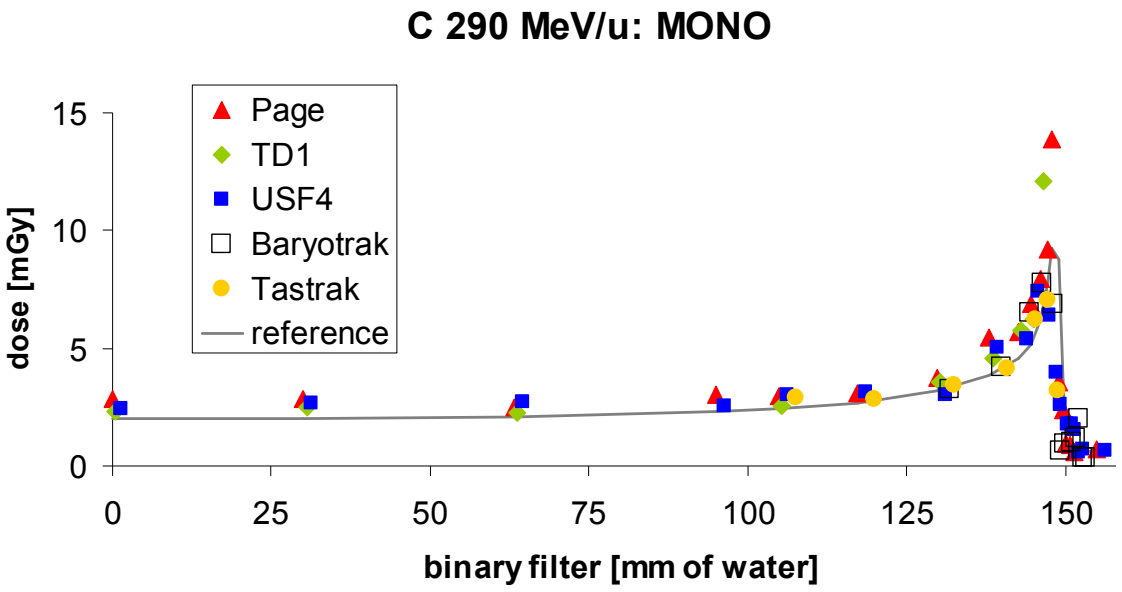

a)

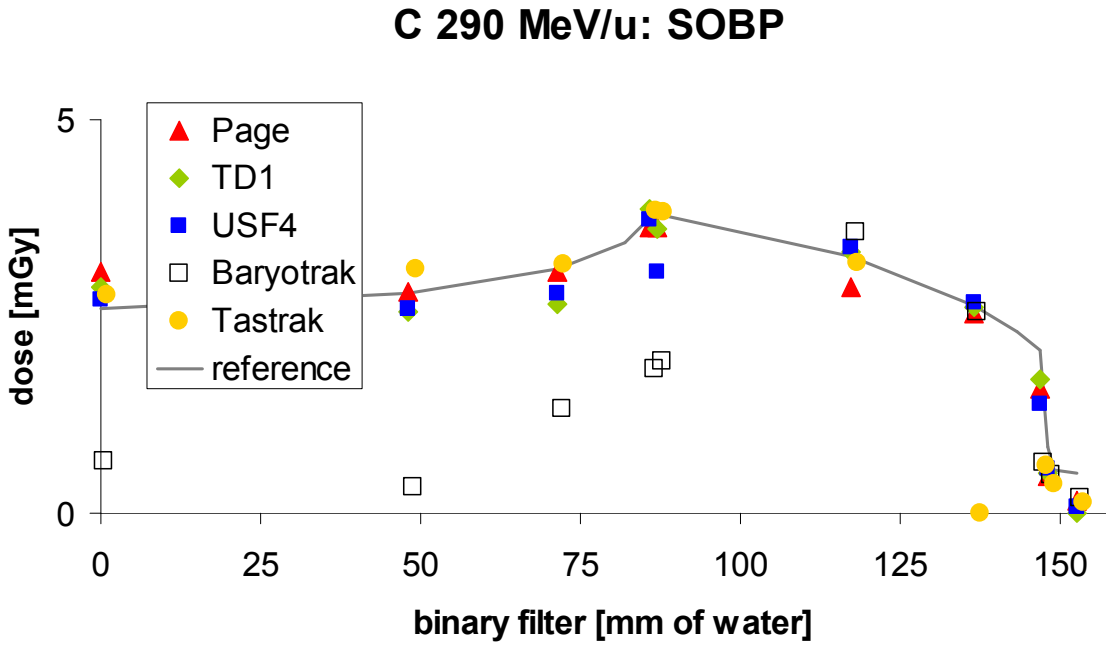

b)

Figure 29 *Depth-dose distribution for MONO (a) and SOBP (b) setup of C 290 MeV/u; comparison of measurement with different track etch detectors (dots) and reference distribution (line)*

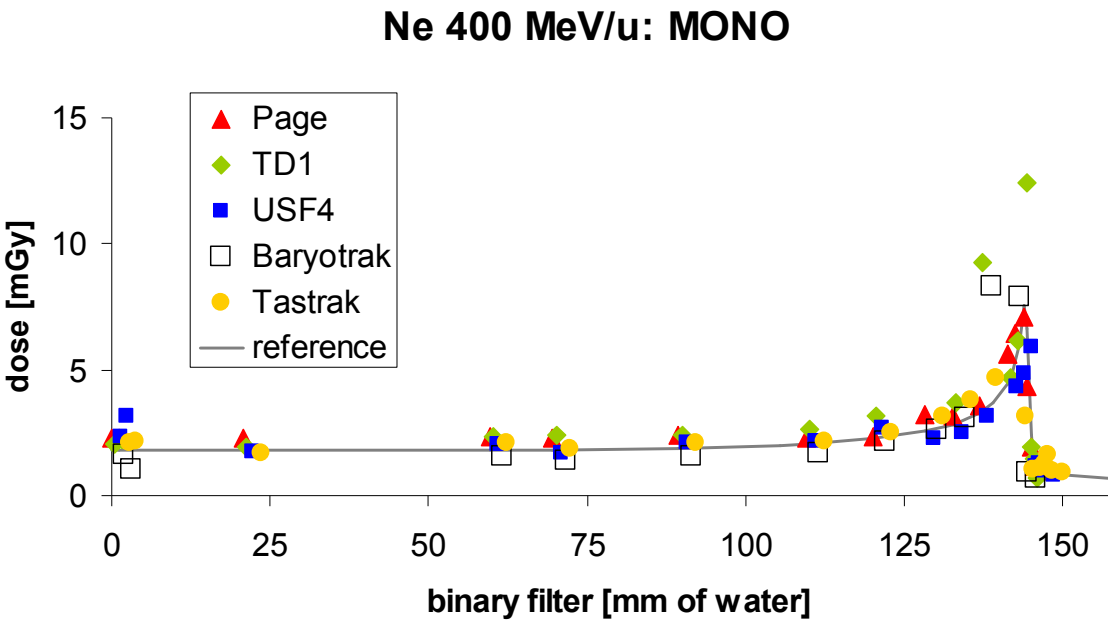

a)

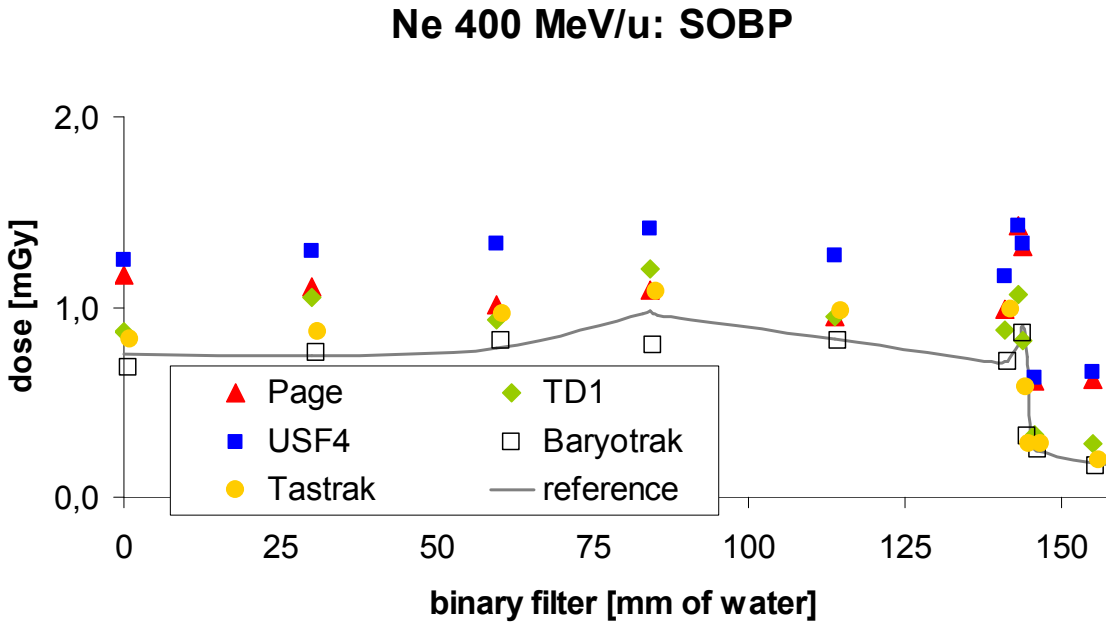

b)

Figure 30 *Depth-dose distribution for MONO (a) and SOBP (b) setup of Ne 400 MeV/u; comparison of measurement with different track etch detectors (dots) and reference distribution (line)*

3.2.3 Spectra of linear energy transfer in Bragg's maximum

Let's get back to higher values of total dose registered right in the area of Bragg's maximum mentioned in previous chapter. First guess of explanation was wrong submission of deleted tracks; part of overlapping tracks had to be erased to achieve readability of image. Their number was recorded and included in calculation of total dose, however it is possible there were not strictly deleted just particles from main peak considering the difficulties to distinguish little variances in their size. Fortunately, TD1 results were measured with HspFit software, where analyzed data are stored and can be reanalyzed. The data were carefully examined without any deleting of any kind of tracks and results remain unchanged. Thus, we focused on corresponding spectra of linear energy transfer and wanted to see, what kind of particles are registered in the Bragg's maximum.

The spectra compiling results for irradiation with carbon beam in Bragg's maximum are figured on 31. The surprisingly high values of total dose were recorded by material TD1 for 146.15 mm and material Page for 147.92 mm; on can see obvious corresponding high number of registered particles in main peak for both cases with linear energy transfer ranging from 100 to 200 keV.μm^{-1}. These particles were not registered, or just partially, with other three materials.

C 290 MeV/u behind binary filters of

146.15 mm **147.92 mm**

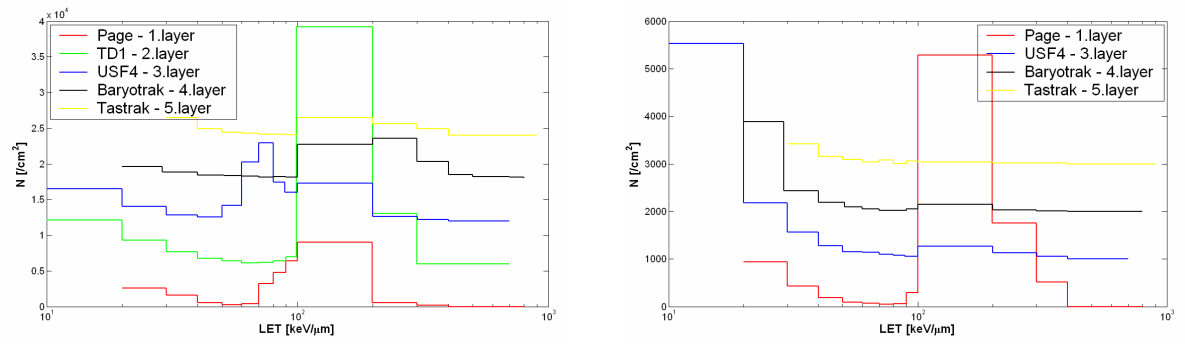

Figure 31 *Detailed examination of spectra in Bragg's maximum of carbon beam behind two thicknesses of binary filters. The spectra are shown with the same LET scale. TD1 results for 147.92 mm are not available.*

Similar Figure 32 was created to describe irradiations with neon beam behind two different thicknesses of binary filter, for which the higher total dose were calculated as well. Materials TD1 and Baryotrak, which recorded high dose behind 136.88 mm of binary filter, have spectra with dominating 100-200 keV.μm^{-1} particles in comparison with other three

materials. The situation is different for spectra recorded behind 143.84 mm. Material TD1 recorded significant group of particles with LET ranging from 300 to 400 keV.μm^{-1}, which leads to increasing of total dose.

Ne 400 MeV/u behind binary filters of

136.88 mm **143.84 mm**

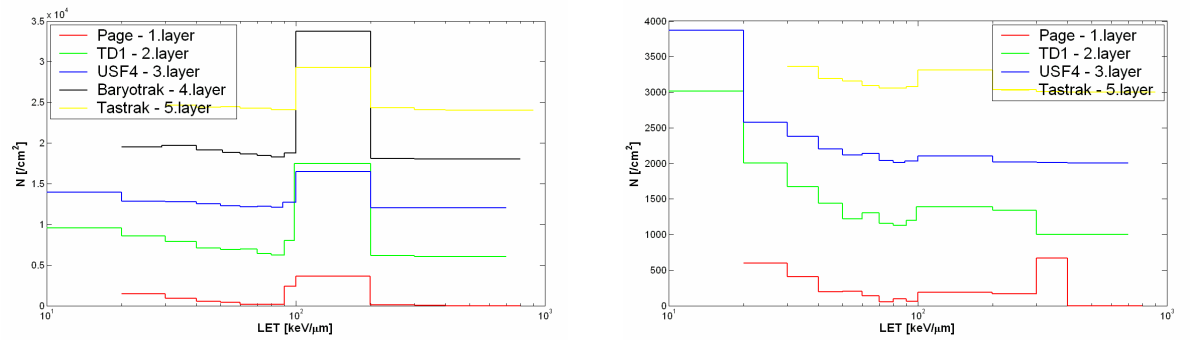

Figure 32 *Detailed examination of spectra in Bragg's maximum of neon beam behind two thicknesses of binary filters. The spectra are shown with the same LET scale. Baryotrak results for 143.84 mm are not available.*

The high doses measured with materials TD1 and USF4 for helium beam behind 135.20 mm are due to high number of low LET particles, which were just partially detected with material Page and entirely passed by other two materials with high detection threshold. Corresponding spectra are figured on 33.

He 150 MeV/u behind binary filter of 135.20 mm

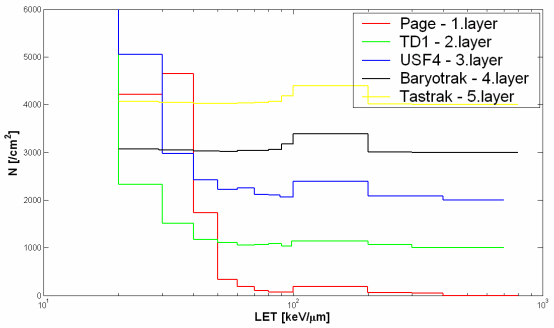

Figure 33 *Detailed examination of spectra in Bragg's maximum of helium beam behind 135.20 mm of binary filters. The spectra are shown with the same LET scale.*

In summary, it is unlikely the differences in registered particles among tested materials are caused by any composition properties. More likely it has connection to unexpected scattering of beam passing through the material layers, as well as mentioned failing of materials as LET spectrometers for particles with short range leading to track over etching.

3.2.4 Fragments contributions to total dose

As was mentioned above, there is a specific interest in the fragmentation processes of primary particles passing through a matter. Created secondary particles can completely change biological effect in therapeutic medicine, when comparing to bare primary particle beam (Golovchenko et al., 1999). Also, since the fragmentations of heavy ions can modify radiation field behind a shielding and heavy ions are component of galactic cosmic ray, also the designers of spacecraft protection shielding have to cover this field (Miller, 2001). From these reasons, the fragmentations have been studied theoretically and experimentally for many years.

In, general, there can be distinguished two kinds of fragmentation: projectile and target. The projectile fragments are characterized by low LET and long particle range, whereas the target fragments are usually notable for high LET and short particle range. The elongation or contraction of particle range results from different fragment proton number, while its velocity is considered to be constant (Zhao et al., 2009). The short particle range is reason why it is not easy to measure this kind of fragments (Miller, 2001). The track etch detectors are one of the few instruments available for fragmentation studies.

In our case, each linear energy spectrum recorded with material Page (placed on the top of materials) was carefully analysed and the peak of primary particles was identified. For the area of plateau, it was possible to distinguish some of the lower-Z fragments (Figure 34). Except the cluster of carbon as the primary ion, there can be observed clusters of boron (B), beryllium (Be), lithium (Li), helium (He) and proton (H). In case of neon, there can be identified additional clusters of carbon (C), nitrogen (N), oxygen (O) and fluorine (F) (Endo et al., 2010; Mrázová et al., 2010). We identified only a part of lower-Z fragments, as it is obvious on Figure 34. The resolution of fragments is not possible for thick binary filters. The fragment energy loss is more spread due to any possible place of their origin in shielding (Golovchenko et al., 1999) and therefore the spectra are overlapped.

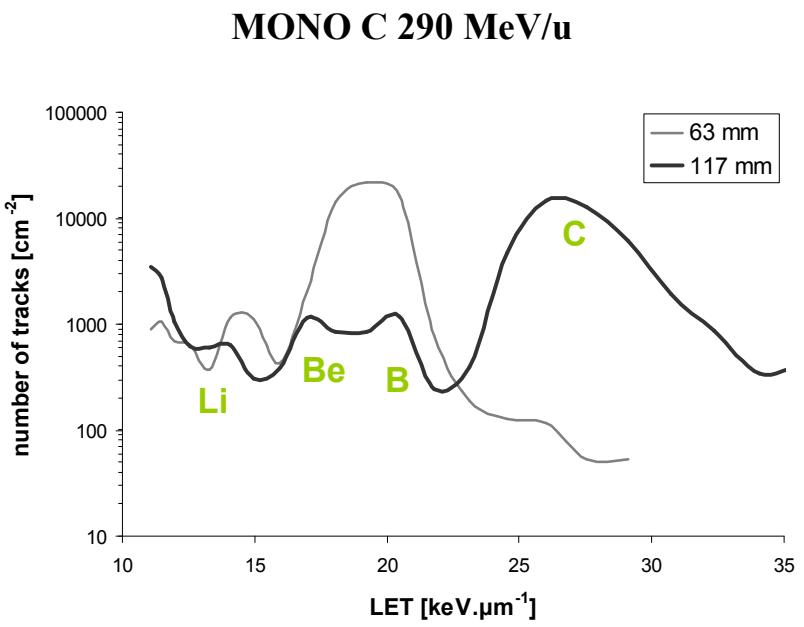

a)

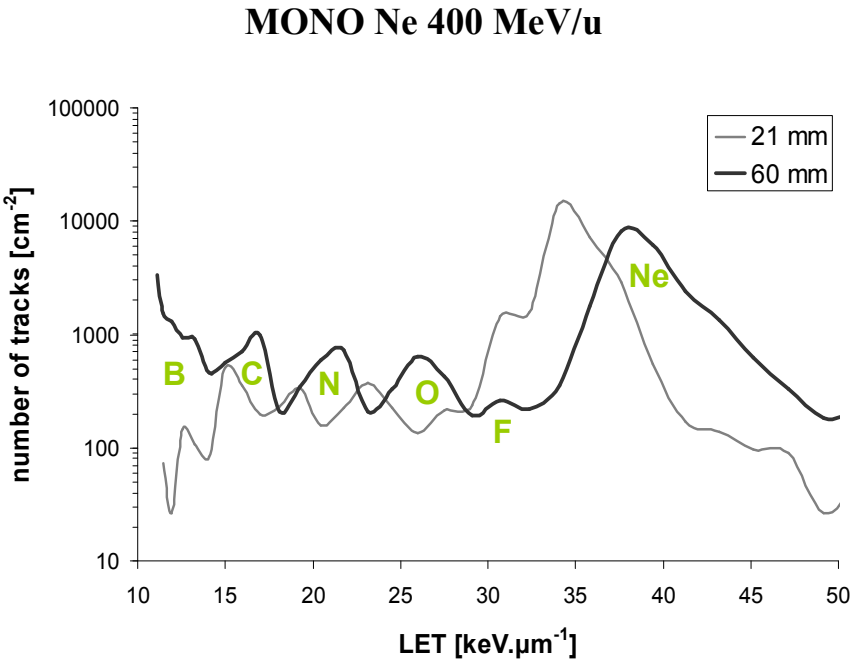

b)

Figure 34 *Fragments identified in LET spectra behind various thicknesses of binary filters for carbon (a) and neon (b) as the primary ion. Note the logarithmic scale on dependent axis.*

Further, it was possible to inspect a contribution of primary and secondary particles to the total incident number. Secondary particles include low LET particles coming from projectile fragmentations, as well as high LET particles coming from target fragmentations. The results for MONO configuration of carbon and neon beam are included on Figure 35. One can see a diminishing of primary particle number together with increase of recorded secondary particles; these trends are more manifest for neon irradiations. The results are consistent with literature, where fragmentation importance was described to be increase with proton number (Matsufuji et al., 2003), depth (Golovchenko et al., 1999), as well as with primary ion energy (Endo et al., 2007), or decrease of proton number of shielding material (Mrázová et al., 2010).

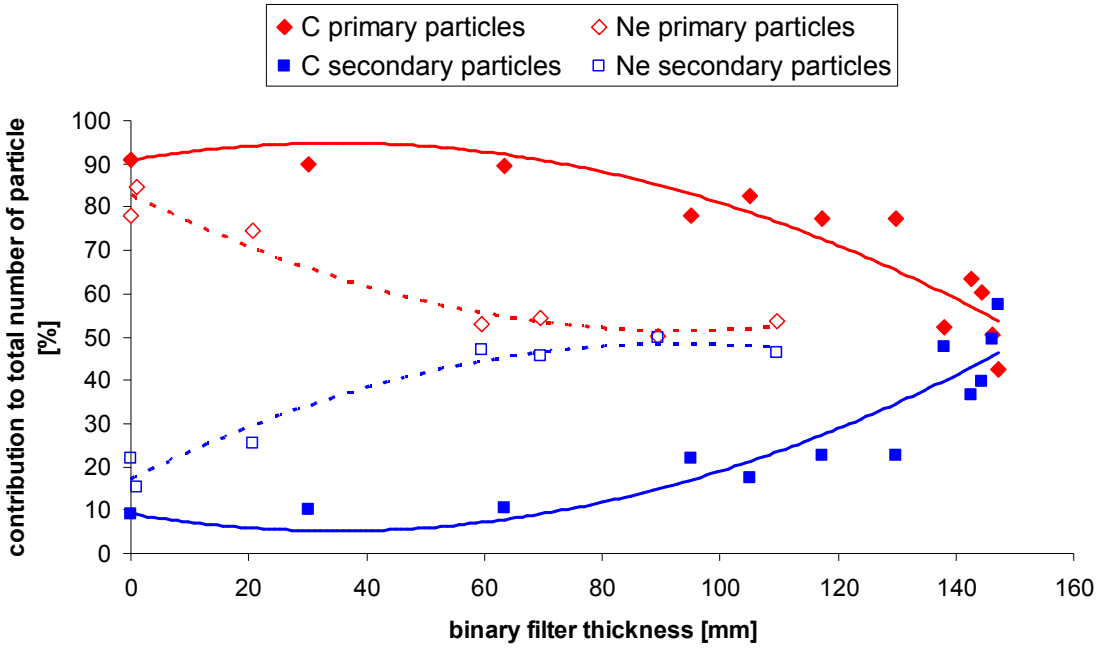

Figure 35 *Percent contribution of primary and secondary particles to the total number of incident in dependence of binary filter thickness (dots). Curves represent polynomial fitting as an eye guide.*

The dose contributions were individually calculated for primary particles and secondary particles with lower or higher LET. Following figures illustrates the dose contributions for carbon (Figure 36) and neon (Figure 37) beams of both setups. The contribution of secondary particles to the total dose is roughly increasing together with corresponding decrease of primary particles contribution. SOBP setup of 290 MeV/u carbon beam results to more rapid increase of high LET fragments with depth compared to MONO

setup. They contribute with 40.6 ± 4.0 % to the total dose behind binary filter with 136 mm for SOBP, which is the last one, where was possible to distinguish peak of primary particles. In comparison to that, high LET fragments contribute only with 18.8 ± 3.0 % to the total dose behind binary filter of 147 mm thickness for MONO setup. High LET neon fragments contribute with 10 ± 1.1 % and with 36.7 ± 4.3 % for MONO neon beam behind 137 mm, or SOBP setup behind 114 mm respectively.

These results are in good agreement with literature (Jadrníčková, 2010; Mrázová et al., 2010; Endo et al., 2010; Endo et al., 2007).

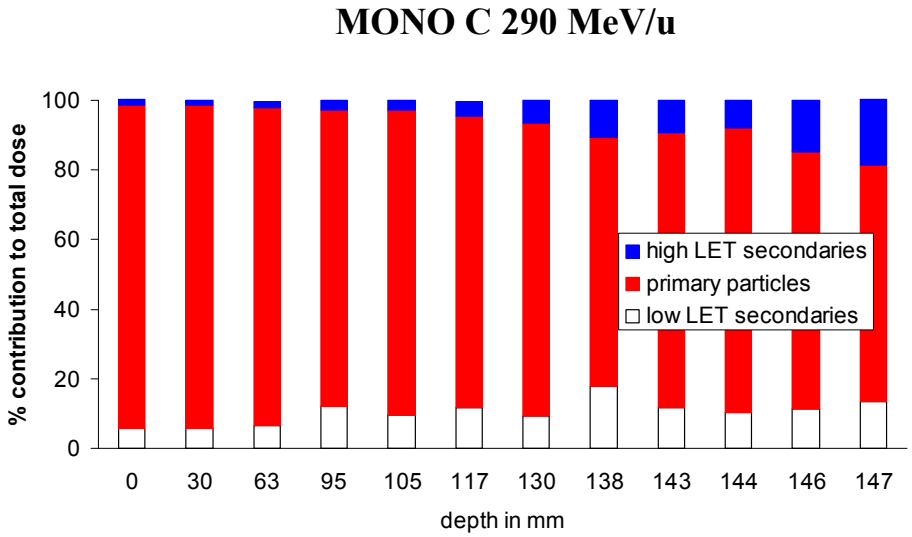

a)

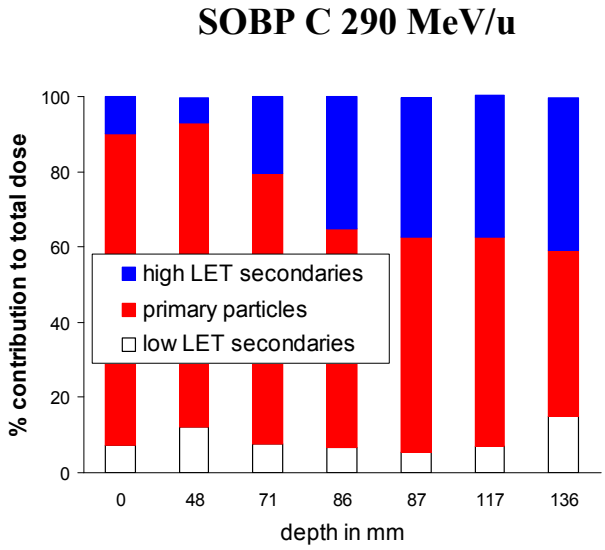

b)

Figure 36 *Contribution to total dose of MONO (a) and SOBP (b) carbon beam from primary and secondary particles, material Page*

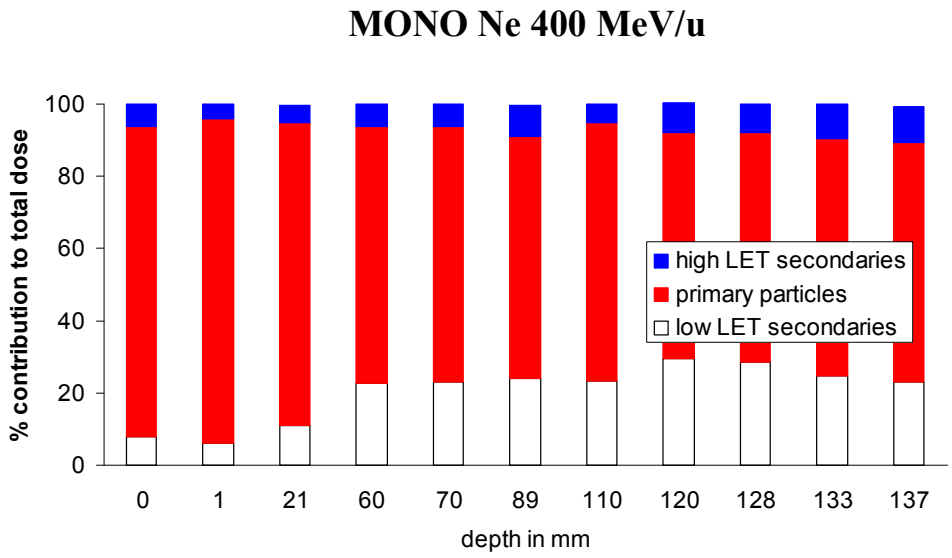

a)

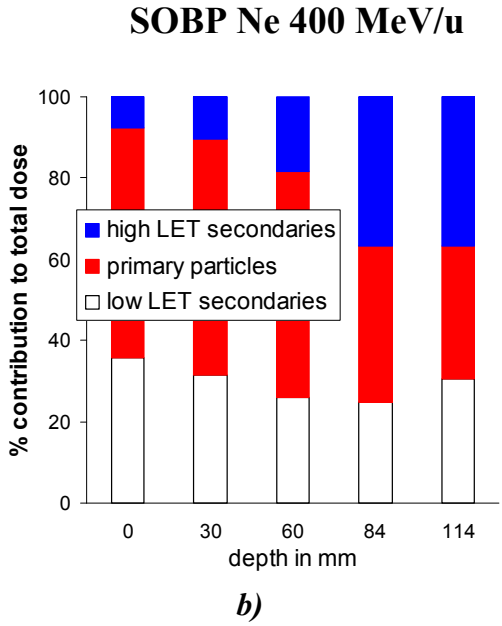

b)

Figure 37 *Contribution to total dose of MONO (a) and SOBP (b) neon beam from primary particles and secondary distinguished by the way described in the text above, material Page*

It should be emphasized; that material Page registers only particles with LET higher than ~ 10 keV.μm^{-1}, but a contribution of fragments with lower LET might be nonnegligible. Further, there were recorded dose contributions related to other then primary particles even for irradiations with no shielding in MONO setup. These particles may originate from fragmentation in the air, but most likely they are caused by a dust and other "false" tracks.

3.3 Neutron dosimetry

Neutron dosimetry, as a complicated research branch, is still looking for new methods and procedures, which would enable to characterize neutron fields. Neutrons are indirectly ionizing radiation; hence their energy is transferred to the matter through the kinetic energy of secondary charged particles. Generally, there are two principles of neutron detection using of two different neutron interactions with the matter. The neutron can be scattered by a nucleus and the recoiling nucleus is detected. Usually, only light nuclei (mainly hydrogen and helium) can be employed for detection purposes. The second approach is a detection of products of neutron nuclear reactions, which can be protons, alpha particles, gamma irradiation or fission fragments. Some of these reactions require threshold of minimal neutron energy. Medium, where neutron interactions take place, can be generally gas, liquid, or solid (Crane and Baker, 1991).

Neutron fields nowadays accompany many human activities and facilities; thus necessity of neutron monitoring rises. They are namely nuclear and research reactors, medical accelerators, high energy particles accelerators (Griffith et al., 2001), and also neutrons can not be avoid from activities taking place in higher altitudes or in space (Spurný et al., 2007). Energy profile of these neutron fields is different; for example common accelerators and nuclear reactors generate neutrons with energies up to 20 MeV. In radiotherapy, there are used either fast neutron beam with energies above 0.1 MeV, or secondary neutrons with energies dependent on energy and kind of primary source. Neutrons field in cosmic radiation include especially energies of few MeV and also energies from 50 to 150 MeV; their potential health risk has been underestimated for long time and only since the nineties has been studied (Tsuda et al., 2003; Oda et al., 2002).

Track etch detectors as possible neutron detectors were recognized in the Seventies (Frank et al., 1974); soon it was realized, that electrochemical etching of TED can be available in personal neutron monitoring system (Benton et al., 1980). Today, electrochemically etched PADC-based neutron dosimeters are one of the most extensively used method of neutron personal dose equivalent assessing in a workplace (Tanner et al., 2001). To extend TED detection abilities, the TED can be covered with a radiator of material consisting of some light element, e.g. TED detection of neutrons with energy less than 500 keV (Durrani and Bull, 1987). Besides, TED can be used as a linear energy transfer spectrometers to inspect also a quality of secondary particle field producing by neutrons.

The most serious complication in neutron dosimetry is that energy absorbed to a matter due to secondary particles resulting from neutron interactions is dependent on the matter. Since we are usually interested in energy absorbed to a tissue, there is strong concern for neutron dosimeter based on a tissue equivalent material. PADC is not tissue equivalent, see Table 8, but neutron interactions are very similar. It is supposed, that neutrons with energy up to 1 MeV are elastically recoiled on hydrogen nuclei producing protons in PADC. If neutron energy increases, heavier recoils and helium nuclei are produced by nuclear reactions with carbon and oxygen nuclei (Spurný, 1995; Brabcová et al., 2009). Neutrons in tissue also react with nitrogen nuclei, which is absent in PADC, producing alpha particles (Brede et al., 1999).

Table 8 *The comparison of composition of pure PADC without additives and soft tissue in mass %*

	H	**C**	**O**	**N**
PADC	6.6	52.6	40.8	-
soft tissue (ICRU 44, 1989)	10.0	14.9	71.6	3.5

3.4 PADC exposed to neutrons

During 2008 we investigated different TED response to quasi mono-energetic neutron beams of different energies; this chapter includes results of two experiments.

The first one was performed at Van der Graaf accelerator at EC-JCR in Belgian Geel. Sets of PADC detectors were exposed to quasi mono-energetic neutron beams induced with protons and deuterons at lithium, deuterium or tritium targets. Detectors were irradiated to seven possible energies ranging from 200 keV to 20 MeV. The second experiment was realized in iThemba laboratory in South Africa. Quasi-mono energetic neutron beam with two possible energies 100 or 200 MeV was induced by protons on Li targets of 6 or 8 mm. Conditions of both experiments were described with reference values of neutron beam fluency, neutron energy spectra, which were measured with Bonner sphere spectrometer (for the two lowest energies) and with IRMM recoil proton telescopes (for remaining energies); and calculated ambient dose equivalent H*(10), the values are included in Table 9. It has to be emphasized that even accelerator-produced neutrons are not fully mono-energetic. Example of neutron spectra for 7 MeV neutron beam is figured on 38.

Materials were irradiated in sandwich arrangement free in the air. All five studied materials were included in Belgian experiment (Page, USF4 and Baryotrak in upper layer; Tastrak and TD1 in bottom layer), while only Page and Tastrak were available for the two highest energies used in Africa (Page above, Tastrak below). All detectors were treated the way described earlier in chapter 2. Thus, we are able to obtain LET spectra and calculated dose equivalent, which can be compared to reference values of H*(10).

Table 9 *Reference ambient dose equivalents H*(10) for experimental neutron energies*

neutron energy [MeV]	H*(10) free in air [mSv]	neutron fluency [cm^{-2}]
0.2	11.4	$6.27.10^7$
0.5	36.7	$1.14.\ 10^8$
1	25.6	$2.67.\ 10^8$
3.5	52.1	$1.27.\ 10^8$
7	89.0	$2.22.\ 10^8$
16	30.1	$5.44.\ 10^7$
20	32.4	$5.47.\ 10^7$

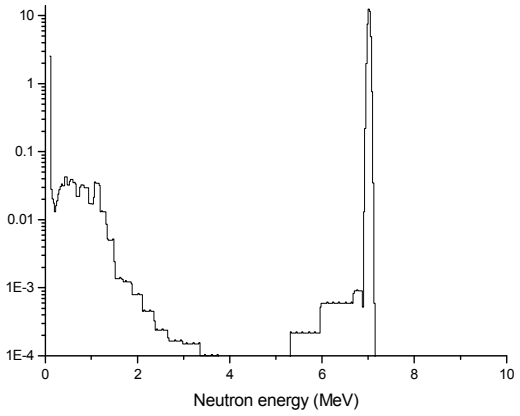

Figure 38 *Example of energetic spectrum for quasi mono-energetic neutron beam with nominal energy 7 MeV.*

3.4.1 Spectra of linear energy transfer

First of all, shapes of induced particles LET spectra were analyzed to inspect complex neutron response of our track etch detectors.

Figure 39 includes LET spectra for all experimental neutron beams with energies from 0.2 to 200 MeV registered with material Page, which were always arranged in the upper layer. Spectra were created with considering of corresponding background response, which was quite high in this experiment (background expressed in dose equivalent was 5.39 ± 1.92 for Belgian experiment and 5.89 ± 1.78 for iThemba in case of Page material). It is obvious, the spectra change with increasing neutron energy. For the energies up to 7 MeV, recoiled protons with LET up to 100 $keV.\mu m^{-1}$ dominate in the contribution to registered tracks. With increasing neutron energy, heavier recoils with LET about 100 $keV.\mu m^{-1}$ and higher start to appear. Their number is rather small, but their contribution to total dose equivalent is dominating regarding to their high quality factors.

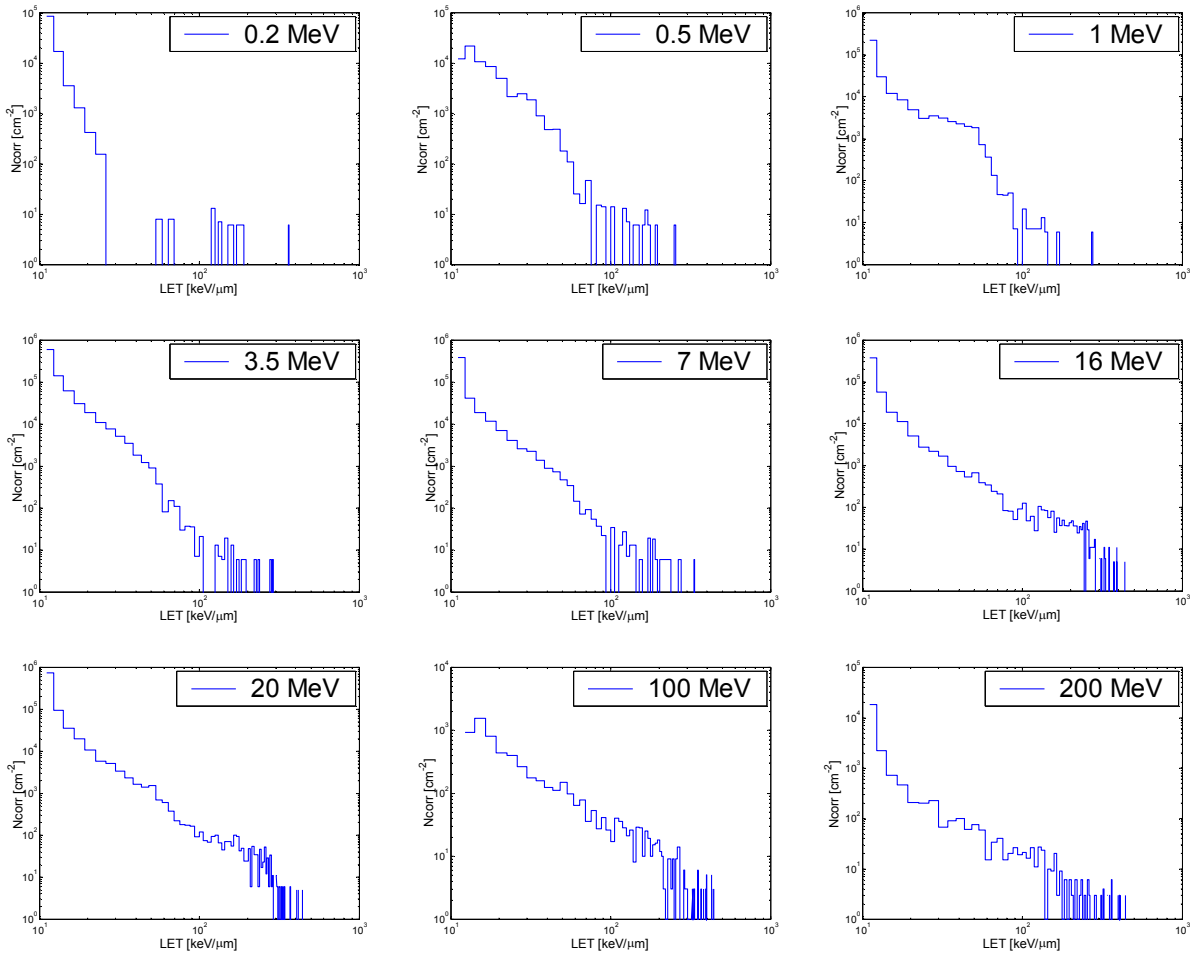

Figure 39 *Spectra of linear energy transfer for quasi mono-energetic neutron beams of energies from 0.2 to 200 MeV, registered with material Page in upper layer*

If we want to inspect possible response differences among used PADC materials, it is necessary to keep on mind, that materials were arranged in layers. Previously, it was suggested, that TED response to neutrons may be dependent on position in a sandwich arrangement; absolute values of dose equivalent distributions were higher for the upper layers for some neutron sources (Jadrníčková, 2010). However, inspection of Page LET spectra results available in African experiment in two possible positions (first and second layer) did not confirm any considerable differences, see Figure 40. Therefore, even if the inspected materials were arranged in two possible layers (Page, USF4 and Baryotrak in the first one; Tastrak and TD1 in the second one), the recorded spectra are considered to be influenced mainly by other factors, which are discussed.

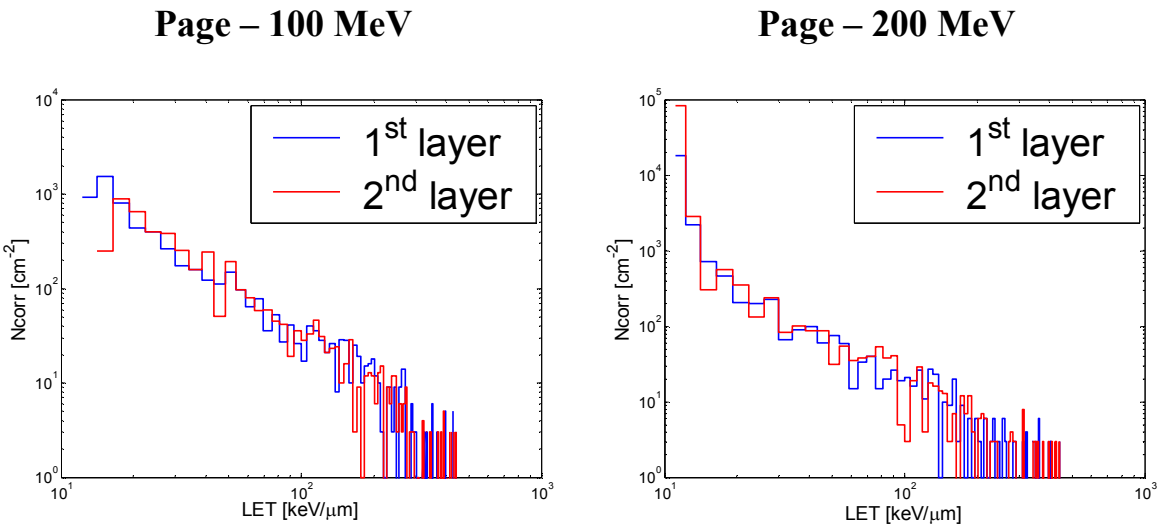

Figure 40 *Comparison of linear energy spectra in two quasi mono-energetic neutron beams registered with material Page arranged in two possible layers*

LET spectra recorded by all available materials in different neutron beams are compared on Figure 41 and 42. There are obvious differences in detection of low LET particles (~ 10 keV.μm^{-1}) according to material detection threshold. Further, there are differences in detection abilities of particles with LET up to 100 keV.μm^{-1}; materials with higher detection threshold (Tastrak and Baryotrak) recorded a higher number of these particles, especially in neutron beams with lower energies. This trend is somehow disappearing with increasing neutron energy. It could have connection to the presence of some chemical additives, like for example antioxidants, with which neither Tastrak nor Baryotrak are doped.

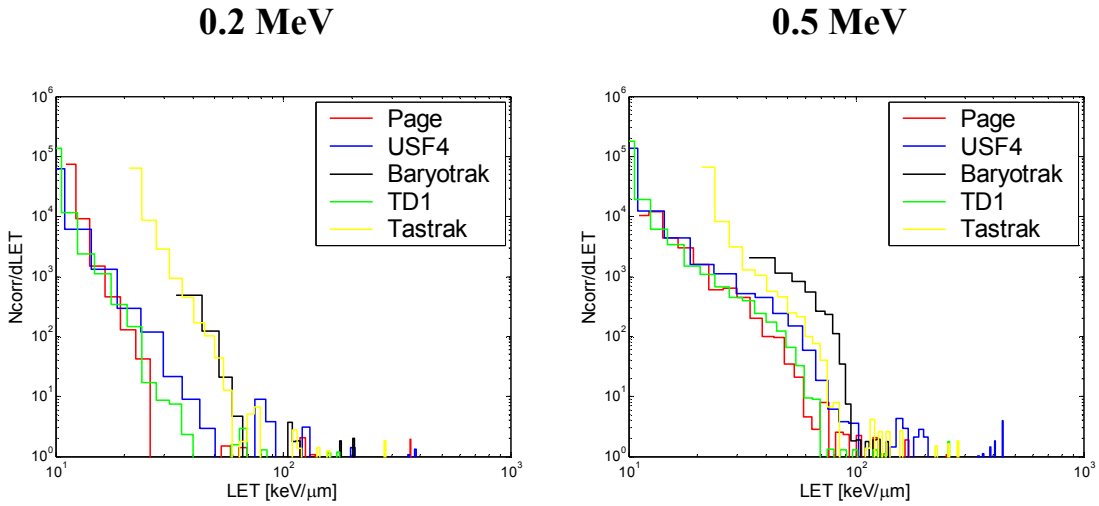

Figure 41 *Linear energy spectra recorded with available PADC employed as LET spectrometers in neutron beams of different energies, note the logarithmic scale on both axis*

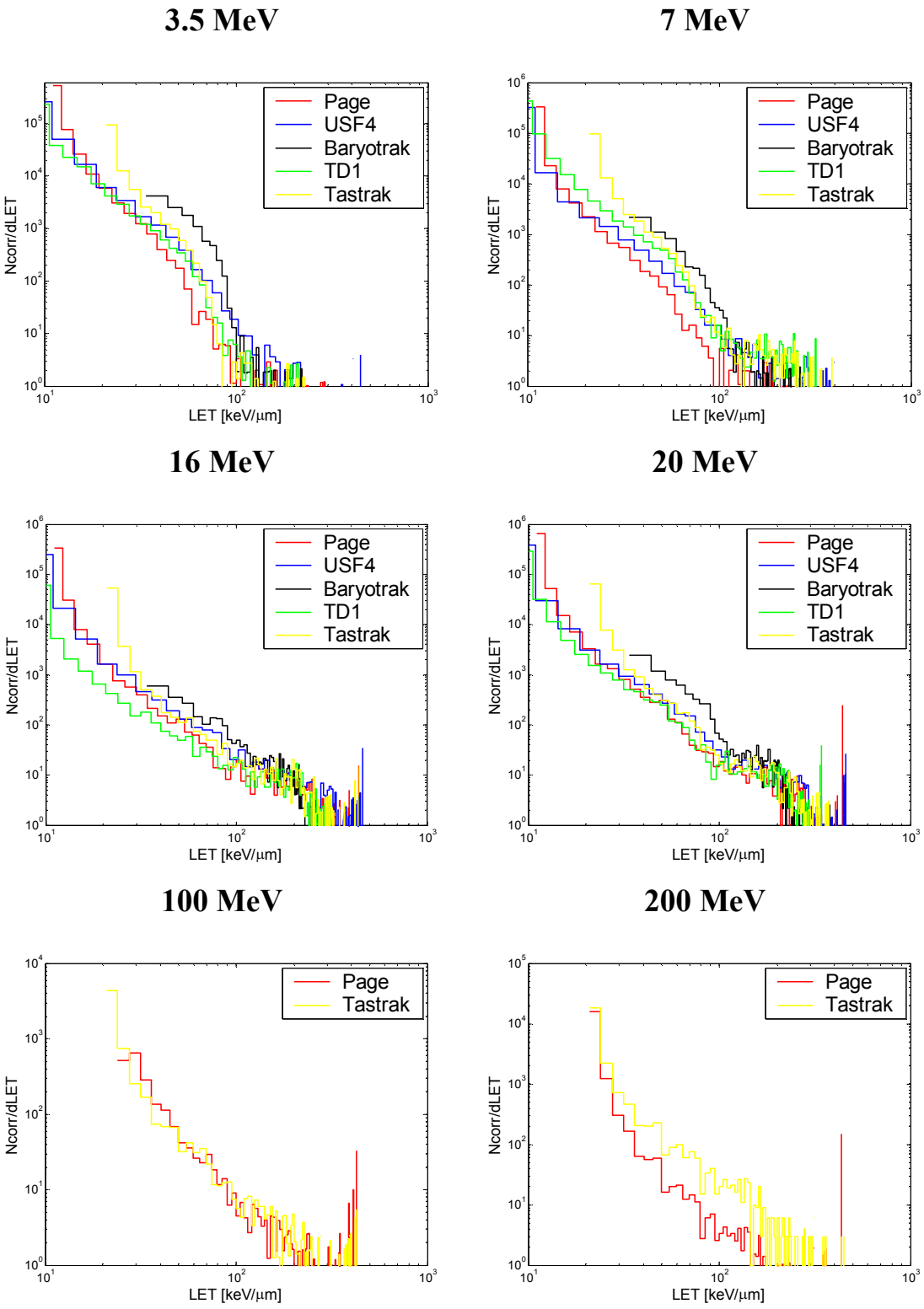

Figure 42 *Linear energy spectra recorded with available PADC employed as LET spectrometers in neutron beams of energies (continuation form the previous page), note the logarithmic scale on both axis. Results of 1 MeV neutron beams are very similar to the results of 0.5 MeV neutron beams and are not included.*

3.4.2 Neutron response

Further, neutron responses were calculated for all applied PADC to inspect eventual differences. Neutron responses were calculated as the ratio of measured dose equivalent and corresponding reference ambient dose equivalent. Ambient dose equivalent H*(10) is operational quantity defined according to (ICRU 60, 1998) as dose equivalent generated in associated oriented and expanded radiation field at the depth of 10 mm on the radius of ICRU sphere, which is oriented opposite to direction of incident radiation. Even if these two quantities represent something different, their comparison can answer the question of PADC neutron response. The Figure 43 shows the response dependence on neutron energy. There are obvious differences among materials.

In summary, PADC response depends on neutron energy in a very complex way. The materials Tastrak and Baryotrak exhibited overestimating response for most of the neutron energies, the overestimation is roughly decreasing. On the other hand, the response of three remaining materials with low detection thresholds is mostly increasing up to neutron energy of 20 MeV, and then it decreases. This behaviour is in agreement with published results (Domingo et al., 2009), where dose equivalent response of TED in mono energetic neutron beams with energies up to 10 MeV was inspected. It was observed transient degrease of dose equivalent response for the lowest and the highest energies. It is explained by production of secondary particles, which are outside of PADC detection range.

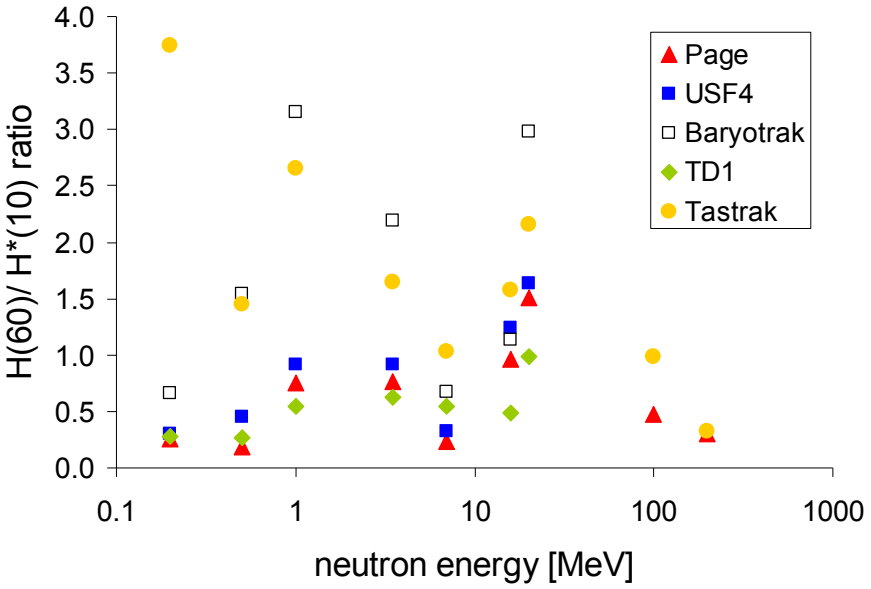

Figure 43 *Neutron response estimation calculated as ratio of measured dose equivalent and reference ambient dose equivalent for different TED detectors based on PADC*

Observed trends can have connection to the different chemical composition of individual PADC, since the materials with higher detection thresholds (and with no antioxidants) Tastrak and Baryotrak detected similarly compared to other materials.

One should also keep on his mind that results might be biased due to probable presence of over-etched tracks. As was mentioned above, today, we do not distinguish these particles and consider them as the normal ones; therefore their assigned LET is overestimated. However, deletion of such tracks would lead to further underestimation of dose equivalent.

3.5 Summary of the previous PADC applications

When we focus on detection abilities in beams of heavy charged particles, we are usually interested in low LET particles, as well as in high LET particles, thus we need the material with as the lowest detection threshold and the highest saturation point as possible. Also, particles with very short range can be expected, especially in Bragg's maximum area. We can consider using of materials with lower etch velocity to diminish risk of such particles to be removed from an etched surface. Hence, etch velocity was inspected via thickness of removed layer by method of fission fragments analysis described in chapter 1.2.2. The averages from more than sixty individual etching are figured in 44; only our standard etching conditions were analysed. There are obvious differences between etch velocities, the thickness of removed Page material was 15.7 ± 0.6 μm, while 13.7 ± 0.6 μm for Baryotrak, which is material with the lowest etch velocity.

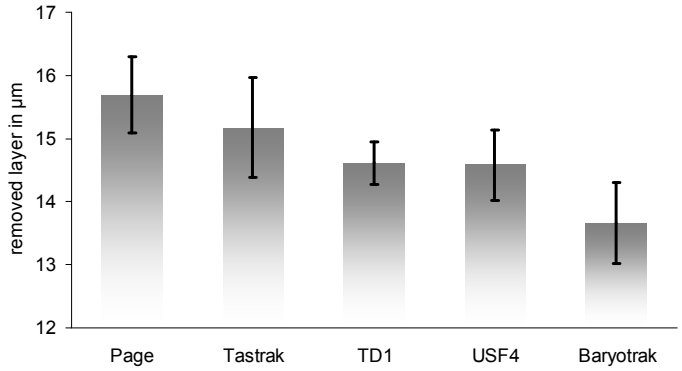

Figure 44 *Removed layers of different PADC under our standard etching conditions; error bars represent statistic errors*

General summary of our neutron tests is that the PADC response depends on neutron energy in a very complex way. The materials Tastrak and Baryotrak exhibited overestimating

response for most of the neutron energies, the overestimation is roughly decreasing. On the other hand, two remaining materials underestimated the response, but this trend is roughly increasing up to neutron energy of 20 MeV. Usually, it is preferable to overestimate radiation quantities from radiation protection viewpoint.

3.6 Track etch detectors in space dosimetry

Earlier, there was recognized a possibility of TED application in study of charged particles (Benton, 1983) or microdosimetric studies (Spurný et al., 1999) onboard of spacecrafts; often in combination with thermoluminiscent detectors (Doke et al., 1995).

Space dosimetry has several special requirements. Except good detection ability in a mixed radiation field, a dosimeter should be able to work for long time without necessity of maintenance and ideally without any power supply. Usually, spatial and weight modesty is also required. Track etch detectors are the excellent choice. TED are small, power independent, autonomous and able to register particles with LET from 5-10 keV.μm^{-1}, which are particles with dominating health impact (Zhou et al, 2009). On the other side, they are able to provide only overall integral signal.

3.6.1 Cosmic radiation flux

Cosmic radiation flux consists especially of protons (88 %), alpha particles (10 %) and heavier nuclei (1 %); among light particles, there are electrons (1 %), positrons and neutrinos (Reitz et al., 1997). Particles are accompanied with high energetic gamma radiation and neutron flux. Primary cosmic energy ranges from 10^9eV to 10^{20}eV, whereas number of incident particles decreases with third power of energy. When cosmic flux reaches approximately 30 km altitude, its primary particles start to interact with nuclei present in atmosphere and secondary particles are formed.

Radiation originated in space contributes to man natural radiation background; however, Earth surface is partially shielded by the atmosphere and by geomagnetic field. Thus, an average annual effective dose is dependent on altitude (0.45 mSv in 1 km, 10 mSv in 8 km), latitude (minimum at the equator), and also on solar activity. Solar activity increases and decreases with eleven year cycle; solar particles generate magnetic field, which partially shield the inner Solar System against low energetic cosmic particles (Ullmann, 2002; Reitz et al., 1997; Heinrich et al., 1999).

3.6.2 Experimental application of TED onboard of spacecrafts

Considering the aspects mentioned in chapter 2.5 and 3.5, the best choice for measuring in mixed field, as it is onboard space vehicle for example, appears to be the combination of USF4, material with the lowest detection threshold, and Baryotrak, material with the highest tolerance to saturation. Thus, the most wide operational range would be achieved, if their results are combined. The combination can be also recommended for partial insensitivity to environmental changes and good detection response for neutrons of Baryotrak.

The possibility of combination is shown on experiment performed on the International Space Station (ISS) during 2009. TED USF4 and Baryotrak were placed inside of ISS in Columbus Module for 136 days; after delivery to our department, they were etched and evaluated by the method described in chapter 2.

Spectra of linear energy transfer were drafted with uniform LET step, 10 keV.μm^{-1} for both applied materials. Afterwards, spectra were combined to create one compiling spectrum, where USF4 results are utilized up to 30 keV.μm^{-1} (Baryotrak detection threshold) and Baryotrak results are used over this value; linear energy spectra and its combination are figured on 45.

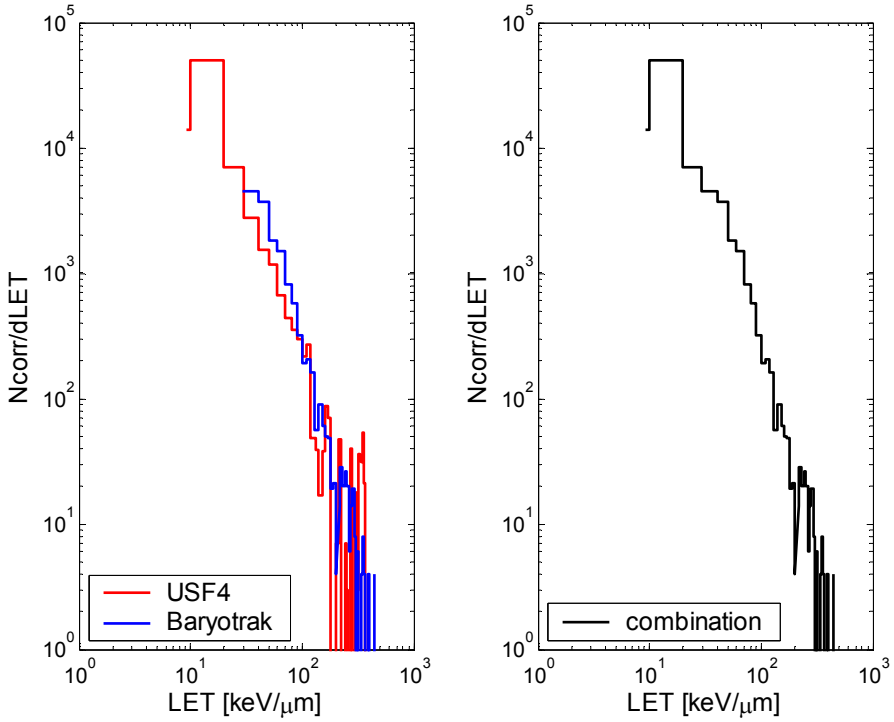

Figure 45 *Spectra of liner energy transfer LET recorded by individual materials (left) with low (USF4) and high (Baryotrak) detection threshold and their combination (right)*

Further, dose equivalent can be calculated according to (9) and compare with results, which would be obtained with USF4 and Baryotrak detectors separately. Dose equivalent rate was estimated as 193 ± 16.5 μSv.day^{-1} by the USF4 detector itself, 206 ± 24.7 μSv.day^{-1} by the Baryotrak detector, and 220 ± 25.2 μSv.day^{-1} by their combination. Dose equivalent is strongly dependent on factors mentioned in chapter 3.6.1 and vary approximately from 200 to 1000 μSv.day^{-1} (Jadrníčková, 2010; Spurný and Jadrníčková, 2005). Spectra of dose equivalent of combined results are figured on 46; the contribution of particles with LET up to or above 100 keV.μm^{-1} is 63 ± 10 %, 37 ± 8.2 % respectively, which agrees with our previous studies (Jadrníčková et al., 2010b; Jadrníčková et al., 2010c; Jadrníčková et al., 2009). Contribution of higher LET particles is affected by high uncertainties due to a small number of present particles.

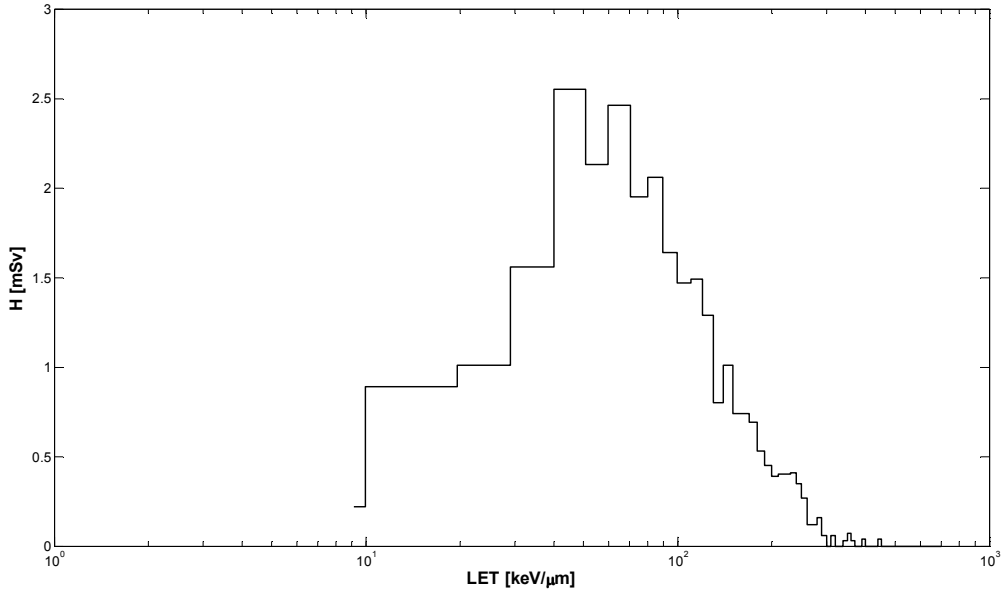

Figure 46 *Distribution of dose equivalent H along linear energy transfer LET inside of ISS; spectrum combines results obtained with USF4 and Baryotrak detectors by the way described in text.*

4. CONCLUSIONS

Track etch detectors are not commonly used as linear energy spectrometer, but they are preferred in some applications, where their advantages of spatial modesty and power independence can be utilized. However, there is still a space for an up-grade of methodology or used materials.

The thesis deals with methodology from various points of view; the obtained results and experience are successfully applied in three experimental fields - dosimetry in heavy ion beams, neutron dosimetry and dosimetry on board of spacecrafts. Five different TED materials were included into all methodological tests, as well as to experiments. Thus, it was possible to compare them and consider differences, which would affect their detection abilities in some particular application. Let me summarize all achieved objectives:

1. First of all, calibration for LET spectrometry and overall uncertainty analysis were performed. So far, such complex analysis has not been available; though the proper estimation of uncertainties, including calibration uncertainties, should be very common component of any calculation and measurement. The basic properties of inspected materials were described, such as detection range, which is of course one of the most important aspect of any detector.

2. Environmental effects on materials were analysed in a long-term experiment. In spite of ambiguous results, it is possible to compare materials at least among themselves. The test outcomes suggest that there is relation between detection threshold and stability in time; the more sensitive material, the more dramatic changes occurred.

3. FT-IR analysis was performed to analyse basic chemical composition of virgin material forms. It was found, that materials differ in composition of aromatic and amid additives and further, some similarities were observed, independently on production origin.

4. Application in heavy ion beams approved TED as an effective instrument. The depth-dose distribution can be satisfyingly described; also it was possible to analyse linear energy transfer spectra and fragments contribution. These results contribute to deeper understanding of beam changes related to biological effects; it might be incorporated into baseline data of any calculation code or serve as confirmation of their accuracy.

5. It is not very common to use TED as linear energy transfer spectrometer in neutron dosimetry, particularly without any additional converters. In our experiments, materials were irradiated in pure form to different energies of neutron beam and their response was analysed, in terms of LET spectra, as well of dose equivalent. Complex response dependent on particular material was observed.

6. All results were considered and the combination of two materials (USF4 and Baryotrak) was recommended for measurements in mixed radiation fields. This combination advantages in the wide detection range, partial stability in time, as well as in optimal detection response to neutrons. The chosen combination was tested in the experiment on board of spacecraft; achieved results are in good agreement with literature and our previous experiments.

However, some unanswered questions still remain. In the future, we should certainly resolve the problem of over-etching tracks. After testing of short and long etching time, we should be able to distinguish the particles with short range and evaluate them properly. Also, the new evaluating software HspFit offers some advantages in comparison to old Lucia system, so far we are searching for upgrading methods of track measuring. Finally, on-going collaboration with HIMAC enables us to even expand the library of dosimetric and microdosimetric characteristics for other ions and energies.

5. ATTACHMENTS

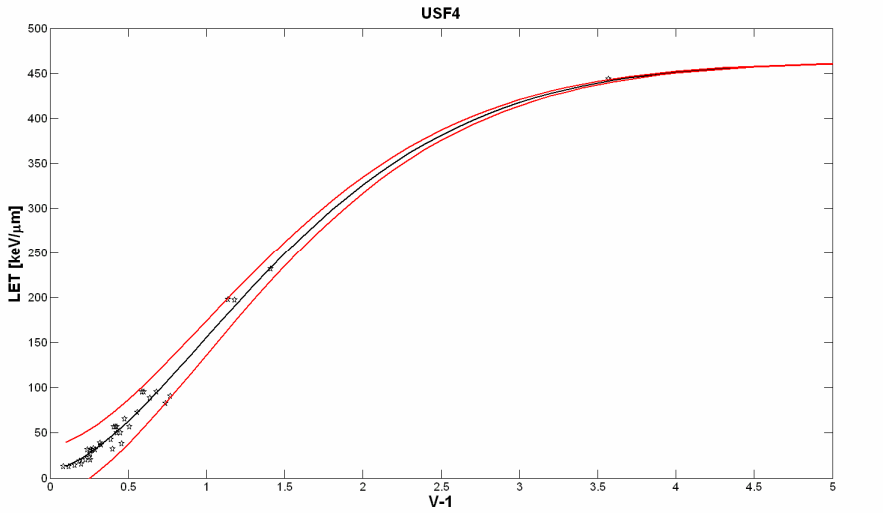

a)

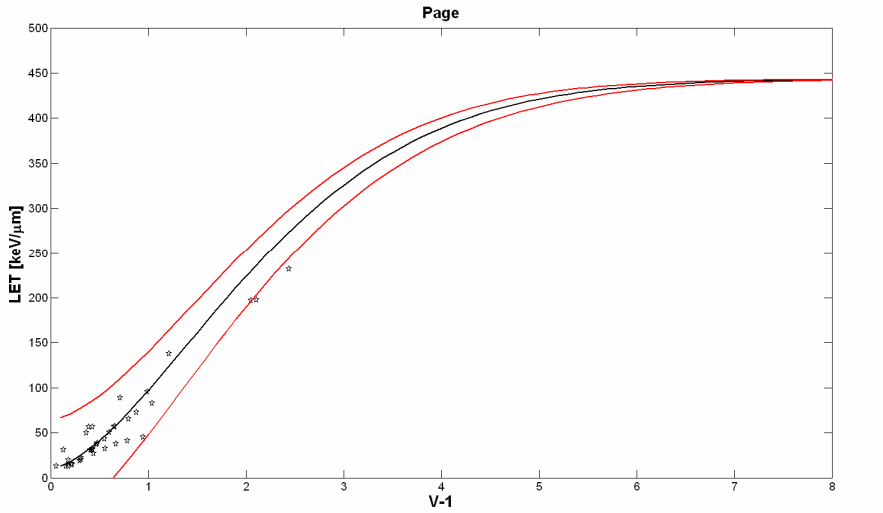

b)

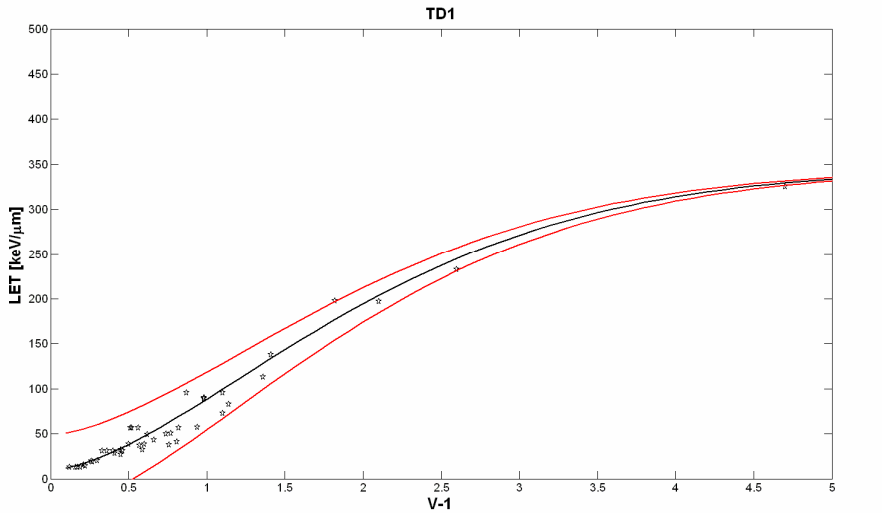

c)

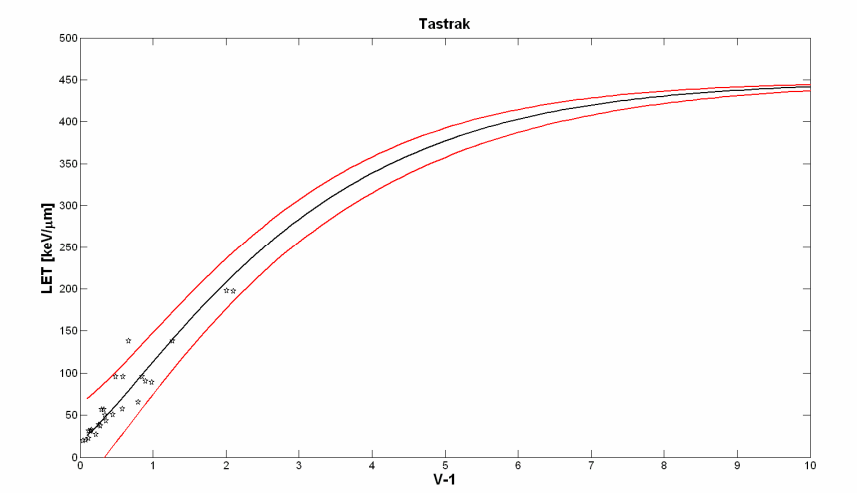

d)

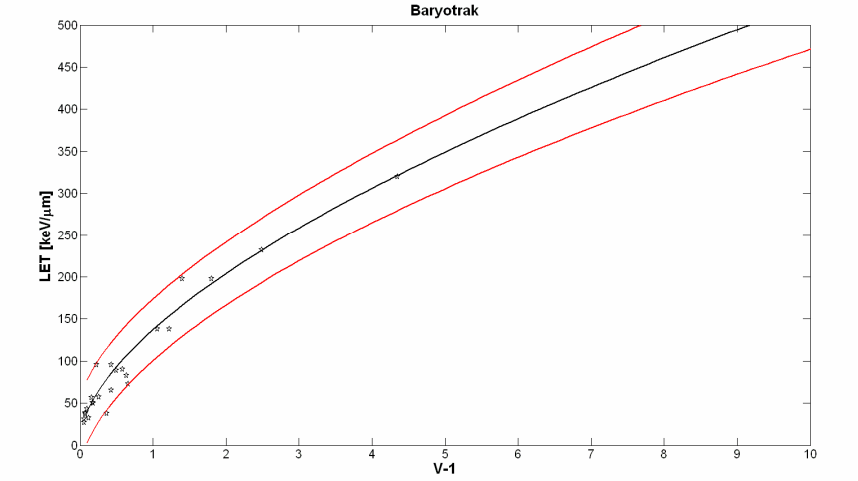

e)

Figure 47 *Fitted calibration curves and measured data (points) for a) USF4, b) Page, c) TD1, d) Tastrak and e) Baryotrak materials applied as linear energy transfer spectrometers; the linear energy transfer in water LET (black) and its 95 % confidence intervals (red) are plotted as function of the shifted etch rate V-1*

6. REFERENCES

Ahmad, S., Stejny, J., 1991. Polymerisation, structure and track recording properties of CR-39, Nuclear Tracks and Radiation Measurements 19(1-4), 11-16.

Amaldi, U., Kraft, G., 2005. Radiotherapy with beams of carbon ions, Rep. Prog. Phys. 68, 1861-1882.

Babkin, V.A. et al., 2010. SOBP forming for carbon therapy, Central European Journal of Physics 8(4), 683-688.

Badhwar, G.D., O'Neill, P.M., 2001. Response of silicon-based linear energy transfer spectrometers: implication for radiation risk assessment in space flights, Nuclear Instruments and Methods in Physics Research, A 466, 464-474.

Bartlett, D.T., 1987. Ageing of and environmental effects of PADC (CR-39), Radiation Protection Dosimetry, 20(1-2), 71-75.

Benton, E.V., 1983. Dosimetric radiation measurements in space, Nuclear Tracks and Radiation Measurements 7(1-2), 1-11.

Benton, E.V. et al., 1986. Applications of nuclear track detectors in space radiation dosimetry, International Journal of Radiation Applications and Instrumentation 12(1-6), 505-508.

Benton, E.V. et al., 1986b. Response of different types of CR-39 to energetic ions, Nuclear Tracks 12(1-6), 79-82.

Benton, E.V. et al., 1980. Proton recording neutron dosemeter for personnel monitoring, Proceedings of the 10th International Conference on Solid State Nuclear Track Detectors, Pergamon Press, 469-475.

Billington, D.S., Crawford, J.H., 1961. Radiation Damage in Solids, Princeton University Press, Princeton, New Jersey.

Böhlke, S., Hermsdorf, D., 2008. Correlation of track etching properties of SSNTDs with the density of free radicals produced by charged particles in PADC, Radiation Measurements 43, S65-S75.

Brabcová, K. et al., 2010. Dosimetry in heavy ion beams using various detectors, Radiation Measurements, in press.

Brabcová, K. et al., 2009. Track etch based LET spectrometry in beams of neutrons with energies from 0.2 to 200 MeV, Radiat. Measur., 44(9-10), 969-971.

Braccini, S., 2007. Progress in hadrontherapy, Nuclear Physics B172, 8-12.

Brede, H.J. et al., 1999. Improvement of response of Cr-39 nuclear track detectors in fast neutron dosimetry, Radiation Protection Dosimetry 85(1-4), 113-116.

Cartwright, B.G. et al., 1978. CR-39: A nuclear-track-recording polymer of unique sensitivity and resolution, Nuclear Instruments and Methods 153, 457-460.

Charvát, J., 1985. Studium polymerních detektorů stop v pevné fázi pro účely spektrometrie lineárního přenosu energie, thesis, ČVUT FJFI.

Chaudhri, M.A., 2007. Production of secondary neutrons from patients during therapy with carbon ions, their dose contributions and potential risks, IFMBE Proceedings 14, 2207-2210.

Courdi, A. et al., 1994. The depth-dependent radiation response of human melanoma cells exposed to 65 MeV protons, British Journal of Radiology 67, 800-804.

Crane, T.W., Baker, M.P., 1991. Neutron detectors in Reilly, D. et al.: Passive nondestructive assay of nuclear materials, Washington DC.

Dachev, Ts, 2009. Characterization of near earth radiation environment by Liulin type instruments, Adv. Space Res. 44, 1441-1449.

Doke, T. et al., 1997. Dip angle dependence on track formation sensitivity in antioxidant doped CR-39 plates, Radiation Measurements 28(1-6), 445-450.

Doke, T. et al., 1995. Estimation of dose equivalent in STS-47 by combination of TLDs and CR-39, Radiation Measurements 24(1), 75-82.

Domingo, C. et al., 2009. Measurements in quasi-monoenergetic neutron beams at the EC-IRMM Van der Graaf accelerator for calibration of the UAB PADC based neutron dosimeter, Radiation Measurements 44, 981-984.

Dorschel, B., 2005. Influence of oxygen on the track etch rate along light ion trajectories in CR-39, Radiation Measurements 40, 234-239.

Drach, J. et al., 1987. Effect of oxygen on response of plastic and glass track detectors, Nuclear Instruments and Methods in Physics Research, B 28(3), 364-368.

Durrani, S.A., Bull, R.K., 1987. Solid State Nuclear Track Detection, Pergamon Press.

Endo, S. et al., 2010. Measurement of microdosimetric spectra produced from a 290 MeV/n Spread Out Bragg Peak carbon beam, Radiat. Environ. Biophys 49, 469-475.

Endo, S. et al., 2007. Microdosimetric evaluation of secondary particles in a phantom produced by carbon 290 MeV/nucleon ions at HIMAC, J. Raidat. Res. 48, 397-406.

Fleischer, R.L. et al., 1975. Nuclear tracks in solids: principles and applications, University of California Press.

Fleischer, R.L. et al., 1965a. Solid-state track detectors: Applications to nuclear science and geophysics, Ann. Rev. Sci. 15, 1-28.

Fleischer, R.L. et al., 1965b. Ion explosion spike mechanism for formation of charged-particle tracks in solids, Journal of Applied Physics 36, 3645-3652.

Fleischer, R.L. et al., 1963. Method of forming fine holes of near atomic dimensions, Rev. Sci. Instr. 34, 510-512.

Fujii, M. et al., 1984. Improvements in the sensitivity and the etching properties of CR-39, Nuclear Instruments and Methods A 226, 496.

Frank, A. I. et al., 1974. A passive neutron spectrometer using a nuclear track detector, Nuclear Instruments and Methods 122, 433-441.

Genz, A., 1992. Numerical computation of multivariate normal probabilities, J. Comp. Graph Stat. 1, 141-149.

Gilvin, P. et al., 1988. Progress in an operational dosimetry system using PADC, Nuclear Tracks Radiation Measurements 15(1-4), 577-581.

Golovchenko, A.N. et al., 1999. Fragmentation of 200 and 244 MeV/u carbon beams in thick tissue-like absorbers, Nuclear Instruments and Methods in Physics Research B 159, 233-240.

Griffith, R.V et al., 2001. Compendium of neutron spectra and detector responses for radiation protection purposes, IAEA TRS-403.

Hardcastle, G.D., Miles, J.C.H., 1996. Ageing and fading of alpha particle tracks in CR-39 exposed to air, Radiation Protection Dosimetry 64(4), 295-298.

Heinrich, W. et al., 1999. Physics of cosmic radiation fields, Radiation Protection Dosimetry, 86(4), 253-258.

Hummel, D.O. and Scholl, F., 1971. Infrared analysis of polymers, resins and additives, an atlas, New York.

Hutchinson, J.M., 1995. Physical aging of polymers, Prog. Polym. Sci. 20, 703-760.

ICRP (International Commission on Radiological Protection), Recommendations, ICRP Publication 60, Ann. ICRP 21(1-3), Oxford Pergamon Press, (1991).

ICRU Report No. 16, 1970. Linear energy transfer.

ICRU Report No. 36, 1983. Microdosimetry.

ICRU Report No. 44, 1989. Tissue substitutes in radiation dosimetry and measurement.

ICRU Report No. 60, 1998. Fundamental quantities and units for ionizing radiation.

Inaniwa, T. et al., 2005. Simulation for position determination of distal and proximal edges for SOBP irradiation in hadron therapy by using the maximum likelihood estimation method, Physics in Medicine and Biology 50, 5829-5845.

Jadrníčková, I., 2010. Spectrometry of linear energy transfer: use in radiotherapy and radiation protection in high-energy particle fields, LAP Lambert Academic Publishing.

Jadrníčková, I. et al.,2010a. Měření ve svazku He 150 MeV/n MONO urychlovače HIMAC pomocí různých detektorů, Bezpečnosť jadrovej energie 18(56), 223-225.

Jadrníčková, I. et al.,2010b. Dose characteristics and LET spectra on and inside the spherical phantom onboard of ISS, Radiation Measurements, accepted.

Jadrníčková, I. et al.,2010c. To monitoring onboard spacecraft by means of passive detectors, Radiation Protection Dosimetry, accepted.

Jadrníčková, I. et al., 2009. Variation of absorbed doses onboard of ISS Russian Service Module as measured with passive detectors, Radiation Measurements 44, 901-904.

Jayaraman, S., Lanzl, J.H.,2004. Clinical radiotherapy physics, second edition, Springer-Verlag, Germany.

JCGM: 104, 2009. Working Group 1 of the Joint Committee for Guides in Metrology: Evaluation of measurement data - An introduction to the "Guide to the expression of uncertainty in measurement" and related documents.

Kanai et al.,1999. Biophysical characteristics of HIMAC clinical irradiation system for heavy-ion radiation therapy, In. J. Radiation Oncology Biol. Phys 44(1), 201-210.

Kania, P., 2007. Infračervená spektrometrie, skripta VŠCHT.

Kodaira, S. et al., 2009. A program for the precise observations of ultra heavy nuclei in galactic cosmic rays, J. Phys. Soc. Jpn. 78, 138-141.

Kodaira, S. et al., 2007. New method of the precise measurement for the thickness and bulk etch rate of the solid-state track detector, Nuclear Instruments and Methods in Physics Research, A 574, 163-170.

Kohno, R. et al., 2005. Measurements of dose-averaged linear energy transfer distributions in water using CR-39 plastic nuclear track detector for therapeutic carbon ion beams, Jpn. J. Appl. Phys. 44, 8722-8726.

Kovář, Z. et al., 1984. Pokroky dozimetrie ionizujícího záření, Academia Praha.

Kraft, G., 2007. Heavy ion tumor therapy: from the scientific principles to the clinical routine, Nuclear Physics News 17, 29.

L'Annunziata, M.F. et al., 2003. Handbook of radioactivity analysis, Academic Press.

Lounis-Mokrani, Z. et al., 2003. Characterization of chemical and optical modifications induced by 22.5 MeV proton beams in CR-39 detectors, Radiation Measurements 36, 615-620.

Matsufuji, N. et al., 2003. Influence of fragment reaction of relativistic heavy charged particles on heavy-ion radiotherapy, Phys. Med. Biol. 48, 1605-1623.

Miller, J., 2001. Recent measurements for hadrontherapy and space radiation: nuclear physics, Physica Medica XVII (1).

Mori, Y. et al., 2009. Radiation chemical yield for loss of carbonate ester bonds in PADC films exposed to gamma ray, Radiation Measurements 44, 211-213.

Mrázová et al., 2010. Fragmentation of Ne ions with energy 400 MeV/u behind targets from different materials measured with PNTD, Radiation Measurements, in press.

Nadkarni, V.S., Samant, S.D., 1996. Development of indigenous polyallyl diglycol carbonate (PADC) films for nuclear track detection, Radiation Measurement 26(5), 651-656.

Nikezic, D., Yu, K.N., 2007. Computer simulation of radon measurements with nuclear track detectors, Computer Physics Research Trends, Nova Science Publisher, Inc.

Nikezic, D., Yu, K.N., 2004. Materials Science and Engineering, R 46, 51-123.

Nikezic, D., Yu, K.N., 2003. Three-dimensional analytical determination of the track parameters: over-etched tracks, Radiation Measurements 37, 39-45.

Novotná, M., 2010, personal communication.

Novovičová, J., 1999. Pravděpodobnost a matematická statistika, skripta ČVUT.

Oda, K. et al., 2002. Characteristic response of plastic track detectors to 40-80 MeV neutrons, Radiation Protection Dosimetry 101(1-4), 569-572.

Ogura, K. et al., 1997. Proton response of high sensitivity CR-39 copolymer, Radiation Measurements 28(1-6), 197-200.

Ogura, K. et al., 1995. Development of copolymer of CR-39 with high sensitivity to low LET particles, Radiation Measurements 25(1-4), 159-162.

Pálfalvi, J.K., 2009. Fluence and dose of mised space radiation by SSNTDs achievements and constraints, Radiation Measurements 44, 724-728.

Pálfalvi, J.K. et al., 2008. Cosmic ray detection on the Foton-M2 satellite by a track etched detector stack, Advances in Space Research 42, 1030-1036.

Ploc, O. et al., 2010. Measurements and analysis of LET distributions at HIMAC BIO: development of the LET distributions database, poster presentation on HIMAC Annual Meeting, April, Chiba.

Portwood, T. et al., 1986. Ageing effects in CR-39, Nuclear Tracks 12(1-6), 109-112.

Portwood, T., Stejny, J., 1984. Analysis of CR-39 and the effect of additives, Nuclear Tracks and Radiation Measurements 8(1-4), 151-154.

Price, P.B., Walker, R.M, 1962. Chemical etching of charged particle tracks in solids, J. Appl. Phys. 33, 3407-12.

Reitz, G. et al., 1997. Results of dosimetric measurements in space missions, Radiation Protection Measurements, 70(1-4), 413-418.

Rytz, A., 1991. Recommended energy and intensity values of alpha particles from radioactive decay, Atomic Data and Nuclear Data Tables, 47(2), 205-239.

Schardt, D. et al., 2007. Nuclear fragments and fast neutrons in carbon ion radiation therapy, Proceedings of Ion beams in biology and medicine, Heidelberg, 9-15.

Sedlák, A., 1989. Mikrodizimetrie a její aplikace, Academia Praha.

Silk, E.C.H., Barnes, R.S., 1959. Examination of fission fragment tracks with an electron microscope, Ohil.Mag. 4, 970-972.

Somogyi, G. et al., 1986. Effect of certain production parameters and post-production treatments on the etching characteristics of CR-39 sheets, Nuclear Tracks 12(1-6), 97-100.

Spurný, F., 2001. Radiation doses at high altitudes and during space flights, Radiation Physics and Chemistry 61, 301-307.

Spurný, F., 1995. Dosimetry of neutrons and high energy particles with nuclear track detectors, Radiation Measurements 25(1-4), 429-436.

Spurný, F. and Jadrníčková, I., 2005. Some recent measurements onboard spacecraft with passive detector, Radiation Protection Dosimetry 116(1-4), 228-231.

Spurný, F. et. al., 2010. Spectra of the linear energy transfer and other dosimetry characteristics as measured in C 290 MeV/n MONO and SOBP ion beams at HIMAC-BIO (NIRS, Japan) with differennt detectors, Radiation Protection Dosimetry, accepted.

Spurný, F. et al., 2009. Measurements and analysis of LET distributions at HIMAC BIO: Development of the LET distributions database, poster presentation on HIMAC Annual Meeting, April, Chiba.

Spurný F., et al., 2007. On the neutron contribution to the exposure level onboard space vehicles, Radiation Protection Dosimetry 126(1-4), 519-523.

Spurný, F. et al., 2005. Upgrading of LET track-etch spectrometer calibration: calibration and uncertainty analysis, Radiation Measurements 40, 343-346.

Spurný, F. et al., 1999. Dosimetry and microdosimetry on board of satellites with track etch detectors, Radiation Measurements 31, 615-618.

Tanner, R.J. et al., 2005. Operational and dosimetric characteristics of etched-track neutron detectors in routine neutron radiation protection dosimetry, Radiation Measurement 40, 549-559.

Tanner, R.J. et al, 2001. Recent enhancements to the understanding of the response of the NRPB neutron personal dosemeter, Radiation Measurements 34, 457-461.

Tanner, R.I. et al., 1995. The time dependence of neutron response for PADC manufactured using two different cure cycles, Radiation Measurements 25(1-4), 465-466.

Tawara, H. et al., 2008. Measurement of a linear energy transfer distribution with antioxidant doped CR-39 correcting for the dip angle dependence of track formation sensitivity, Jpn. J. Appl. Phys. 47, 7324-7327.

Tsuda, S. et al., 2003. Synthesis and characterization of a soft-tissue substitute for neutron dosimetry, Journal of Nuclear Science and Technology 40(12), 1027-1031.

Tripathy, S.P. et al., 2001. Modification induced by proton irradiation in polyallyldiglycol carbonate (PADC), Radiation Measurements 34, 15-17.

Ullmann, V., 2002. Jaderná fyzika a fyzika ionizujícího záření, Klinika nukleární medicíny, Fakultní nemocnice s poliklinikou Ostrava, available on http://astronuklfyzika. cz/Fyzika-NuklMed.htm.

Waker, A.J. et al., 2002. Classical microdosimetry in radiation protection dosimetry and monitoring, Radiation Protection Dosimetry 99(1-4), 311-316.

Yamauchi, T., 2003. Studies on the nuclear tracks in Cr-39 plastics, Radiation Measurements 36, 73-81.

Yamauchi, T. et al., 2008. Loss of carbonate ester bonds along Fe ion tracks in thin CR-39 films, Radiation Measurements 43, 106-110.

Yasuda, N., 2010, personal communication.

Yasuda N. et al., 2008. Verification of angular dependence for track sensitivity on several types of CR-39, Radiation Measurements 43, 269-273.

Yasuda, N. et al., 2006a. The intercomparison of cosmic rays with heavy ion beams at NIRS (ICCHIBAN) project, Radiation Protection Dosimetry 120(1-4), 414-420.

Yasuda, N. et al., 2006b. Extremely high dose neutron dosimetry using CR-39 and atomic force microscopy, Radiation Protection Dosimetry 120 (1-4), 470-474.

Yasuda, N. et al., 2005. Development of a high speed imaging microscope and new software for nuclear track detector analysis, Radiation Measurements 40, 311-315.

Yasuda, H. et al., 2000. Effective Dose Equivalent on the Ninth Shuttle-Mir Mission (STS-91), Radiation Research 154, 705-713.

Yasuda, N. et al., 1998. Measurement of bulk etch rate of CR-39 with atomic force microscopy, Nuclear Instruments and Methods B 142, 111.

Young, D.A., 1958. Etching of radiation damage in lithium fluoride, Nature 1982, 375-377.

Zhao, Q. et al., 2009. Secondary beam fragments produced by 200 and 400 Mev/u $^{12}C^{6+}$ ions in water, Chin. Phys. Lett. 26(9).

Zhou, D. et al., 2010. Radiation measured for MATROSHKA-1 experiment with passive dosimeters, Acta Astronautica 66, 301-308.

Zhou, D. et al., 2009. Research on sensitivity fading on CR-39 detectors during long time exposure, Radiation Measurements 44, 909-912.

Ziegler, J.F. et al., 2008. SRIM: The stopping and range of ions in matter, Pergamon Press, New York; see also www.SRIM.org.